Mix, A.C., Tiedemann, R., Blum, P., et al., 2003
Proceedings of the Ocean Drilling Program, Initial Reports Volume 202

3. Site 1232[1]

Shipboard Scientific Party[2]

INTRODUCTION

Site 1232 (proposed Site SEPAC-9A) is located at 39°53.45′, 75°54.08′W in the Chile Basin between the Mocha and Valdivia Fracture Zones, ~50 km west of the Chile Trench (Fig. F1). The water depth of 4072 m is ideal to monitor the influx of Circumpolar Deep Water into the Chile Basin. The crustal age is not well defined but was expected to be between 19 and 29 Ma as derived from magnetic lineations in the region.

The tectonic backtrack path of Site 1232 on the Nazca plate is approximately parallel to its latitudinal position and to surface-ocean gradients such as sea-surface temperatures in the subpolar transition zone. Thus, Site 1232 should have been situated close to the northernmost reaches of the westerly winds and the Antarctic Circumpolar Current during the Neogene. Today, Site 1232 lies ~300 m below the lysocline depth.

The total thickness of the sedimentary section was estimated at ~470 m based on site survey seismic profiles (80-in³ water gun at 30–400 Hz and 3.5-kHz shallow profiler) (Mix et al., 1997, 1998). The seismic data reveal well-stratified, flat-laying, moderately reflective layers (Fig. F2). Basement appears as a highly reflective surface that outcrops or is thinly covered with sediment on abyssal hills to the north and south of the basin. North of Site 1232, a Parasound profile indicated turbidite deposits in this terrain, as the upper 30 m of seismic penetration were marked by diffuse reflection. A 10-m-long piston core from the location of Site 1232 (RR9702A-26PC; Oregon State University) taken during the site survey cruise recovered hemipelagic sediments containing only a few centimeter-scale turbidite deposits.

The primary objectives at Site 1232 were to

F1. Site location and oceanographic features off southern and central Chile, p. 16.

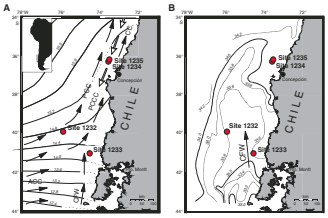

F2. Seismic profile at Site 1232, p. 17.

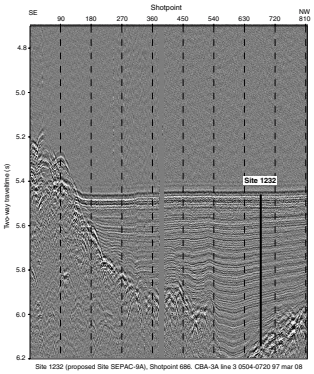

[1]Examples of how to reference the whole or part of this volume.
[2]Shipboard Scientific Party addresses.

Ms 202IR-103

1. Examine the long-term Neogene response of the southeast Pacific to major tectonic and climatic events, such as the opening of the Drake Passage (creating the Antarctic Circumpolar Current), the closing of the Isthmus of Panama (terminating the Atlantic-Pacific exchange of water masses), the uplift of the Andes (modifying the atmospheric circulation pattern) and the glaciation of the Antarctic;
2. Assess short-term variations in the character and expansion of Antarctic Circumpolar Deep Water on orbital timescales (Fig. **F3**); and
3. Monitor variations in the southernmost reaches of the northward-flowing Peru-Chile Current, based on planktonic fauna and flora, allowing comparisons to other sites of the latitudinal transect (Fig. **F1**).

Site 1232 revealed a dramatically different sequence than expected. The sediment record consists of an expanded Pleistocene section (<0.8 Ma) of silty clay (inferred turbidites and hemipelagic sediments) interbedded with thin beds of sandy silt (basal parts of distal turbidites), considerably limiting the paleoceanographic opportunity to fully achieve the outlined objectives.

F3. North-south cross section of water masses, p. 18.

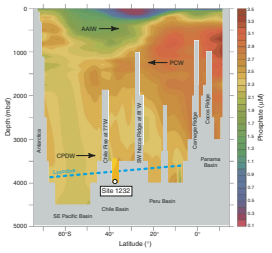

OPERATIONS

Valparaiso Port Call and First Transit

Leg 202 began at 1120 hr on 29 March 2002, when the first line was passed ashore in Valparaiso, Chile. The scientific party was aboard by 2 April. Two Chilean (Pedro Crignola and Flavia Velásquez Ruiz) and one Peruvian (Robert Herrera) observers joined the scientific party in compliance with demands associated with the permissions to operate in their national waters. The three individuals were to leave the ship later in the cruise upon exiting Peruvian waters and be replaced by an Ecuadorian observer. The port call was extended by 24 hr because we had to leave the pier and anchor in the harbor to allow a fruit freighter to occupy the berth.

At 0718 hr on 4 April, the last line was released and the vessel began the journey to the first site of the leg. Based on an assessment of available time and scheduled drilling program, we added the top-priority contingency Site SEPAC-19A to the operational plan. Because this site is positioned farther south than any of the first-priority sites, it was most effective to drill it as the first site. A 3.5-kHz survey was conducted over proposed Sites SEPAC-14A and SEPAC-13B before we proceeded to Site SEPAC-19A.

By midnight, the winds were gusting to 38 kt and the seas began to build. The vessel's speed had to be reduced to limit violent rolling and pitching. The next morning up to 60-kt gusts and blinding rain followed, and the seas and swell were estimated to be 30 ft and greater. As the vessel approached the position of Site SEPAC-19A, the captain ordered the vessel to reverse course. The speed was reduced to ~4 kt to maintain heading into the Force 8 storm. As the vessel proceeded on this northwesterly course, the weather gradually improved, but not to the extent that would have allowed us to return to Site SEPAC-19A. The most effective option was to proceed to Site SEPAC-9A. As the storm gradually abated, the speed of the vessel increased to 8 kt.

Site 1232

In the morning of 7 April, the vessel slowed and approached the Global Positioning System (GPS) coordinates of Site 1232 (proposed Site SEPAC-9A). The thrusters were lowered, and at 1100 hr the vessel was holding station at Site 1232 using the GPS. The voyage from Valparaiso lasted 74.5 hr and covered 645 nmi at an average speed of 8.6 kt.

The corrected precision depth recorder measurement indicated a depth of 4091.4 meters below rig floor (mbrf), relative to the dual elevator stool on the rig floor. A 136-m-long advanced piston corer (APC) and extended core barrel (XCB) bottom-hole assembly (BHA) was made up. This type of BHA was used at all sites during Leg 202. The initial pipe trip of the leg was extended to accomplish routine preparations and maintenance.

Hole 1232A

Hole 1232A was initiated with the APC at 0505 hr on 8 April with the bit placed at 4089 mbrf. The first core was a full recovery (Table T1), and hole-to-hole correlation later showed that the core top was 6.1 m below the seafloor (mbsf). Piston coring advanced to 112.5 mbsf, where the formation became too stiff to continue with the APC. Although the last two cores (11H and 12H) achieved full stroke, the barrels became firmly stuck in the formation and could not be released with a force of 80 klb. The core barrels were subsequently drilled over and released. The APC portion of the hole cored 112.5 m and recovered 104.5 m (recovery = 93%). Cores were oriented starting with Core 3H. Four attempts at collecting downhole temperature data were unsuccessful because of tool problems (Cores 3H, 6H, and 7H) or excessive motion at the bit (Core 8H).

T1. Operations summary, p. 37.

The wireline parted during the recovery of Core 5H, and the core barrel dropped from ~150 mbrf. The core barrel, tensor tool, and sinker bars were successfully recovered in the first fishing attempt with the wireline.

Vessel heave was responsible for the mechanical parting of the APC shear pin when the core barrel for Core 5H apparently landed too hard in the BHA. The barrel was actually pumped into the formation during the pressuring up of the drill string and did not successfully fire in the normal fashion. The resulting core was mostly flow-in, which probably occurred during the extraction of the barrel from the sediment.

Following APC refusal, the XCB was deployed and advanced from 112.5 to 371.3 mbsf. We planned originally to deepen the hole to acoustic basement at ~500 mbsf. This plan was abandoned and the hole was terminated because (1) the recovered sequence consisted of Pleistocene turbidites, and seismic data indicated that this sequence continued to basement and (2) inferred sediment accumulation rates were much higher than expected, which made the prospect of recovering pre-Pleistocene sediments unlikely. The XCB cored 258.8 m and recovered 184.31 m (recovery = 71.2%). In total, 371.3 m was cored and 288.8 m was recovered in Hole 1232A (recovery = 78%) (Table T1).

Hole 1232B

The vessel was offset 30 m north, and Hole 1232B was initiated with the APC at 1820 hr on 10 April. In an attempt to obtain a good mudline core and a stratigraphic overlap with the initial hole, the bit was posi-

tioned at 4080 mbrf. The core was still too deep by 2.2 m, however, as determined later. Based on the drill string measurement, the seafloor depth was 4080.4 m. Piston coring advanced to 90.1 mbsf, where the hole was terminated. The average recovery was 106.9% (Table T1). Cores were oriented starting with Core 2H. A bottom-water temperature measurement (1.60°C) was obtained with the APC temperature (APCT) tool before we initiated the hole. Four attempts at collecting downhole temperature data were unsuccessful because of tool problems (Cores 3H, 4H, 6H, and 8H). The bit was pulled free of the seafloor at 0815 hr on 11 April.

Hole 1232C

The vessel was offset 30 m north, and Hole 1232C was initiated with the APC at 1010 hr on 11 April. The bit was positioned at 4075 mbrf. The mudline was recovered in Core 1H, and the seafloor depth was determined to be at 4079.8 mbrf based on the drill string measurement. Piston coring was concluded after advancing to 33.2 mbsf. The average recovery was 95.4%. Because of the shallow depth objective, no cores were oriented. One downhole temperature measurement was attempted (Core 4H) but yielded bad data. The overall cored interval at this site was 494.6 m with 416.8 m recovered (recovery = 84.3%) (Table T1).

The vessel was secured for transit and left location at 2330 hr on 12 April.

COMPOSITE SECTION

We built a meters composite depth (mcd) scale and a splice (as defined in "Composite Section," p. 4, in the "Explanatory Notes" chapter) that ranged from the top of Core 202-1232C-1H to the bottom of Section 202-1232B-4H-7 (Tables T2, T3). The splice extends from 0.0 to 42.58 mcd. Splice construction below this interval was precluded by incomplete core recovery and by alignment of core gaps. We constructed a discontinuous ("floating") splice (see "Composite Section," p. 4, in the "Explanatory Notes" chapter) for the interval 42.67–100.34 mcd (Sections 202-1232B-5H-1 through 202-1232A-9H-7). Below that interval, cores were appended according to the cored interval if nominal recovery was <100% or to the recovered interval if recovery was >100%.

The mcd scale and the splice are based on the stratigraphic correlation of whole-core OSU Fast Track magnetic susceptibility measurements (OSUS-MS) collected at 2.5-cm depth increments using 1-s integration times (Fig. F4; Tables T4, T5). Correlations were checked using multisensor track (MST) data collected at 2.5- to 5-cm depth increments. We then constructed spliced records of magnetic susceptibility (MST-MS), gamma ray attenuation (GRA) bulk density, and natural gamma radiation (NGR) data (Fig. F5).

Magnetic susceptibility was the most useful stratigraphic tool for correlation at Site 1232. GRA density was helpful in some intervals where magnetic susceptibility structure was ambiguous. Correlation between cores from different holes was poor in the top and bottom ~1 m of many cores. We interpret this lack of correlation as evidence for disturbance resulting from the effects of the coring process at Site 1232. We constructed the mcd scale by assuming that the uppermost sediment (the "mudline") in Core 202-1232C-1H was the sediment/water interface. Core 202-1232C-1H, the "anchor" in the composite depth scale, is

T2. Composite depth scale, p. 38.

T3. Splice tie points, p. 39.

F4. Magnetic susceptibility vs. depth for the spliced record, p. 19.

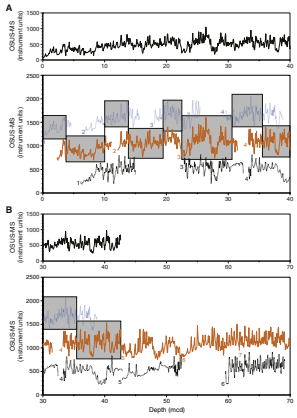

T4. OSUS-MS measurements, Hole 1232A, p. 40.

T5. OSUS-MS measurements, Hole 1232B, p. 41.

F5. Spliced records of L*, NGR, GRA density, and MST-MS, p. 21.

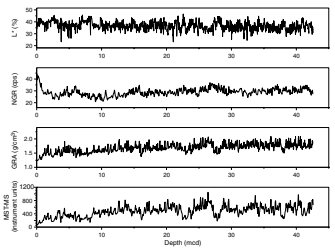

the only core in which depths are the same on the mbsf and mcd scales. From this anchor we worked downhole, correlating the stratigraphy on a core-by-core basis.

Although cores from different holes in the interval 42.67–100.34 mcd could not be tied directly to the splice, they could be correlated with each other. We placed them on the composite depth scale by adding the cumulative offset from the splice above to the mbsf depths for Cores 202-1232B-5H through 10H except where the bottom of a core overlapped with the top of the core below. In this case, the lower core was shifted down to prevent overlap and the new cumulative offset propagated downhole. Cores from Hole 1232A were then correlated with cores from Hole 1232B. At depths >100.34 mcd, cores in Hole 1232A were assigned an mcd by adding the cumulative offset of Core 202-1232A-9H, the deepest core correlated with a core in Hole 1232B, to their mbsf depth except when the recovered interval exceeded the cored interval. In these cases, the difference (typically <0.3 m) was added to the offset to avoid stratigraphic overlap.

A comparison of the mcd and mbsf depth scales (Fig. F6) shows that within the splice the mcd scale is an average of 22% greater than the mbsf scale. In addition, Hole 1232A shows an overall step in the offsets below Core 202-1232A-6H and can be best correlated to Core 202-1232B-7H in the composite section. This additional offset reflects the fact that Core 202-1232A-5H was recovered after operational problems and contained significant flow-in. We concluded that the core, and all subsequent cores, were recovered from deeper in the section than was recorded by the driller.

To facilitate the calculation of mass accumulation rates (MARs), we provide corrected meters composite depth (cmcd) in Tables T2 and T3 for depths within the splice. A comparison of the mcd and mbsf depth scales (Fig. F6) shows that the mcd scale within the splice is an average of 22% longer than the mbsf scale.

F6. Mcd vs. mbsf, p. 22.

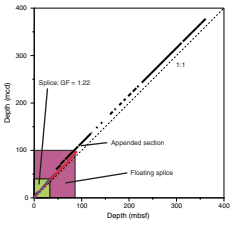

LITHOSTRATIGRAPHY

A sediment section extending to 362.1 mbsf (381.7 mcd) was recovered from three holes at Site 1232. The sediment record is dominated by turbidite deposits and is characterized by siliciclastic silty clay and clay (dominant lithology) and sandy silt (minor lithology). Clay minerals and feldspars are common, whereas amphiboles, pyroxenes, and quartz are present in minor amounts. Biogenic components are generally rare to absent. Sediment dry bulk density and GRA bulk density are variable, with mean values that do not shift markedly between the uppermost and lowermost sediments, except for slightly lower values in the uppermost 15 mbsf. Magnetic susceptibility is generally very high and variable, and sediment reflectance is low. All measured parameters display high variability on decimeter (0.2–0.5 m) scales. Color changes are subtle and gradational within the dominant lithology but contrast sharply with the minor lithologies.

A single lithologic Unit I was defined for the site on the basis of visual core description, smear slide examination, diffuse reflectance spectrophotometry, magnetic susceptibility, GRA bulk density, natural gamma emissions, and moisture and density (MAD) measurements (Table T6). The dominant lithology consists of massive light gray to gray silty clay and clay. Lithologic variability mainly consists of the interbedding of coarser layers within the silty clay and clay sediments. The

T6. Lithologic Unit I, p. 42.

coarser-grained layers are generally 1 to 10 cm thick and are present throughout the section at irregular intervals averaging ~30 cm. These layers contain a sharp basal contact and grade upward to gradational, poorly defined contacts with the dominant lithology. They are interpreted as the basal portion of turbidite sequences. The interbedding of coarse-grained layers with the silty clay exerts a predominant influence on the magnitude and length-scale of variability displayed by all of the measured parameters.

Description of Lithologic Unit

Unit I

Intervals: Cores 202-1232A-1H through 39X; Cores 202-1232B-1H through 10H; and Cores 202-1232C-1H through 4H
Depths: Hole 1232A: 0–362.1 mbsf (5.94–381.7 mcd); Hole 1232B: 0–90.4 mbsf (2.24–98.8 mcd); and Hole 1232C: 0–33.2 mbsf (0–38.9 mcd)
Age: late Quaternary (<0.78 Ma)

The dominant lithology defining Unit I displays little visual variability. It is primarily a massive unit with few sedimentary structures. Sediment color ranges from light greenish gray to light gray to medium gray, and most color transitions are gradual. Some mottling, occasional light brown nodules, and thin silt layers are present. Sand content is negligible within the dominant lithology, and silt content varies from ~10% to 40%.

A second important lithology is interbedded with the dominant silty clay and clay throughout Unit I. It consists of coarser sediment, typically silty sand or sandy silt, overlying a sharp basal contact and grading upward over several centimeters to silty clay (Fig. F7). The interbedding occurs on decimeter scales and displays strong contrasts in texture and most physical properties, although not in mineralogy.

A total of 1328 coarse layers were observed (Table T7), with 772 present in the 289 m of core recovered in Hole 1232A (371 m deep) (Fig. F8). This extrapolates to 991 layers over the drilled interval (2.7/m on average), although variability is detected on all depth scales. The coarse lower portions of the layers vary in thickness from <0.5 to 118 cm, measured from the basal contact to the first shift in texture and color above the darkest interval (Fig. F7). The combined length of these coarse intervals represents ~15% of the undisturbed sediment recovered by the APC at the site (Table T6). The basal contacts of the coarse layers are generally sharp, although rarely planar. Many of the contacts have centimeter-scale, possibly erosional, relief. Many of the contacts and layers are deformed and inclined from subparallel to nearly perpendicular to the overall bedding, perhaps due to drilling disturbance. Because the coarse layers grade upward into the silty clay of the overlying sediments, in most cases it is difficult to determine the exact top of the entire sedimentary packet. Some or all of the silty clay that is defined as the dominant lithology may be associated with the deposition of the coarse sediment. Some of the coarse layers present in the upper part of the stratigraphic section are soupy and disturbed.

The coarse, graded layers generally thin downcore. From 235 to 293 mcd (217.3–275.0 mbsf; Cores 202-1232A-24X through 29X), an interval of nearly complete recovery, no coarse-grained layers thicker than 4 cm are present, whereas the coarse layers shallower than 120 mcd have

F7. Typical interbedded sequence, p. 23.

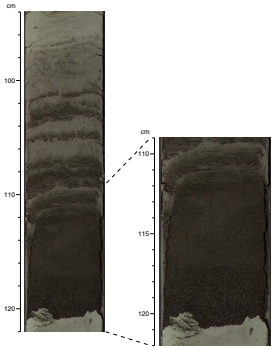

T7. Coarse-grained layers, p. 43.

F8. Basal depth and thickness of coarse-grained layers, p. 24.

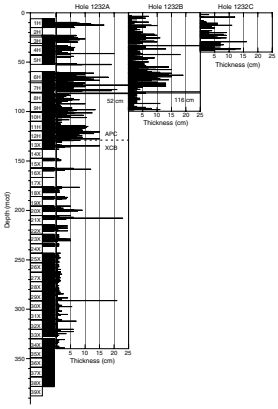

an average thickness >4 cm. Although this may reflect an environmental shift in the source areas of the turbidites, the deeper interval is also strongly influenced by coring disturbance.

Silt-sized components of the dominant silty clay lithology consist primarily of feldspars, with lesser amounts of amphibole, pyroxene, and quartz (Fig. F9). Minerals that are present in trace abundance include mica, rutile, garnet, zircon, brown volcanic glass, and palagonite. The mineralogy of the coarser interbedded layers is similar to that of the dominant silty clay lithology, with the exception of containing fewer clay minerals. Biogenic components are present in trace abundances, with a few exceptions (Fig. F9). Several thin layers contain abundant nannofossils, and one sediment pod contains abundant siliceous microfossils. Subtle shifts in mineralogy occur downcore. For example, opaque minerals are present throughout all cores from Site 1232 but generally reach minimum concentrations in the interval from 220 to 250 mcd (Fig. F9). Zircon and rutile are absent from this interval, although they are present in trace abundances shallower and deeper in the section. Similarly, titanite is absent above 250 mcd and is present in trace abundances downhole. These changes in mineralogy generally follow shifts in the thickness of interbedded coarse-grained layers.

Thin ash layers are present in interval 202-1232A-34X-3, 116–116.5 cm (336.61 mcd), and Section 202-1232B-3H-1, 110 cm (22.88 mcd).

Slight to moderate bioturbation is evident within some intervals, particularly in the cores recovered by APC. Bioturbation is particularly apparent above color transitions and is expressed as smoothly perforated contacts and sediment mottling. A highly bioturbated minor lithology consisting of light brown clayey calcareous ooze is entirely present as diffuse light brown mottling within medium gray clay in Section 202-1232A-13X-3.

Core logging data are highly variable superimposed on a more or less constant background, with the exception of the uppermost 22 mcd, which are characterized by lower magnetic susceptibility and NGR and lower than average GRA densities (Fig. F10). This high variability is the consequence of primarily textural and secondarily mineralogical changes (e.g., ferromagnetic mineral content that increases in coarser layers) between fine-grained and coarse layers. Density and porosity suggest a slight downhole trend resulting from sediment compaction and dewatering with increased overburden (Fig. F11). However, this trend is well within the superimposed variability generated by differences in lithology. The different characteristics of the upper 20 m are more evident in the MAD data than in the core logging data (Fig. F11) with high porosity, high water content, and, consequently, low bulk density. Several samples in this upper sequence also suggest grain densities that are higher than the downcore average. In general, a contrast in the large-scale texture and interbedding is present along with the switch to XCB coring at 112.5 mbsf in Hole 1232A (129.7 mcd) (Figs. F8, F9). This may indicate a bias in the recovery that favors collection of finer lithologies and thinner coarse-grained layers. Alternatively, the change to XCB coring may have been required by a true change in lithology, as clay-rich sediments often cause high pullout tensions during APC coring, although some of the shift to thinner coarse layers occurs below the shift to XCB coring. Drilling disturbance within the XCB cores increases downcore and may explain the muting of many measured parameters below ~120 mcd. Below this depth, changes in mineralogy are subtle and primarily influence components that are present

F9. Mineralogy acquired from smear slide data, p. 25.

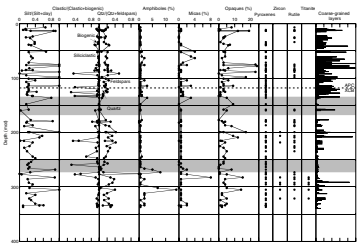

F10. Lithostratigraphic summary, p. 26.

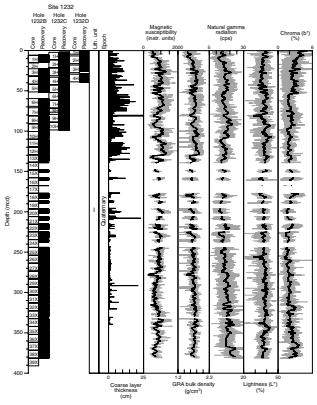

F11. Moisture and density, p. 27.

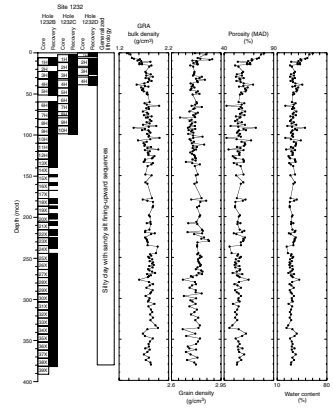

only in trace abundances (Fig. F9). Therefore, no unit or subunit divisions are defined based on these changes.

In general, the GRA and MAD measurements are well correlated (r^2 = 0.997) (Fig. F12). Thus, the linear relationship between MAD bulk density and dry bulk density can be applied to the GRA density data in order to calculate predicted dry bulk densities, which are necessary for calculating MARs.

Magnetic susceptibility, GRA density, reflectance spectroscopy data (primarily b*, but also L*) vary in relation to observed textural changes. Coarse layers are characterized by high magnetic susceptibility and GRA density and low b* and L* values. In the a*-b* color space, almost all color measurements at Site 1232 plot in the "yellow" domain (~a* = 0) (Fig. F13) with silty sand layers plotting at the lower end (b* < 2) (Fig. F14). Smear slide estimates suggest that the presence of coarser grains (silt and sand) reduces the chroma (~b*) even in finer sediments.

Interpretation and Depositional History

The physiographic setting of Site 1232, ~200 km from a continental source and seaward of the trench, is consistent with the accumulation of hemipelagic sediments. For example, such sediments are present within the uppermost interval (202-1232C-1H-1, 0–8 cm) and contain ~15% biogenic components. However, the sediments of Unit I are predominantly siliciclastic, and the accumulation of 362 m of sediment in <0.8 m.y. suggests a sedimentation rate of >450 m/m.y., which is much higher than might be expected from typical hemipelagic sedimentation alone. The trace abundances of biogenic components within the dominant lithology are therefore mostly a result of dilution by terrigenous sediments. Analyses of surface sediments demonstrate that the trench system is not an effective barrier to sediments derived from the continent (Lamy et al., 1998). In addition, the interbedded coarse layers constitute a significant fraction of the stratigraphic column and contain negligible biogenic components. The sharp basal contacts, erosive scour relief, graded bedding, strong change in physical properties, and finer, gradational tops all indicate that these are turbidite sequences. Because some fine-grained overlying sediment may have been deposited along with the coarser basal portion of the interbedded layers as a turbidite sequence, the measured occurrence of coarse lithologies within 15% of Unit I provides only a minimum estimate of the influence of these turbidites at Site 1232.

The mineralogy of the sediments within the turbidites and the dominant silty clay is similar and is characterized by a very immature mineralogical assemblage (i.e., low quartz, high plagioclase, and significant amounts of amphiboles and pyroxenes), suggesting a predominantly andesitic to basaltic provenance. This provenance is compatible with the proximity and mineralogy of the Andes rather than a plutonic (i.e., Coastal Range) or a mafic oceanic source. This is consistent with the modern mineralogical composition off the central Chile region (Thornburg and Kulm, 1987b; Lamy et al., 1998). Compared to the Chile margin sediments farther north and south, both trench and continental slope surface sediments suggest the most immature mineralogical assemblages off central Chile are due to the overwhelming contribution of highly erodible source rocks from the Andes supplied by the high discharge of river systems in this region (Thornburg and Kulm, 1987b; Lamy et al., 1998). Sediments are transported downslope within large submarine fan systems in this region and are further distributed along

F12. GRA and MAD bulk density, p. 28.

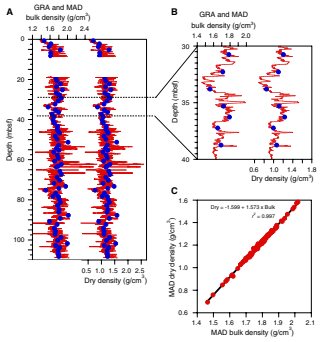

F13. Color measurements, p. 29.

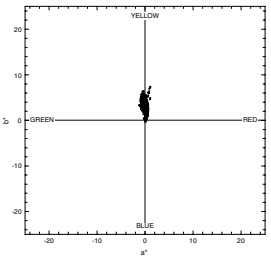

F14. Coarse layer characteristics, p. 30.

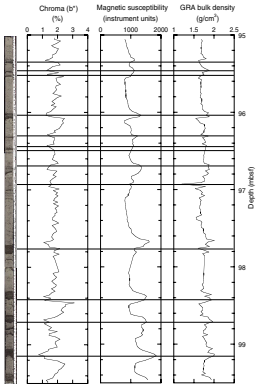

the trench toward the north (Thornburg and Kulm, 1987a). Therefore, it is difficult to say how far or via what exact path the turbidites traveled to the site, although they are more likely to have come from the south, where the trench is filled and where the sediment source is largest. The erosive contacts and similar mineralogies of the interbedded dominant and secondary lithologies indicate the possibility that some portion of the vertical pelagic sedimentation has not been preserved at this site. The persistently similar mineralogy indicates little change in the character of the sediment source through the last few hundred thousand years. The 772 layers recovered from Site 1232 represent a minimum estimate that does not include layers that were eroded by subsequent events or were not recovered during drilling. Therefore, the average time step for turbidite deposition is most likely on the order of a few centuries within the 0.78-Ma maximum age of the section. Their recurrence may reflect paleoseismic activity or other processes that affect slope instability. The presence of thinner interbedded coarse-grained layers in the lower half of the section may reflect a more distant origin of the older turbidites or less intense events.

BIOSTRATIGRAPHY

Calcareous nannofossils, planktonic and benthic foraminifers, and diatoms were examined at Site 1232. The abundance of calcareous microfossils is generally low, and their preservation is generally poor to moderate. Reworking of microfossils is apparent in all the fossil groups examined. In particular, freshwater and benthic diatoms are present in most of the samples, indicating relatively persistent redeposition from the upper continental margin. Calcareous nannofossils and planktonic foraminifers suggest that the entire sequence cored at the site is Pleistocene in age.

Calcareous Nannofossils

All the core catcher samples, plus additional samples from the split cores, were examined for calcareous nannofossils. Calcareous nannofossils are generally rare to few in most samples and barren in a number of samples. The preservation of nannofossils is generally poor to moderate. Reworking of nannofossils (mostly Neogene in age) is apparent in many samples.

Emiliania huxleyi was observed down to 143.7 mcd (Sample 202-1232A-13X-CC) (Table T8). Thus, an age of 0.26 Ma can be assigned to the interval of 137.9–138.8 mcd (Samples 202-1232A-13X-CC and 14X-1, 29 cm). One specimen of *Pseudoemiliania lacunosa* was found in each of the following samples: Samples 202-1232A-26X-CC (263.5 mcd), 30X-CC (303.0 mcd), and 32X-CC (322.7 mcd). This suggests that the interval from Section 202-1232A-26X-CC (273.4 mcd) downhole is older than 0.46 Ma. Medium-sized *Gephyrocapsa* spp. are present down to the bottom of the hole, which suggests a basal age younger than 1.69 Ma.

T8. Distribution of calcareous nannofossils, p. 47.

Planktonic Foraminifers

Planktonic foraminifers were examined in all core catcher samples from Hole 1232A and in selected samples from Cores 202-1232A-1H and 8H. The soft clay in the samples was easily removed by being

soaked in warm water and washed through a 63-µm sieve. The abundance of planktonic foraminifers at Site 1232 fluctuates markedly (between >50% and <1% of the >63-µm residue), and a few samples are barren. Preservation varies significantly, and evidence of dissolution, frequent test breakage, and test infills are observed, particularly in samples with low test abundance.

The planktonic foraminiferal assemblage includes *Globorotalia truncatulinoides, Globorotalia inflata, Globigerina bulloides, Globigerinita glutinata, Globigerina falconensis, Neogloboquadrina pachyderma,* and *Orbulina universa* (Table T9). This assemblage is present intermittently down to the base of Hole 1232A (Sample 202-1232A-39X-CC), indicating the Pleistocene Zone Pt1 of Berggren et al. (1995). *Globorotalia tosaensis* and *Globorotalia crassaformis* are both present in the lower part of the section in the interval from 273.4 to 317.5 mcd (interval 202-1232A-26X-CC through 36X-CC). *G. tosaensis* is the species used by Berggren et al. (1995) to subdivide the zone into two the Subzones Pt1a (present–0.65 Ma) and Pt1b (0.65–1.77 Ma). However, it is difficult to apply here for a similar purpose, as poor preservation makes reliable recognition of the taxon difficult. Therefore, the true last appearance of the taxon cannot be precisely determined in this section. The composition of the assemblage generally reflects temperate transitional climatic conditions.

T9. Distribution of foraminifers, p. 48.

Benthic Foraminifers

Benthic foraminifers were studied in all core catcher samples from Holes 1232A and in selected samples from Cores 202-1232A-1H and 8H. Benthic foraminifers are present in many of the samples studied. However, abundance varies markedly, and the ratio of benthic to planktonic foraminifers fluctuates significantly. Preservation is generally moderate or poor. The Pleistocene assemblage includes *Cibicidoides* spp., *Coryphostoma* sp., *Eggerella bradyi, Globobulimina pacifica, Globocassidulina subglobosa, Globulina* spp., *Gyroidinoides orbicularis, Hoeglundina elegans, Melonis affinis, Melonis pompilioides, Oridorsalis umbonatus, Pullenia bulloides, Pyrgo murrhina, Pyrgo serrata, Uvigerina peregrina,* and *Uvigerina hispida*.

Tests appear frequently blackened with mud infill and abraded, showing clear evidence of reworking. Samples 202-1232A-8H-5, 136–138 cm; 8H-5, 145–147 cm; and 8H-5, 148–150 cm, respectively (below, within, and above a distinct turbidite layer), were analyzed to detect any changes in provenance and assemblage composition related to lithology. Composition did not vary significantly in the three samples studied. Even samples from the presumed "hemipelagic" intervals above and below the distinct turbiditic interval were found to contain some blackened abraded tests with mud infills (in particular *Uvigerina* spp. and *Cibicidoides* spp.), suggesting significant reworking prior to sediment deposition.

Diatoms

All core catcher samples from Hole 1232A as well as some additional samples from the split cores were analyzed. Most samples contain diatoms; abundance varies between common and trace, and preservation is poor to moderate. Preservation deteriorates and abundance decreases below Core 202-1232A-20X. Diatom assemblages vary in character between typical upwelling and freshwater dominated.

Upwelling-related assemblages were defined based on the dominance of resting spores of the genus *Chaetoceros* and the common occurrence

of *Thalassiosira,* mainly forms of the *eccentrica* group. Freshwater-dominated assemblages are mainly composed of *Aulacoseira granulata* with minor contributions of *Eunotia, Fragilaria, Melosira, Cymbella,* and *Cyclotella* spp. Freshwater assemblages are mainly associated with the coarser sediments but are present in most samples. Benthic forms such as *Cocconeis* and *Navicula* are also present in most samples, except for the intervals between Cores 202-1232A-11H and 13X, 31X and 33X, and 34X and 39X. Given that these forms can only live in shallow waters (water depth of <100 m), they were interpreted as displaced.

Typical oceanic warm-water forms such as *Azpeitia nodulifer, Fragilariopsis doliolus,* and *Hemidiscus cuneiformis* are found as minor contributors in "hemipelagic" layers sampled from the split cores (Samples 202-1232A-4H-2, 10 cm; 7H-3, 121 cm; 7H-5, 44, 60, and 65 cm; 8H-5, 55 and 80 cm; 19X-1, 93 cm; 34X-3, 120 cm; and 34X-5, 54 cm) (Table T10).

Because no biostratigraphically useful marker species were found, age assignments were not possible.

T10. Distribution of diatoms, p. 49.

PALEOMAGNETISM

Natural Remanent Magnetization

The natural remanent magnetization (NRM) of archive halves of APC and XCB cores recovered at Site 1232 was measured using the shipboard pass-through cryogenic magnetometer. Measurements were made at 5-cm intervals. Sections obviously affected by drilling disturbance were not measured. Cores 202-1232A-1H through 20X and 34X were initially measured and then remeasured after demagnetization at peak alternating fields (AF) of 10, 15 and 20 mT. Cores 202-1232A-23X through 30X and Cores 1202-232B-1H through 6H were initially measured and then remeasured after demagnetization at peak AF fields of 10 and 20 mT. Cores 202-1232A-31X through 33X and 35X through 39X were initially measured and then remeasured after demagnetization at a peak AF field of 20 mT.

Initial NRM intensities were extremely high, ranging from 0.5 to >3.5 A/m (Fig. F15). Intensities in Hole 1232A cores were lower in the XCB section (mean ≈ 0.6 A/m) than in the APC section (mean ≈ 1.4 A/m). The high NRM intensities are consistent with a magnetic overprint that has been attributed to the drill string. This overprint, characterized by steep positive inclinations averaging 71° for Hole 1232A (Fig. F15), was substantially reduced (typically by 75%) by demagnetization at peak AF fields as low as 10 mT. After 20-mT AF demagnetization, inclinations observed (Fig. F15) were closer to the expected axial-geocentric-dipole inclination (–59°) for the site latitude (~40°S). Although the positive overprint is substantially reduced through AF demagnetization, some overprint still remains, as evidenced by mean inclinations of –30° with a median value of –39° after 20-mT AF demagnetization (Fig. F15). High NRM intensities are still observed after 20-mT AF demagnetization, with lower values in the XCB section (0.14 A/m) than in the APC section (0.21 A/m). Declinations prior to demagnetization are consistently near 0° and 360°. These directions are consistent with a drill string overprint that is removed in the APC but not the XCB cored section after demagnetization (Fig. F15). The tensor orientation tool was employed below the second core of the APC section of both Holes 1232A and 1232B.

F15. NRM before and after 20-mT demagnetization, p. 31.

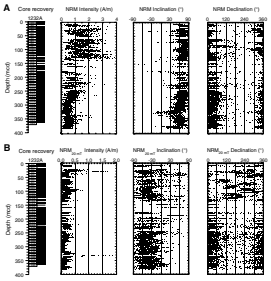

Magnetic Polarity

The magnetic polarity at Site 1232 is normal and attributed to the Brunhes Chron (0–0.78 Ma). However, many intervals of positive (reversed) or shallow inclination are observed (Figs. F15, F16). These anomalous inclinations do not reflect geomagnetic field behavior, but rather artifacts of the drill string magnetic overprint combined with decimeter-scale changes in grain size and magnetic susceptibility (see "Lithostratigraphy," p. 5). Intermittent coring deformation of the silt-rich intervals may also contribute to the anomalous inclinations.

Initial NRM intensity and magnetic susceptibility values are generally in phase within the uppermost 130 mcd of all holes showing similar variability at the decimeter to dekameter scale (Fig. F16). The large-scale (tens of meters) variability is generally consistent with the incidence/thickness of turbidites at Site 1232 (see "Lithostratigraphy," p. 5). Higher intensities are present in stratigraphic intervals having more/thicker turbidites, whereas lower intensities are present in stratigraphic intervals having fewer/thinner turbidites. This pattern is less obvious in the XCB cored interval, possibly due to incomplete recovery (Fig. F15). The high intensity of the drill string overprint and the similarity between the NRM intensity and magnetic susceptibility (Fig. F17) may reflect the coarse-grained, highly terrigenous nature of these turbidite-rich sediments with the drill string–overprinted NRM accentuated by the coarser magnetic grains. This relationship is generally lost after AF demagnetization through the removal of much of the strong viscous remanent magnetization (Fig. F17).

F16. NRM compared among Holes 1232A, 1232B, and 1232C, p. 32.

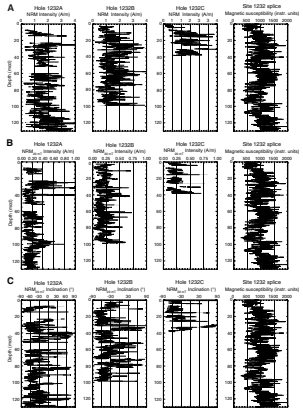

F17. NRM vs. whole-core low-field MS, p. 34.

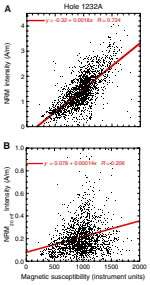

GEOCHEMISTRY

Sediment Gases

Concentrations of headspace gases were routinely monitored in sediments from Hole 1232A according to shipboard safety and pollution prevention considerations. Methane concentrations above ambient background first appeared in a headspace gas sample at 27.3 mcd (Table T11; Fig. F18). Methane concentrations increased to ~9000 ppmv by 64.2 mcd, then remained typically above 10,000 ppm. High methane concentrations and the absence of higher molecular weight hydrocarbon gases (Table T11) indicate that the methane is of biogenic origin, probably originating from in situ degradation via microbial diagenesis (methanogenesis) of sedimentary organic matter. A biogenic origin for the methane is supported by the low values of sulfate in interstitial water at depths below ~20 mcd (Fig. F19). The presence of interstitial sulfate inhibits methanogenesis in marine sediments (Claypool and Kvenvolden, 1983).

T11. Headspace gas concentrations, p. 51.

F18. Headspace methane vs. depth, p. 35.

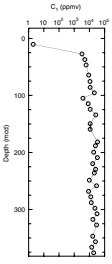

Interstitial Water Geochemistry

We collected 30 interstitial water samples from Site 1232, 20 from Hole 1232A and 10 from Hole 1232B. These are treated as constituting a single mcd profile. Chemical gradients at this site (Table T12) reflect the influence of organic matter diagenesis, some degree of biogenic opal dissolution, and other processes.

Chlorinity ranges from 559 to 576 mM, with low values near the sediment/water interface and from 159.2 to 277.9 mcd (Fig. F19). Salinity,

measured refractively as total dissolved solids, ranges from 33 to 35. Sodium concentrations measured by ion chromatography were, on average, within <2% of those estimated by charge balance reported here (Table **T12**).

Alkalinity increases to peak values >30 mM from 26.3 to 159.2 mcd then decreases to <20 mM at 248.5 mcd, with values in deeper samples >25 mM. Sulfate concentrations decrease to values <2 mM by 26.3 mcd, remaining low with increasing depth except for a small maximum of ~5 mM at 248.5 mcd. Dissolved manganese concentrations generally decrease with increasing depth from 37 µM at 6.7 mcd to 7 µM from 56.6 to 66.3 mcd. Manganese concentrations reach a secondary maximum, with values increasing from 12 µM at 75.5 mcd to 22 µM at 85.7 mcd; farther downhole, values are generally <10 µM. Dissolved iron concentrations increase with increasing depth, with values generally >20 µM from 36.9 to 124.2 mcd and lower values in deeper samples. The iron data show considerable scatter, and many samples have concentrations close to the detection limit (~6 µM). Phosphate concentrations are >50 µM throughout. Ammonium concentrations increase from 0.9 mM at 6.7 mcd to values generally >2 mM by 36.9 mcd. Slightly lower ammonium concentrations are found from 93.4 to 124.2 mcd.

Dissolved silicate concentrations are always <600 µM, indicating that the interstitial waters are not at saturation with respect to biogenic opal. Barium concentrations are generally <20 µM, with a pronounced barium peak up to 34 µM from 83.6 to 95.4 mcd and with values typically >20 µM from 219.7 to 366.2 mcd. Boron concentrations generally decrease with increasing depth, from 472 µM at 6.7 mcd to 325 µM at 366.2 mcd.

Calcium concentrations decrease sharply to values <6 mM by 27.2 mcd and increase to values >6 mM from 64.1 to 75.0 mcd, with a sharp minimum <4 mM from 93.4 to 104.9 mcd. Magnesium concentrations range from 45 to 55 mM, with no pronounced variations with depth. Magnesium/calcium ratios increase from 5.6 at 6.7 mcd to ~8–9 from 26.3 to 76.0 mcd, reach a sharp maximum >14 from 93.4 to 104.9 mcd, decline to <10 from 124.2 to 134.1 mcd, and then remain >11 until the deepest sample. Strontium and potassium concentrations generally decrease slightly with increasing depth (Fig. **F19**).

Sedimentary Inorganic Carbon, Organic Carbon, and Nitrogen Concentrations

Inorganic carbon (IC), total carbon (TC), and total nitrogen (TN) concentrations were determined on sediment samples from Holes 1232A and 1232B (Table **T13**). Organic matter carbon/nitrogen ratios were used to characterize the organic matter.

Total organic carbon (TOC) concentrations are very low throughout the sediment column, with a range between 0.05 and 0.35 wt% (average = 0.17 wt%). Most of the sediment samples contain <0.25 wt% TOC, which is typical of open-ocean sediments. TN values at Site 1232 are very low and vary between 0.1 and 0.8 wt% (average = 0.02 wt%) (Table **T13**). In some sediment samples, nitrogen contents are too low to be measured accurately. Calcium carbonate concentrations range between 0.3 and 27 wt%, and most sediment samples contain <2 wt% calcium carbonate (Table **T13**). These generally low concentrations agree with the paucity of microfossils (coccoliths and foraminifers) and the high abundance of continental clastic sediments at this site.

F19. Interstitial water geochemical data, p. 36.

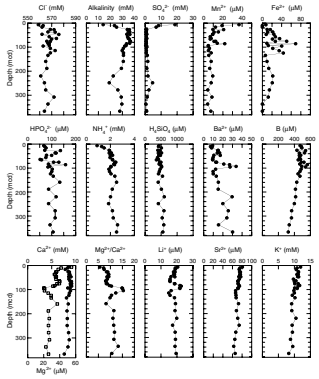

T12. Interstitial water geochemical data, p. 52.

T13. IC, $CaCO_3$, TC, TOC, TN, and TOC/TN ratios, p. 53.

Most TOC/TN ratios are below 12 (average = 8) (Table T13), indicating a predominance of marine organic matter throughout the record (Emerson and Hedges, 1988; Meyers, 1997). Most of the samples in which turbidites are observed have very low TOC contents (e.g., Samples 202-1232A-3H-3, 72–73 cm; 8H-6, 75–75 cm; 10H-3, 74–75 cm; and 11H-6, 74–75 cm) (Table T13) and nitrogen contents too low to be accurately measured.

AGE MODEL AND MASS ACCUMULATION RATES

A 390.6 mcd thick (371.3 mbsf) late Pleistocene turbidite sequence with intercalated hemipelagic sediment was recovered at Site 1232. The basal age of the core is 0.78 Ma, as the entire record is of normal polarity and within the Brunhes Chron (1n; see "Paleomagnetism," p. 11). This paleomagnetic interpretation is in agreement with the biostratigraphic age constraints (0.46–1.69 Ma; see "Biostratigraphy," p. 9). A conservative estimate of the average sedimentation rate is therefore ~475 m/m.y. A detailed age-depth model was not created aboard ship, as polarity chrons and biostratigraphic datums are not abundant enough at this site of extremely high sedimentation rates.

REFERENCES

Berggren, W.A., Kent, D.V., Swisher, C.C., III, and Aubry, M.-P., 1995. A revised Cenozoic geochronology and chronostratigraphy. *In* Berggren, W.A., Kent, D.V., Aubry, M.-P., and Hardenbol, J. (Eds.), *Geochronology, Time Scales and Global Stratigraphic Correlation*. Spec. Publ.—SEPM, 54:129–212.

Brandhorst, W., 1971. Condiciones oceanográficas extivales frente a la costa de Chile. Revista Biologica Marina (Valparaiso), 14:45–84.

Claypool, G.E., and Kvenvolden, K.A., 1983. Methane and other hydrocarbon gases in marine sediment. *Annu. Rev. Earth Planet. Sci.,* 11:299–327.

Emerson, S., and Hedges, J.I., 1988. Processes controlling the organic carbon content of open ocean sediments. *Paleoceanography,* 3:621–634.

Lamy, F., Hebbeln, D., and Wefer, G., 1998. Terrigenous sediment supply along the Chilean continental margin: modern regional patterns of texture and composition. *Geol. Rundsch.,* 87:477–494.

Lamy, F., Rühlemann, C., Hebbeln, D., and Wefer, G., 2002. High- and low-latitude control on the position of the southern Peru-Chile current during the Holocene. *Paleoceanography,* 17(2).10.1029/PA000727.

Meyers, P.A., 1997. Organic geochemical proxies of paleoceanographic, paleolimnologic, and paleoclimatic processes. *Org. Geochem.*, 27:213–250.

Mix, A.C., Pisias, N.G., Bloomer, S.F., and Mayer, L.A., 1998. *Southeast Pacific Paleoceanographic Transects, Site Survey Data Package 3: 3.5 kHz Data, Genesis Leg III, R/V* Roger Revelle, *Feb.–Apr. 1997:* Corvallis (Oregon State Univ.).

Mix, A.C., Pisias, N.G., Goldfinger, C., West, B., Mayer, L.A., and Bloomer, S.F., 1997. *Southeast Pacific Paleoceanographic Transects, Site Survey Data Package 2: Genesis Leg III, R/V* Roger Revelle, *Feb.–Apr. 1997:* Corvallis (Oregon State Univ.).

Ocean Climate Laboratory, 1999. *World Ocean Atlas 1998 (WOA98)* [CD-ROM]. Available from: National Climatic Data Center, Asheville NC 28801-5001, USA.

Strub, P.T., Mesias, J.M., Montecino, V., Rutllant, J., and Salinas, S., 1998. Coastal ocean circulation off western South America. *In* Robinson, A.R., and Brink, K.H. (Eds.), *The Sea* (Vol. 11): *Coastal Oceans:* New York (Wiley), 273–313.

Thornburg, T.M., and Kulm, L.D., 1987a. Sedimentation in the Chile Trench: depositional morphologies, lithofacies, and stratigraphy. *Geol. Soc. Am. Bull.,* 98:33–52.

————————, 1987b. Sedimentation in the Chile Trench: petrofacies and provenance. *J. Sediment. Petrol.,* 57:55–74.

Figure F1. Locations of Site 1232–1235 and oceanographic features off southern and central Chile (ACC = Antarctic Circumpolar Current, PCC = Peru-Chile Current, PCCC = Peru-Chile Countercurrent, CC = Chile Coastal Current, CFW = Chilean Fjord Water) (after Strub et al., 1998, and Lamy et al., 2002). **A.** Modern mean annual sea-surface temperatures (SSTs) (contours are in degrees Celsius, after Ocean Climate Laboratory, 1999; dashed isotherms are extrapolated). **B.** Modern sea-surface salinities (SSSs) measured during the *Marchile* cruise in February to March 1960 (Brandhorst, 1971).

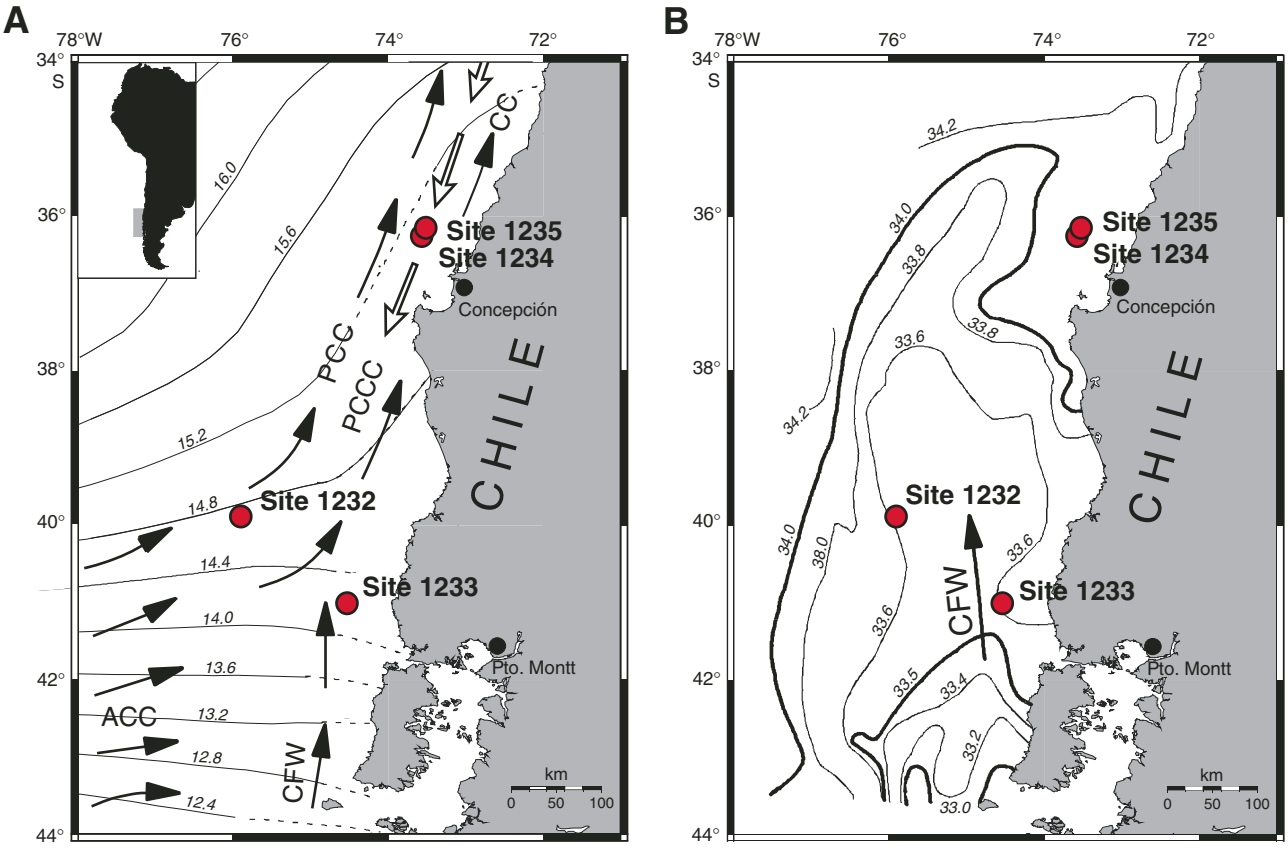

Figure F2. Seismic profile at Site 1232 (*Revelle* line 970308; 80-in³ water gun at 30–400 Hz).

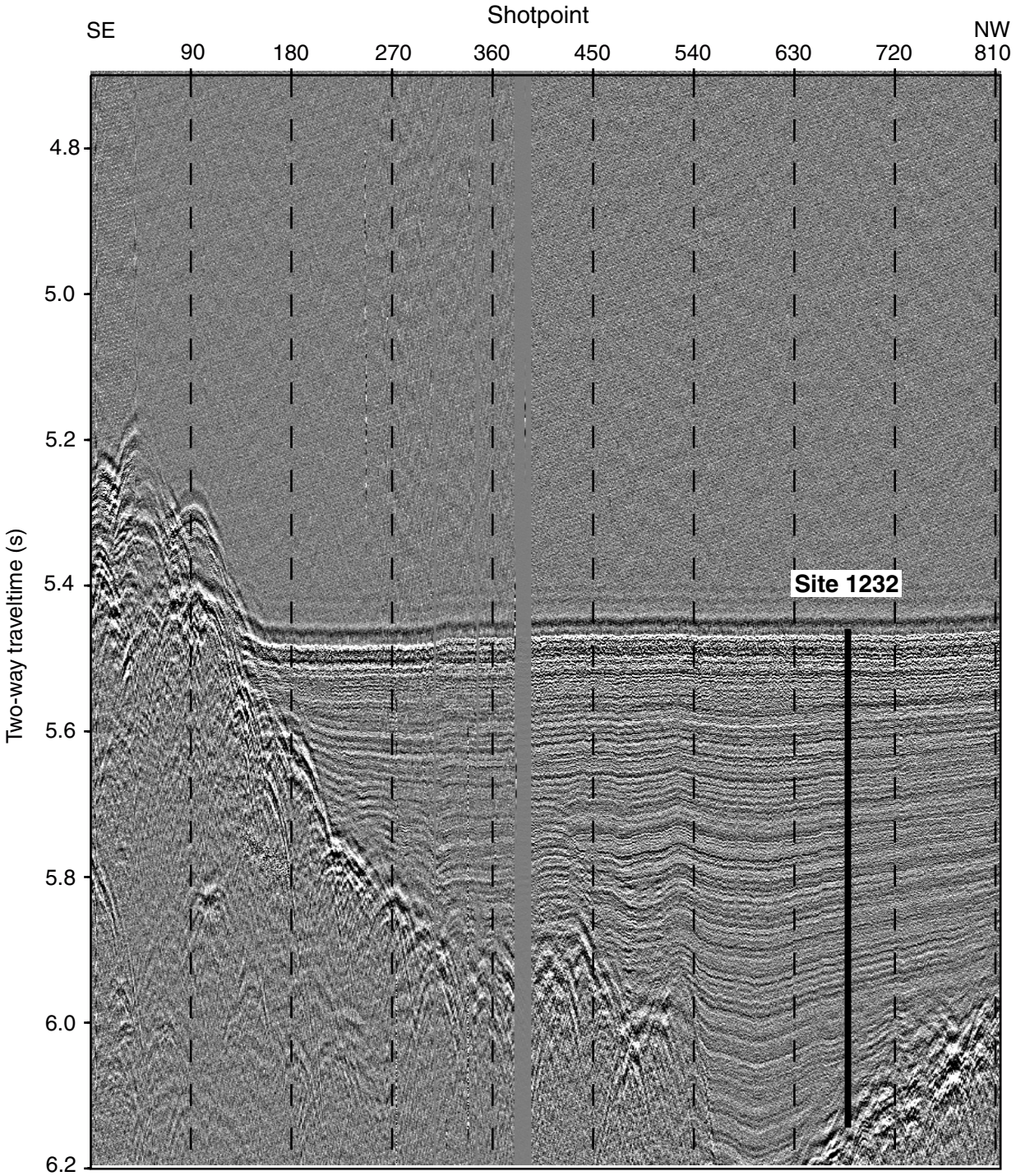

Figure F3. North-south cross section (87°W) of water masses, as indicated by phosphate concentrations in the southeast Pacific (Ocean Climate Laboratory, 1999). Site location and lysocline depth are indicated. PCW = Pacific Central Water, AAIW = Antarctic Intermediate Water, CPDW = Circumpolar Deep Water. Bathymetry is schematic.

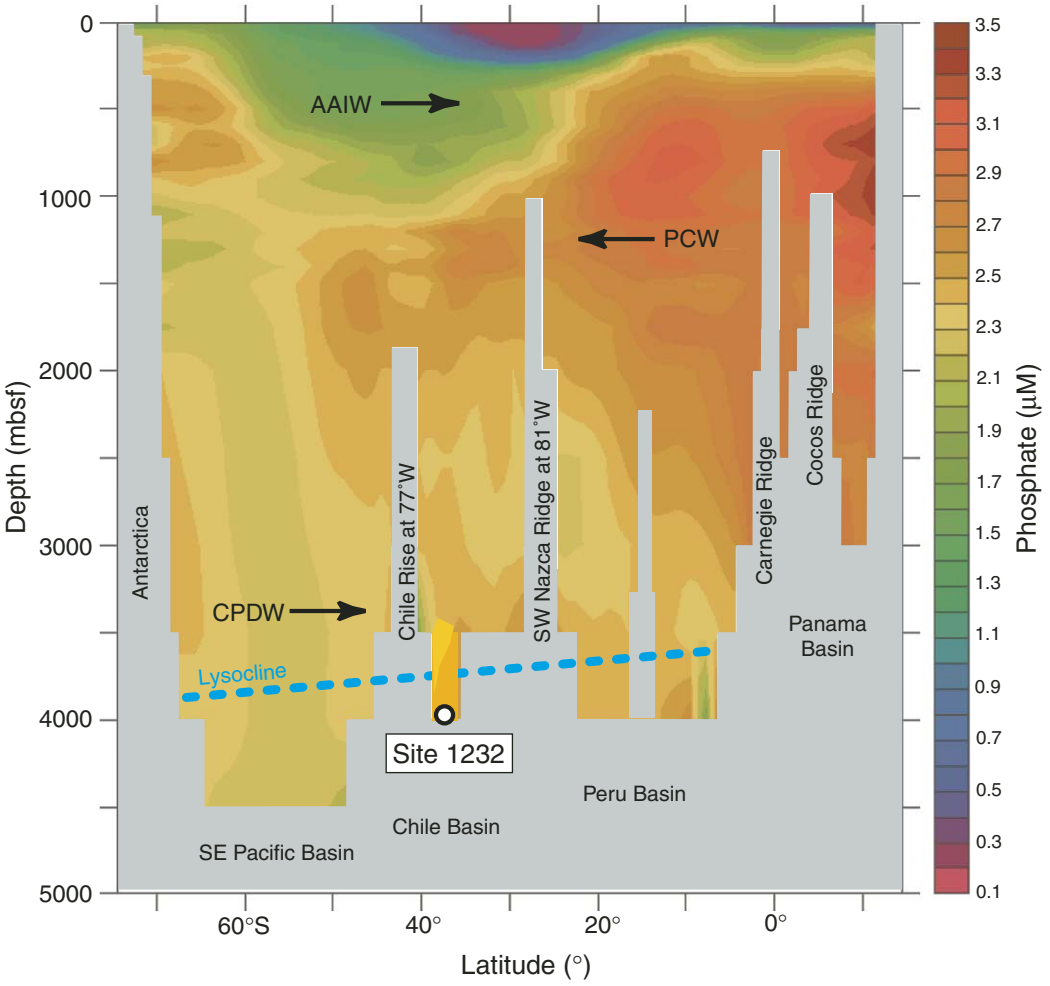

Figure F4. OSU Fast Track magnetic susceptibility data (OSUS-MS) vs. mcd for the spliced record for Holes 1232A through 1232C. Gray boxes indicate the portions of cores that are in the splice. **A.** 0–40 mcd. **B.** 30–70 mcd. (Continued on next page.)

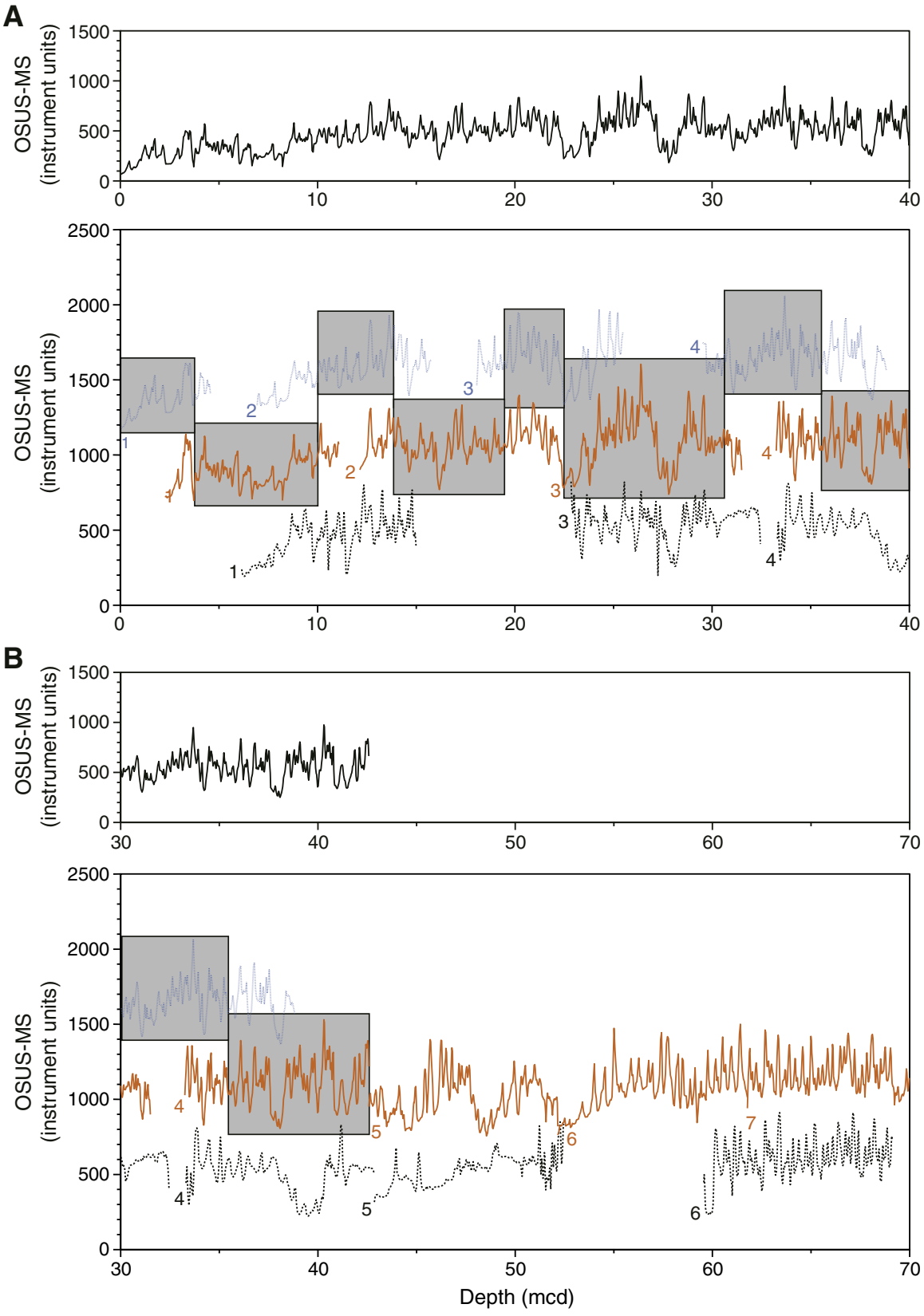

Figure F4 (continued). C. 60–100 mcd. D. 90–130 mcd. E. 120–160 mcd.

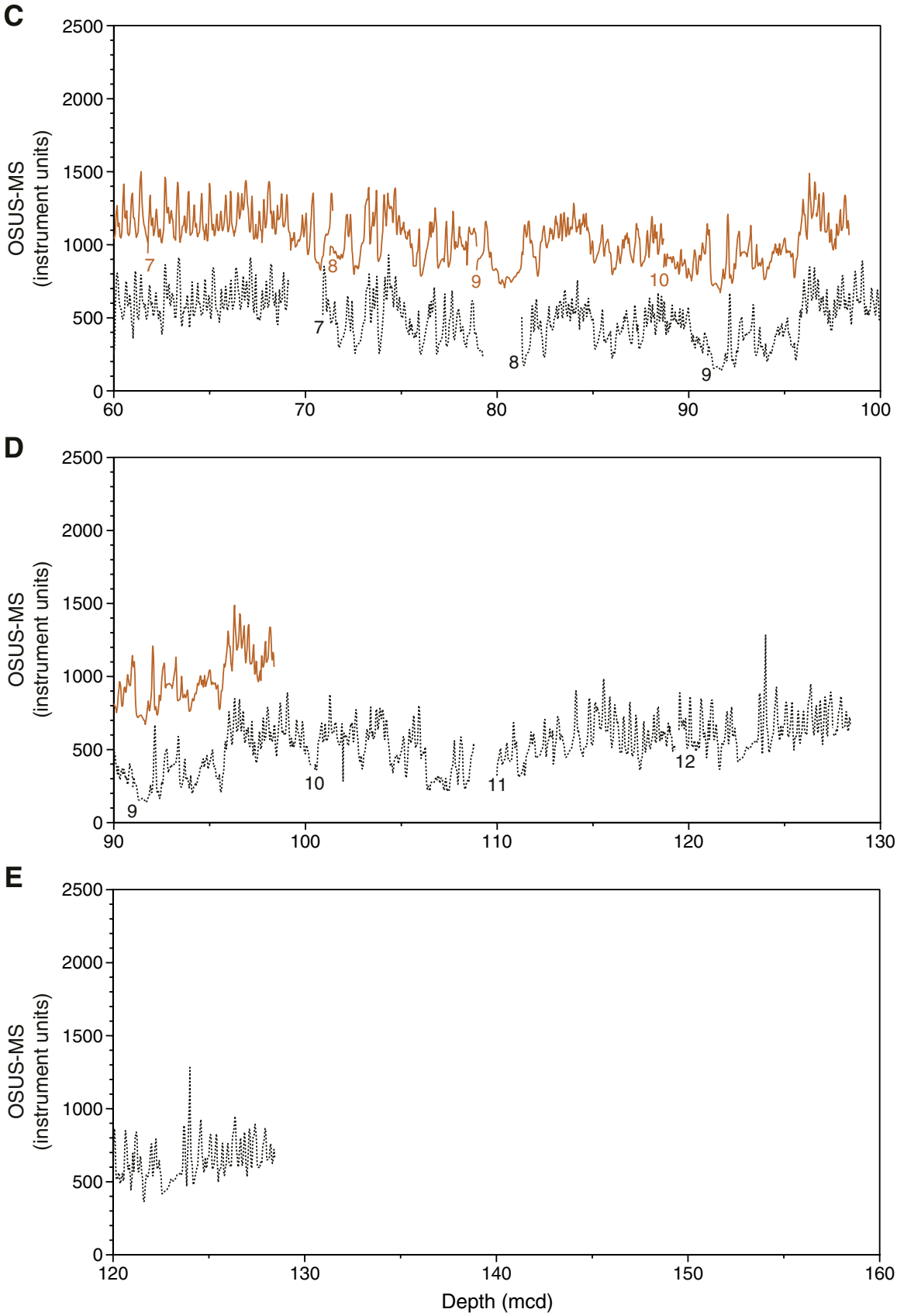

Figure F5. Spliced records of reflectance (L*), NGR, GRA bulk density, and magnetic susceptibility data (MST-MS) from Site 1232.

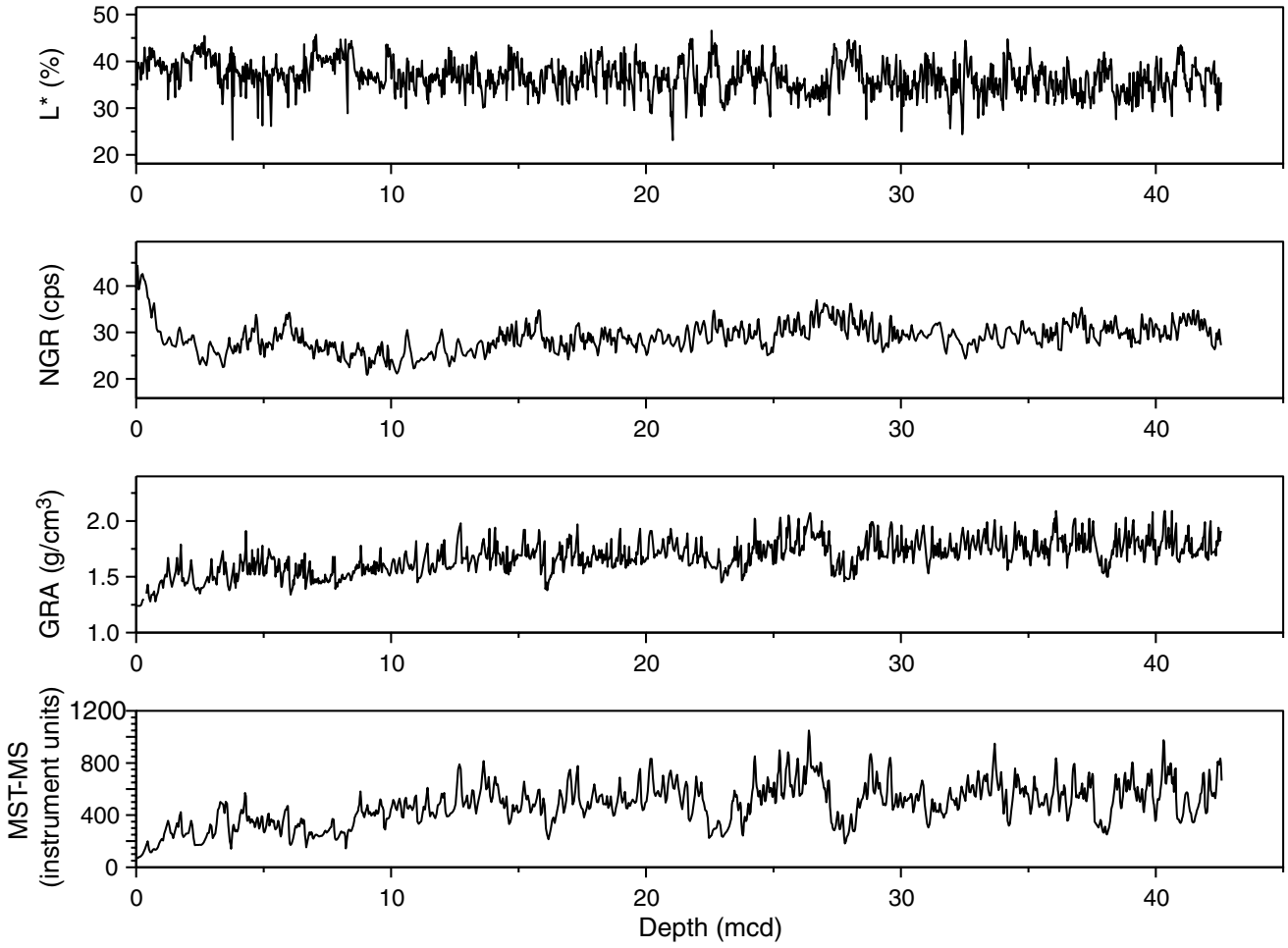

Figure F6. Mcd vs. mbsf depths for Holes 1232A, 1232B, and 1232C. The green box shows the region of the splice. On average, mcd is 22% greater than mbsf in this splice (0–42.58 mcd). The purple box shows the floating splice interval. The 1:1 (mbsf:mcd) line is also shown for comparison. GF = growth factor.

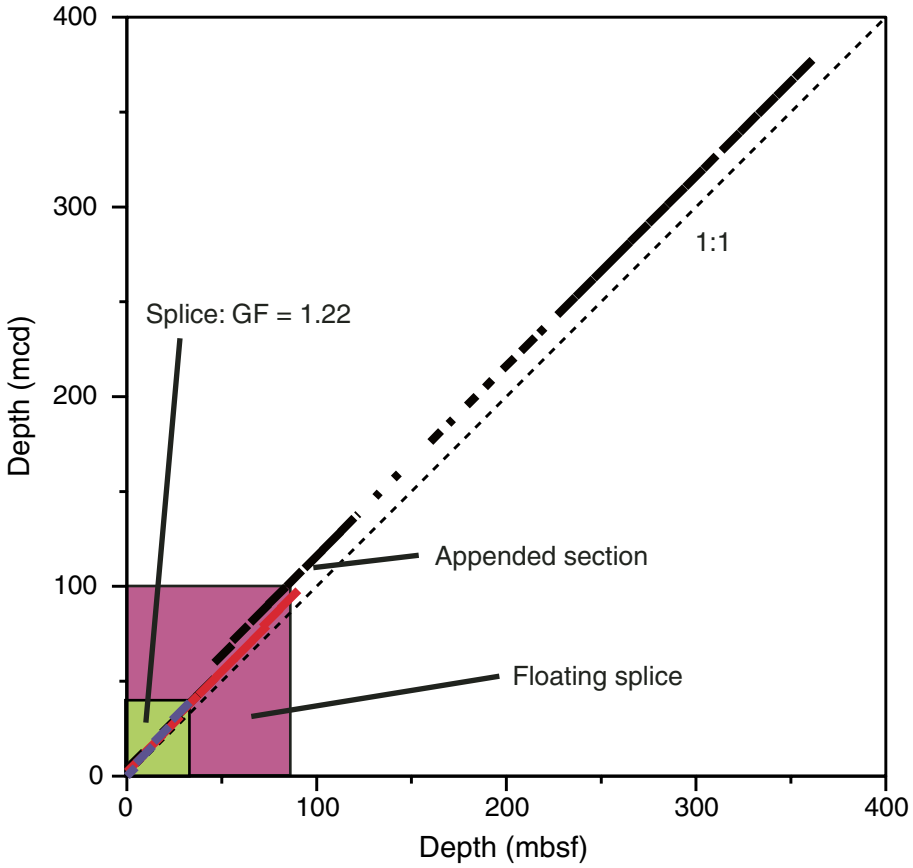

Figure F7. Close-up photograph of typical interbedded sequence (interval 202-1232B-7H-6, 94–122 cm).

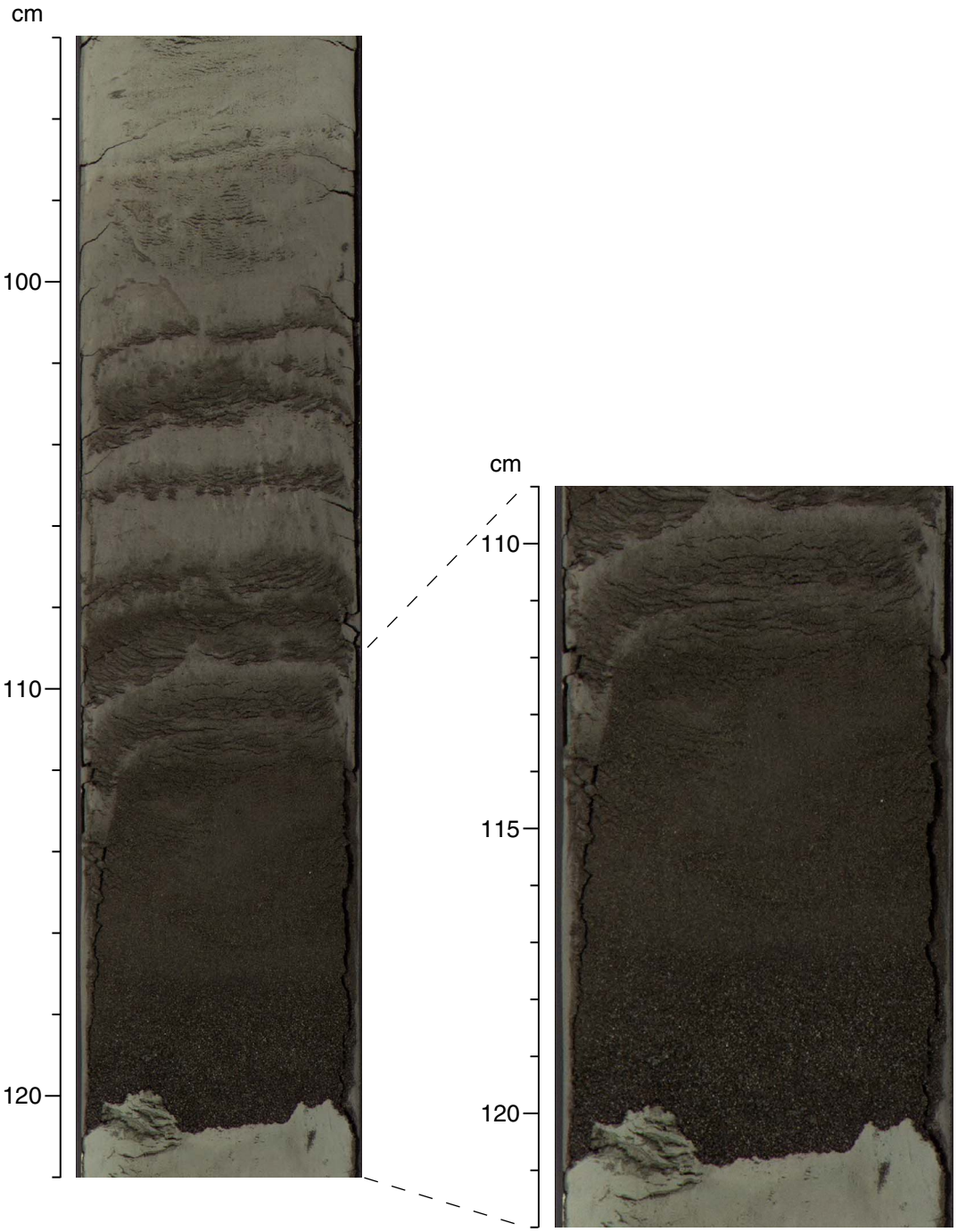

Figure F8. Depths and thicknesses of coarse-grained layers. APC = advanced piston coring, XCB = extended core barrel.

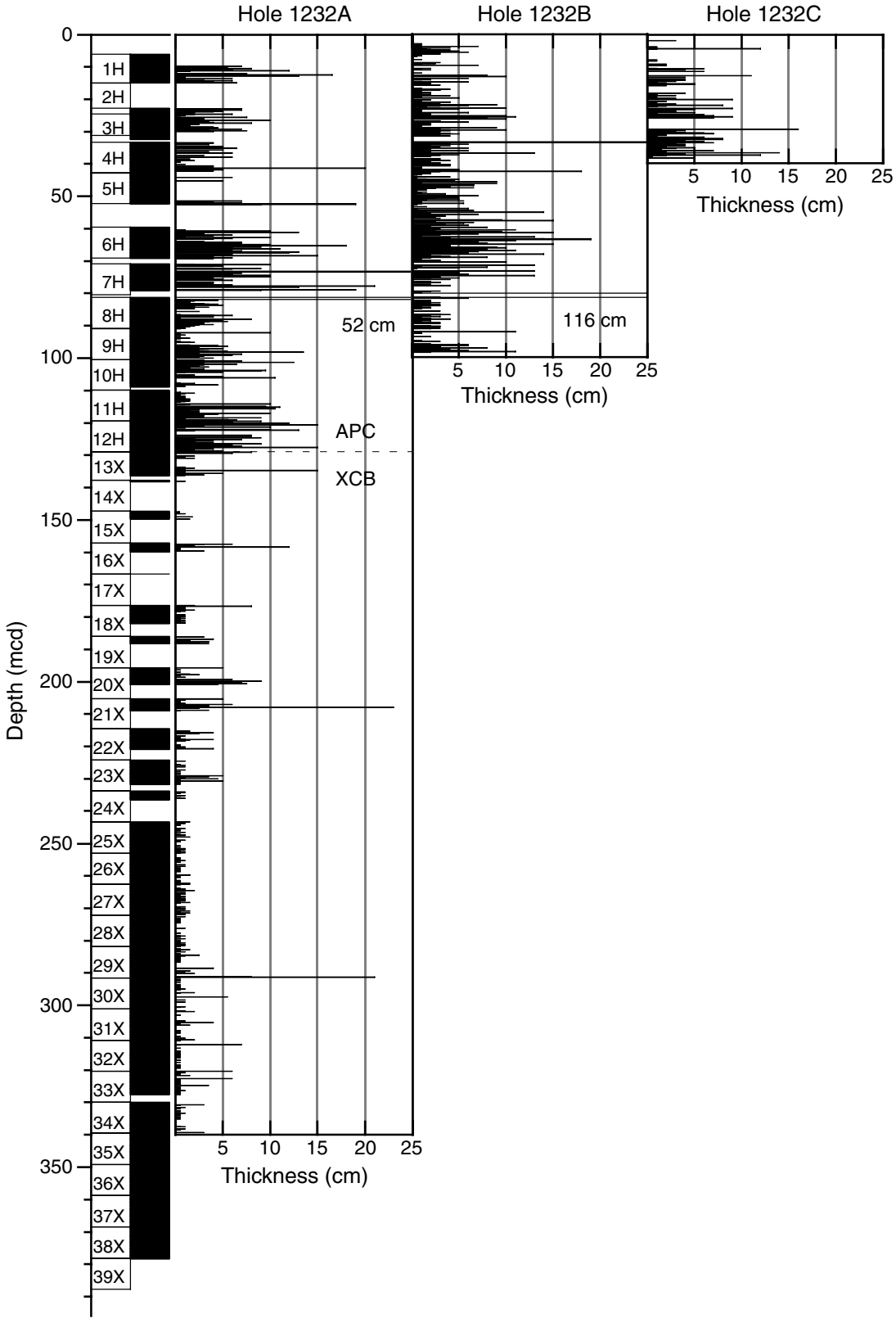

Figure F9. Mineralogy acquired from smear slide data. Shaded intervals indicate low quartz/feldspar ratio. APC = advanced piston corer, XCB = extended core barrel.

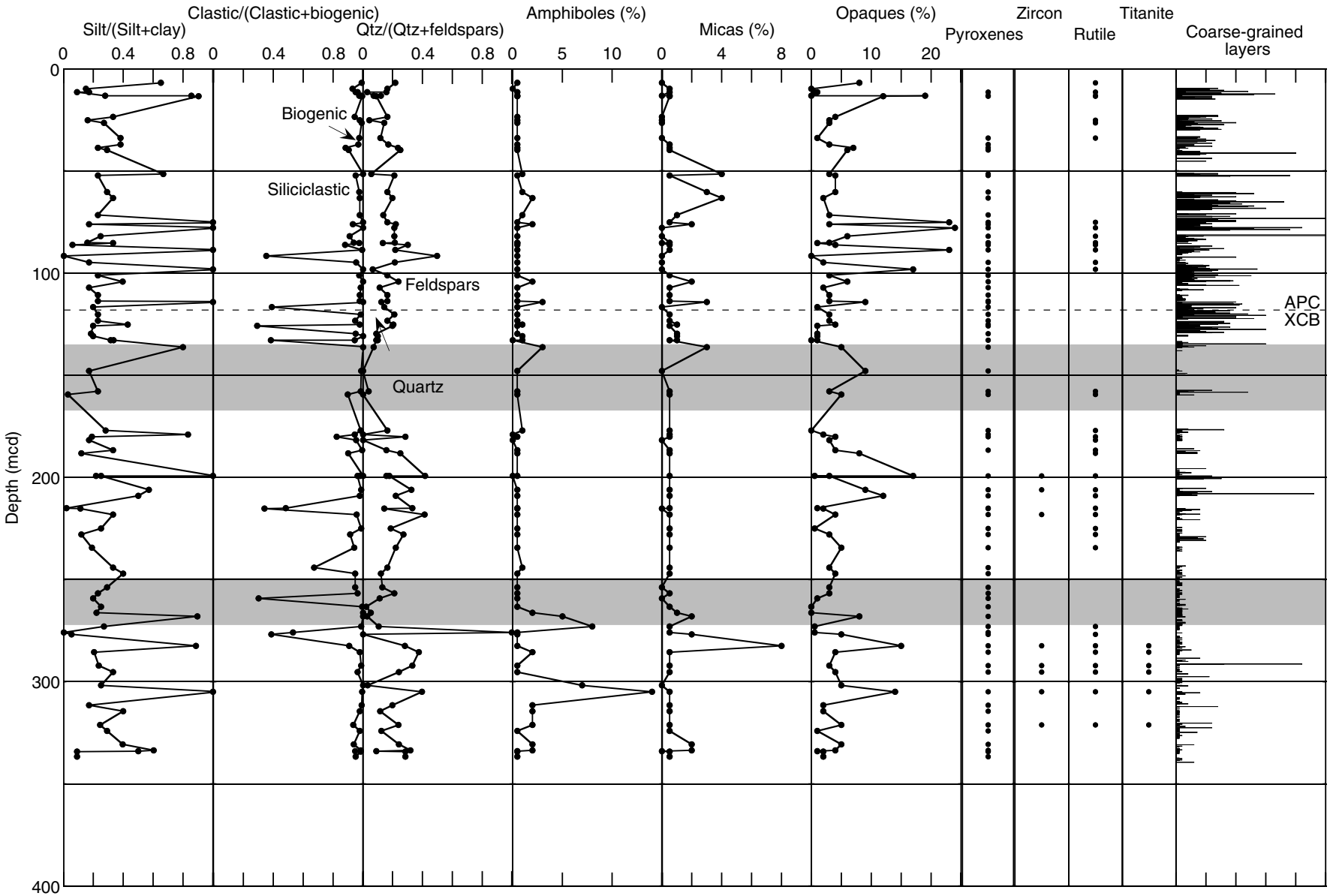

Figure F10. Lithostratigraphic summary for recovered sediments from Site 1232. Locations of sharp contacts (turbidites) are shown in the column adjacent to the generalized lithostratigraphy. GRA = gamma ray attenuation.

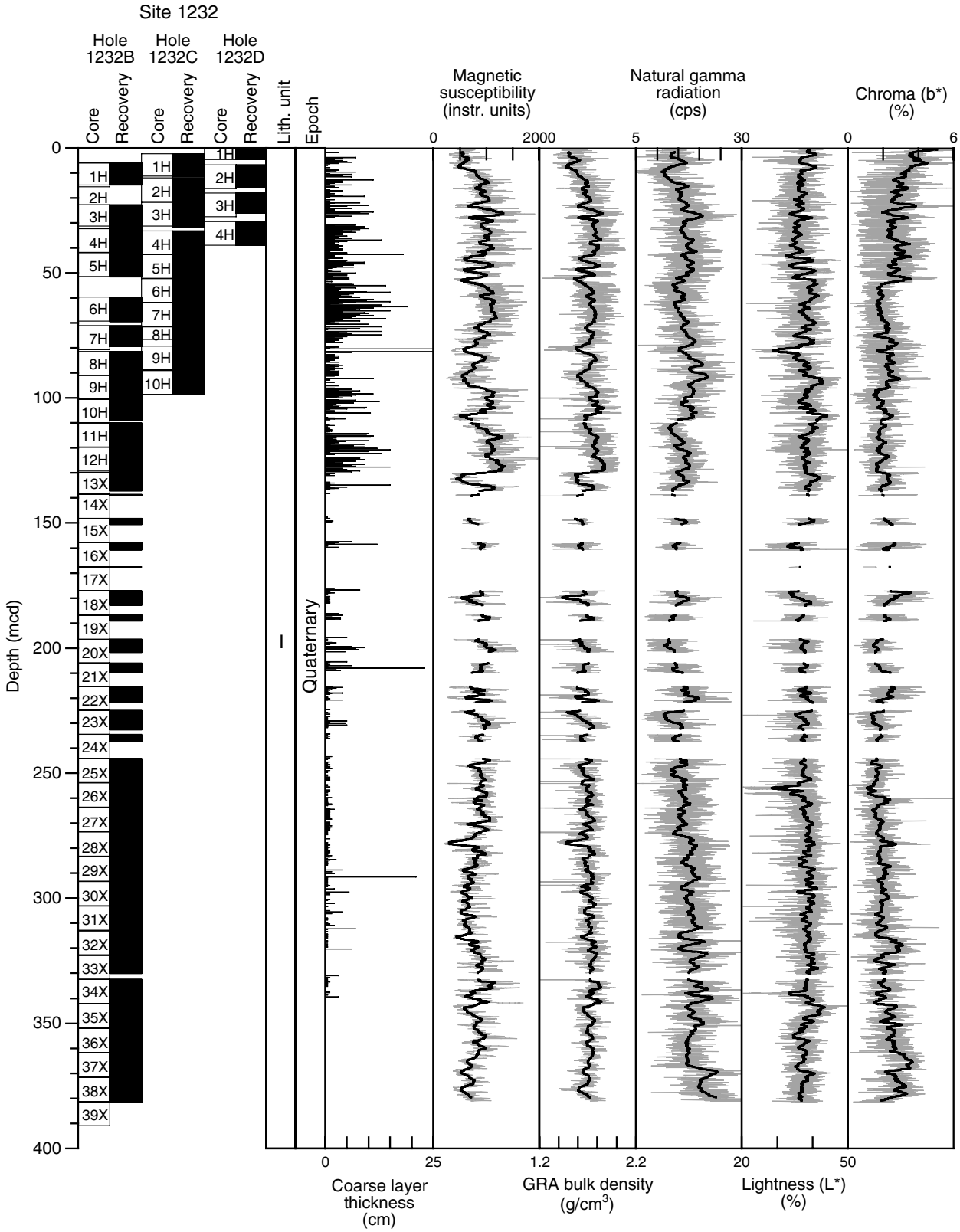

Figure F11. Moisture and density (MAD) data for Site 1232. Core recovery, lithology, bulk density, grain density, porosity, and water content are shown. GRA = gamma ray attenuation.

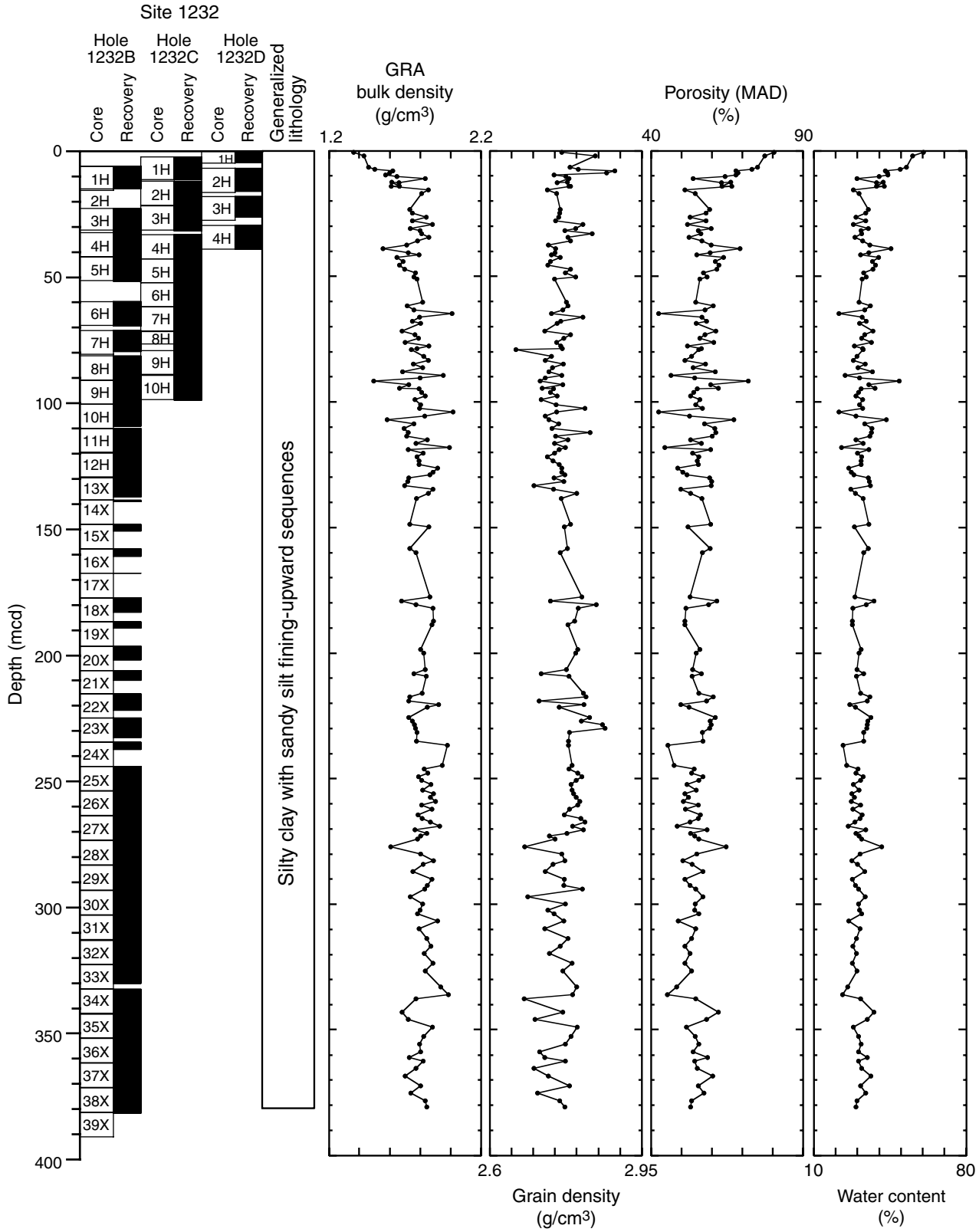

Figure F12. A, B. Comparison of gamma ray attenuation (GRA) (red lines) and moisture and density (MAD) bulk density data (blue circles). **C.** Dry density was calculated from GRA density by applying the relationship between MAD bulk density and MAD dry density measurements.

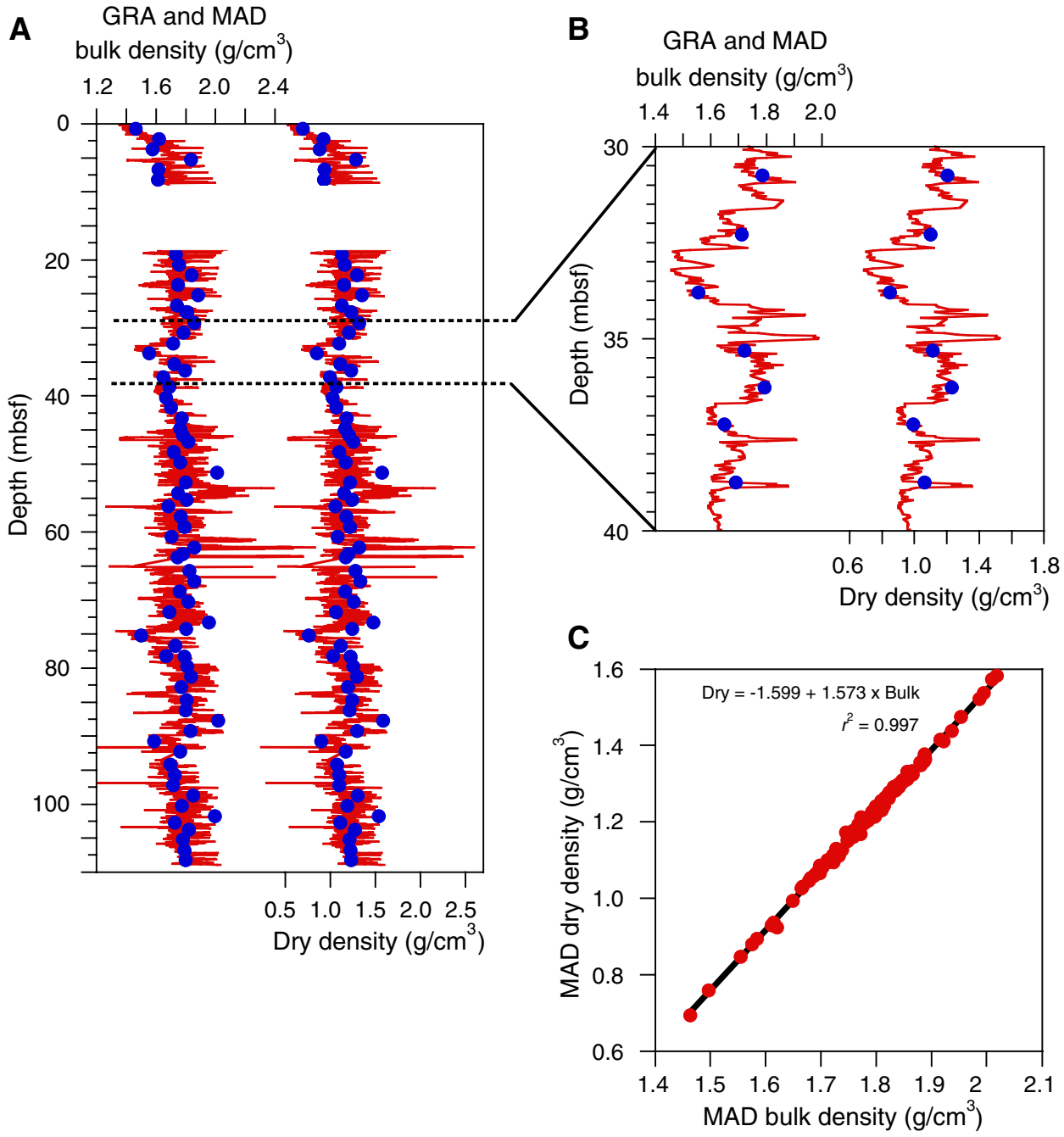

Figure F13. Color measurements plotted in the a*-b* color plane.

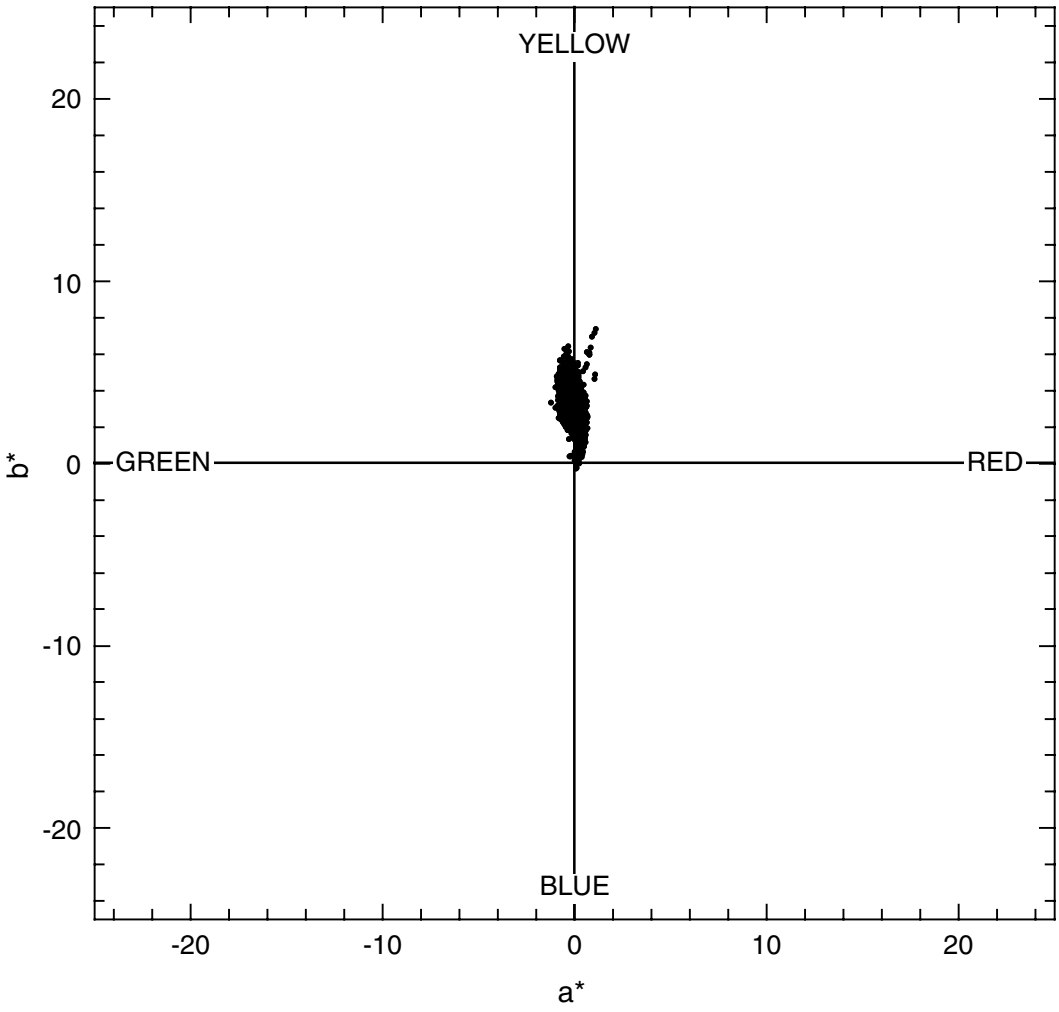

Figure F14. Coarse layers are darker (low L*, not shown) and less chromatic (b* < 2), denser (gamma ray attenuation [GRA] bulk density high), and contain more ferromagnetic minerals (increased magnetic susceptibility).

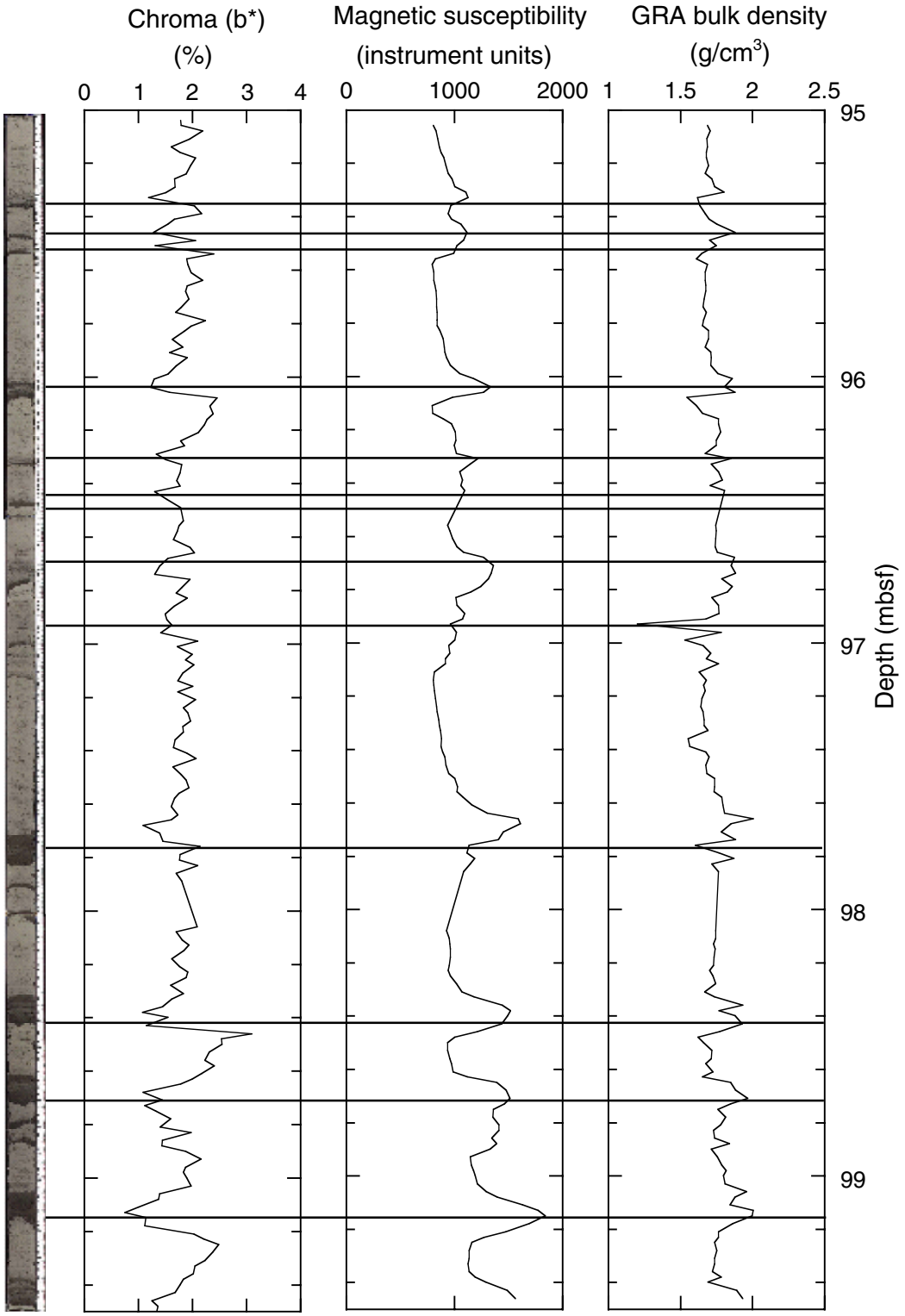

Figure F15. A. Natural remanent magnetization (NRM) within Hole 1232A before AF demagnetization. Notice the extremely high NRM intensities, especially within the APC section, and the high positive inclinations throughout. These inclinations are interpreted to be the result of a drill string magnetic overprint. **B.** NRM within Hole 1232A after 20-mT AF demagnetization. Notice the significantly reduced intensities (although still high in value) and significant shift of most inclinations to negative values. We interpret these results to indicate normal polarity (Brunhes Chron) throughout Hole 1232A.

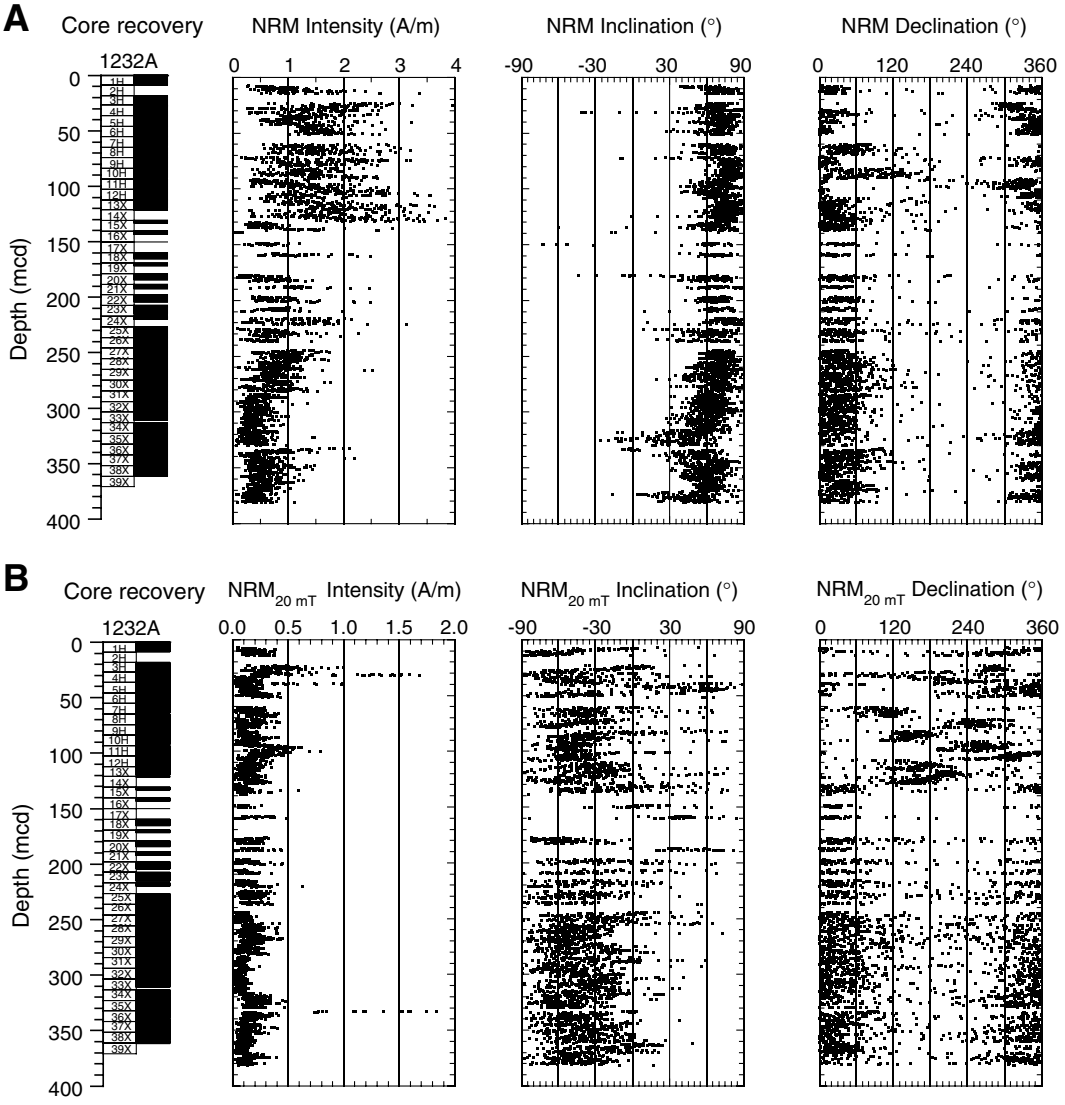

Figure F16. A. Initial natural remanent magnetization (NRM) intensities within the uppermost 130 mcd (cored with the APC) in Holes 1232A, 1232B, and 1232C are compared to magnetic susceptibility values for Hole 1232A. The similarity between the NRM intensity prior to demagnetization and magnetic susceptibility suggest that the drill string magnetization is enhanced by the coarse terrigenous-rich sediments. **B.** Demagnetized NRM intensities (20 mT AF) within the uppermost 130 m in Holes 1232A, 1232B, and 1232C are compared to magnetic susceptibility values for Hole 1232A. **C.** Demagnetized inclinations (20 mT AF) for the uppermost 130 m of Holes 1232A, 12332B, and 1232C. The noisy intervals of reversed inclinations are not easily correlated between holes and are considered to result from variably removed drill string overprints. (**Figure shown on next page.**)

Figure F16 (continued). (Caption shown on previous page.)

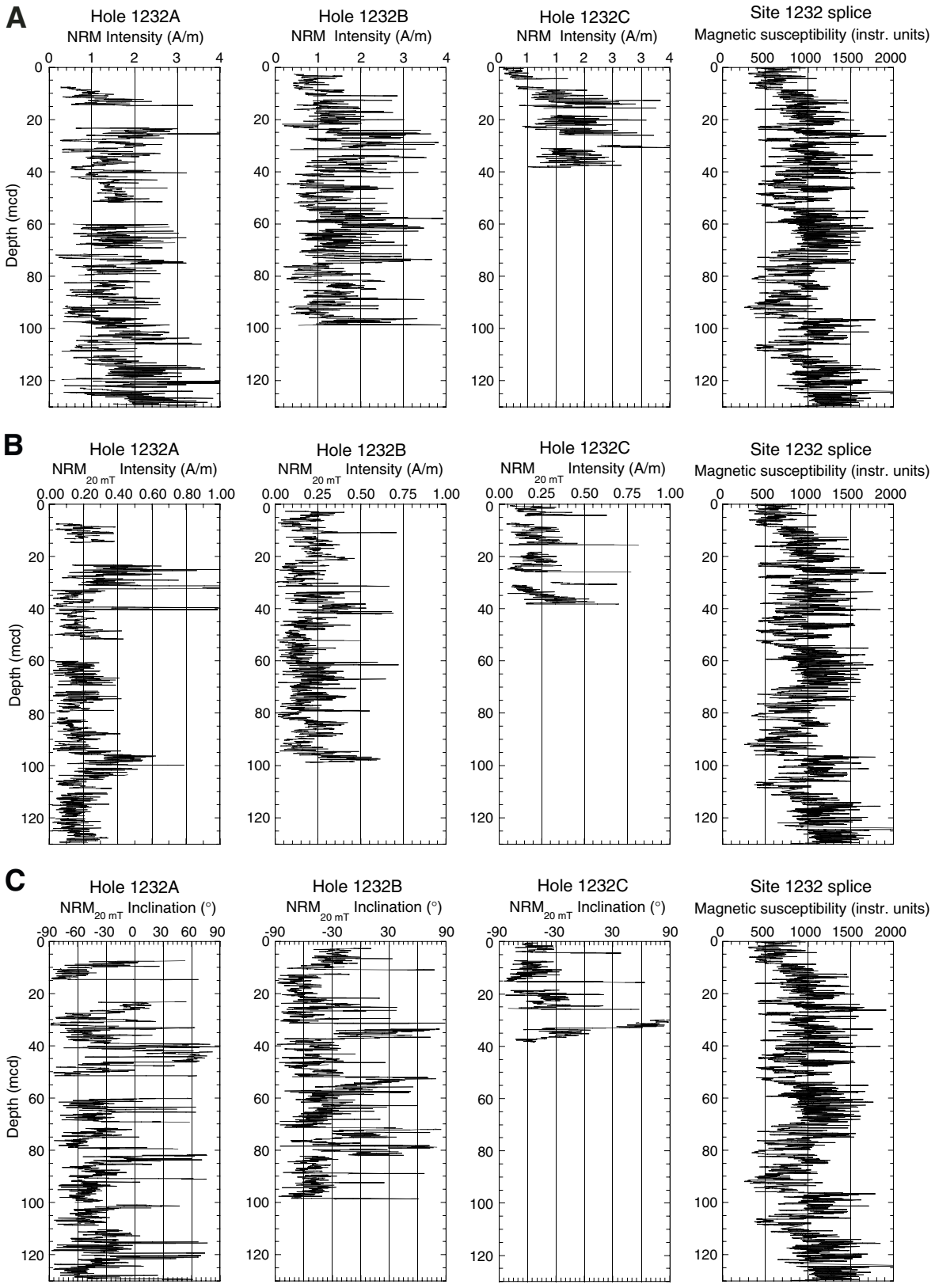

Figure F17. A. Natural remanent magnetization (NRM) intensity prior to demagnetization vs. the shipboard whole-core low-field magnetic susceptibility. **B.** NRM intensity after 20-mT AF demagnetization vs. the shipboard whole-core low-field magnetic susceptibility.

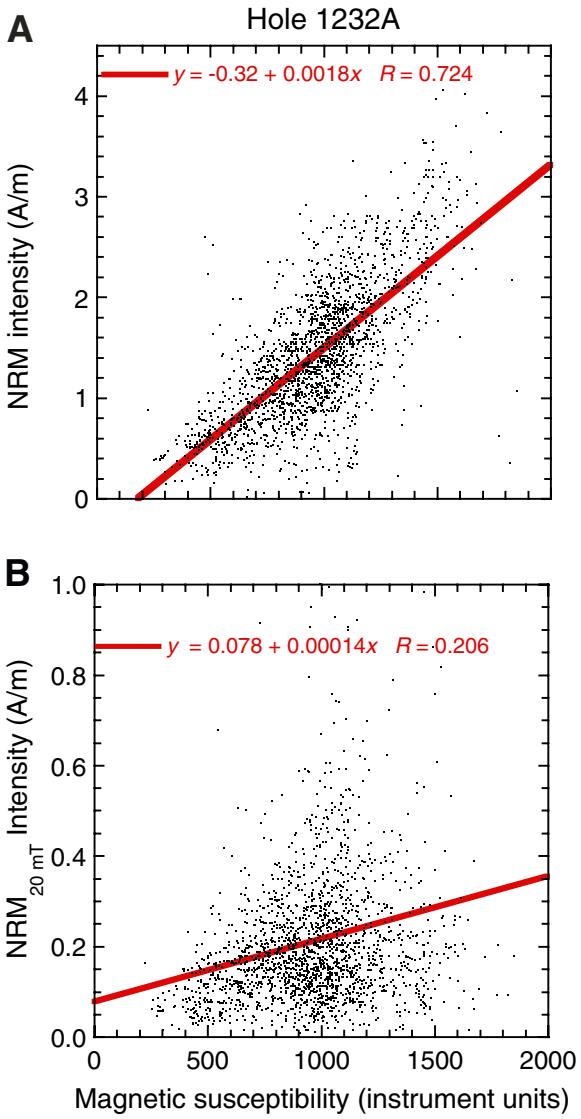

Figure F18. Headspace gas concentrations vs. depth for Hole 1232A.

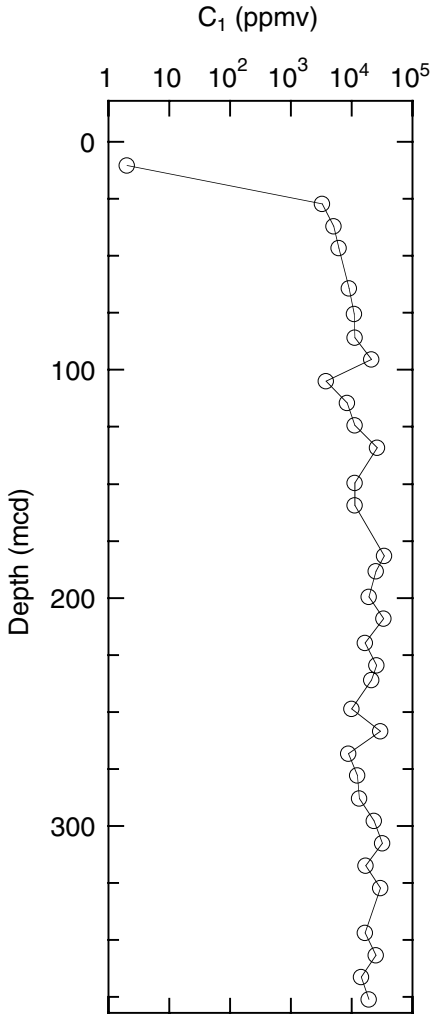

Figure F19. Interstitial water geochemical data for Site 1232. Open squares = calcium concentrations.

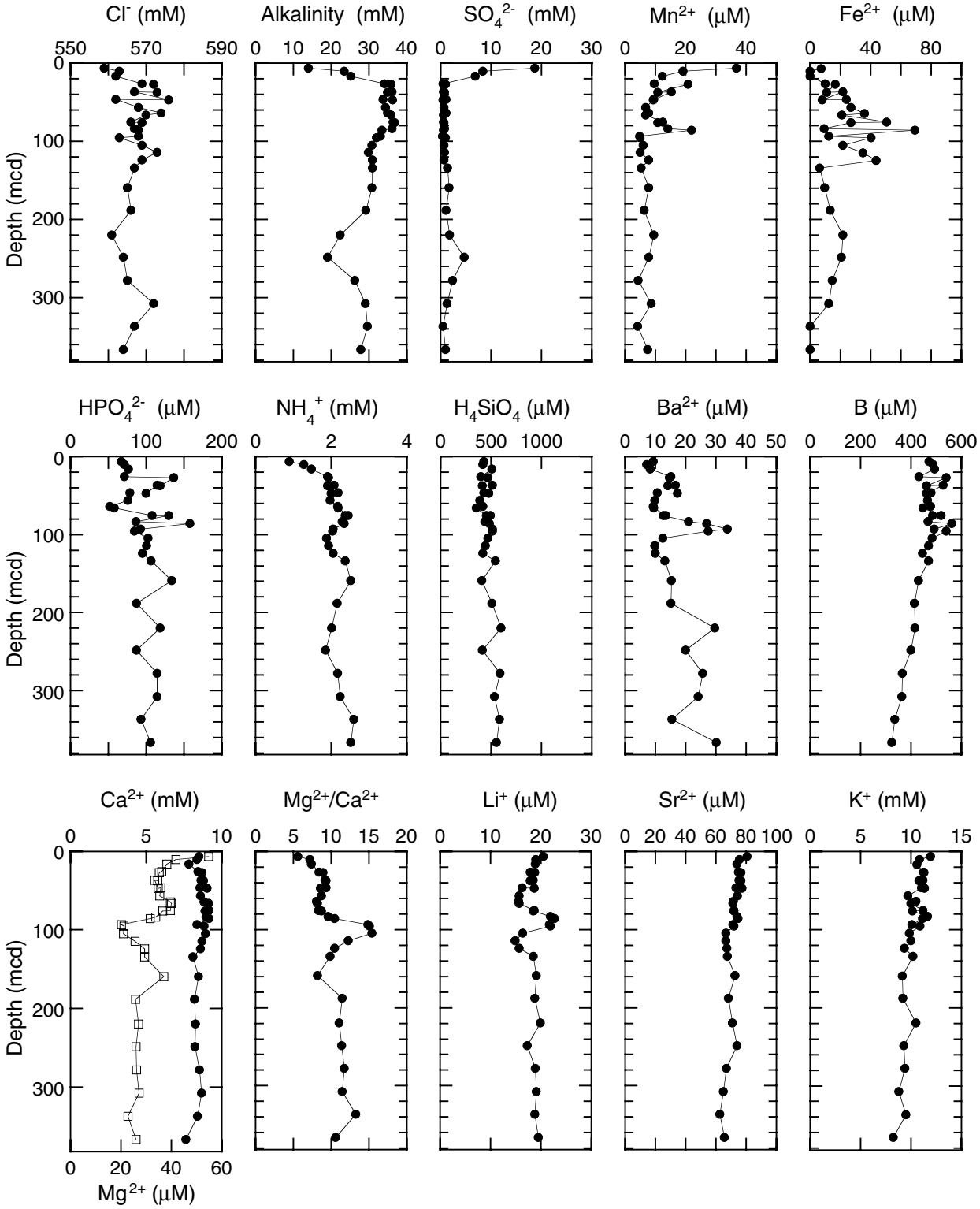

Table T1. Operations summary, Site 1232.

Core	Date (Apr 2002)	Local time (hr)	Depth (mbsf) Top	Depth (mbsf) Bottom	Length (m) Cored	Length (m) Recovered	Recovery (%)	APCT	Orientation
202-1232A-									
1H	8	0530	0.0	9.0	9.0	9.00	100.0		
2H	8	0655	9.0	18.5	9.5	0.00	0.0		
3H	8	0845	18.5	27.0	8.5	9.82	115.5	X	Tensor
4H	8	1040	27.0	36.5	9.5	9.81	103.3		Tensor
5H	8	1615	36.5	46.0	9.5	9.78	103.0		Tensor
6H	8	1733	46.0	55.5	9.5	9.88	104.0	X	Tensor
7H	8	1915	55.5	65.0	9.5	8.42	88.6	X	Tensor
8H	8	2130	65.0	74.5	9.5	9.89	104.1	X	Tensor
9H	8	2245	74.5	84.0	9.5	9.44	99.4		Tensor
10H	9	0015	84.0	93.5	9.5	8.69	91.5		Tensor
11H	9	0325	93.5	103.0	9.5	9.78	103.0		Tensor
12H	9	0525	103.0	112.5	9.5	9.95	104.7		Tensor
13X	9	0655	112.5	121.3	8.8	7.51	85.3		
14X	9	0800	121.3	130.9	9.6	0.69	7.2		
15X	9	0910	130.9	140.6	9.7	2.60	26.8		
16X	9	1020	140.6	150.3	9.7	3.04	31.3		
17X	9	1125	150.3	159.9	9.6	0.13	1.4		
18X	9	1245	159.9	169.5	9.6	5.89	61.4		
19X	9	1400	169.5	179.2	9.7	2.57	26.5		
20X	9	1512	179.2	188.8	9.6	5.40	56.3		
21X	9	1625	188.8	198.1	9.3	3.94	42.4		
22X	9	1738	198.1	207.7	9.6	6.56	68.3		
23X	9	1855	207.7	217.3	9.6	7.78	81.0		
24X	9	2010	217.3	226.9	9.6	2.92	30.4		
25X	9	2120	226.9	236.5	9.6	9.82	102.3		
26X	9	2235	236.5	246.1	9.6	9.83	102.4		
27X	9	2350	246.1	255.7	9.6	9.75	101.6		
28X	10	0120	255.7	265.3	9.6	9.91	103.2		
29X	10	0230	265.3	275.0	9.7	9.88	101.9		
30X	10	0345	275.0	284.7	9.7	9.83	101.3		
31X	10	0455	284.7	294.3	9.6	9.92	103.3		
32X	10	0610	294.3	303.9	9.6	9.80	102.1		
33X	10	0710	303.9	313.5	9.6	7.33	76.4		
34X	10	0820	313.5	323.1	9.6	9.82	102.3		
35X	10	0930	323.1	332.7	9.6	9.78	101.9		
36X	10	1035	332.7	342.3	9.6	9.72	101.3		
37X	10	1155	342.3	352.0	9.7	9.85	101.6		
38X	10	1310	352.0	361.7	9.7	9.73	100.3		
39X	10	1430	361.7	371.3	9.6	0.31	3.2		
			Cored totals:		371.3	288.77	77.8		
202-1232B-									
1H	10	1845	0.0	9.1	9.1	9.14	100.4	X	
2H	10	2015	9.1	18.6	9.5	10.13	106.6		
3H	10	2130	18.6	28.1	9.5	9.85	103.7	X	Tensor
4H	10	2300	28.1	37.6	9.5	9.49	99.9	X	Tensor
5H	11	0010	37.6	47.1	9.5	9.83	103.5		Tensor
6H	11	0145	47.1	56.6	9.5	10.12	106.5	X	Tensor
7H	11	0300	56.6	66.1	9.5	9.92	104.4		Tensor
8H	11	0435	66.1	71.1	5.0	7.91	158.2	X	Tensor
9H	11	0550	71.1	80.6	9.5	10.10	106.3		Tensor
10H	11	0725	80.6	90.1	9.5	9.81	103.3		Tensor
			Cored totals:		90.1	96.30	106.9		
202-1232C-									
1H	11	1040	0.0	4.7	4.7	4.73	100.6		
2H	11	1210	4.7	14.2	9.5	9.18	96.6		
3H	11	1310	14.2	23.7	9.5	8.25	86.8		
4H	11	1445	23.7	33.2	9.5	9.52	100.2	X	
			Cored totals:		33.2	31.68	95.4		
				Site totals:	494.6	416.75	84.3		

Notes: APCT = advanced piston corer temperature tool (stainless steel housing is cutting shoe). X = APCT was used. Tensor = brand name for core-barrel orientation tool.

Table T2. Composite depth scale, Site 1232.

Core	Depth of core top		Depth offset		Translation to cmcd	
	Drillers (mbsf)	Composite (mcd)	Cumulative (m)	Differential (m)	Growth factor*	Depth (cmcd)†
202-1232A-						
1H	0.0	5.94	5.94	6.09	1.22	4.87
3H	18.5	22.78	4.28	–1.66	1.22	18.67
4H	27.0	32.38	5.38	1.10	1.22	26.54
5H‡	36.5	41.93	5.43	0.05	ND	ND
6H‡	46.0	59.65	13.65	8.22	ND	ND
7H‡	55.5	71.11	15.61	1.96	ND	ND
8H‡	65.0	81.30	16.30	0.69	ND	ND
9H‡	74.5	90.98	16.48	0.18	ND	ND
10H	84.0	100.48	16.48	0.00	ND	ND
11H	93.5	109.98	16.48	0.00	ND	ND
12H	103.0	119.76	16.76	0.28	ND	ND
13X	112.5	129.71	17.21	0.45	ND	ND
14X	121.3	138.51	17.21	0.00	ND	ND
15X	130.9	148.11	17.21	0.00	ND	ND
16X	140.6	157.81	17.21	0.00	ND	ND
17X	150.3	167.51	17.21	0.00	ND	ND
18X	159.9	177.11	17.21	0.00	ND	ND
19X	169.5	186.71	17.21	0.00	ND	ND
20X	179.2	196.41	17.21	0.00	ND	ND
21X	188.8	206.01	17.21	0.00	ND	ND
22X	198.1	215.31	17.21	0.00	ND	ND
23X	207.7	224.91	17.21	0.00	ND	ND
24X	217.3	234.51	17.21	0.00	ND	ND
25X	226.9	244.11	17.21	0.00	ND	ND
26X	236.5	253.93	17.43	0.22	ND	ND
27X	246.1	263.76	17.66	0.23	ND	ND
28X	255.7	273.51	17.81	0.15	ND	ND
29X	265.3	283.42	18.12	0.31	ND	ND
30X	275.0	293.30	18.30	0.18	ND	ND
31X	284.7	303.13	18.43	0.13	ND	ND
32X	294.3	313.05	18.75	0.32	ND	ND
33X	303.9	322.85	18.95	0.20	ND	ND
34X	313.5	332.45	18.95	0.00	ND	ND
35X	323.1	342.27	19.17	0.22	ND	ND
36X	332.7	352.05	19.35	0.18	ND	ND
37X	342.3	361.77	19.47	0.12	ND	ND
38X	352.0	371.62	19.62	0.15	ND	ND
39X	361.7	381.35	19.65	0.03	ND	ND
202-1232B-						
1H	0.0	2.24	2.24	2.25	1.22	1.84
2H	9.1	12.00	2.90	0.66	1.22	9.84
3H	18.6	21.78	3.18	0.28	1.22	17.85
4H	28.1	33.17	5.07	1.89	1.22	27.19
5H‡	37.6	42.67	5.07	0.00	ND	ND
6H‡	47.1	52.22	5.12	0.05	ND	ND
7H‡	56.6	61.86	5.26	0.14	ND	ND
8H‡	66.1	71.51	5.41	0.15	ND	ND
9H‡	71.1	79.17	8.07	2.66	ND	ND
10H‡	80.6	89.01	8.41	0.34	ND	ND
202-1232C-						
1H	0.0	0.00	0.00	0.00	1.22	0.00
2H	4.7	6.84	2.14	2.14	1.22	5.61
3H	14.2	17.98	3.78	1.64	1.22	14.74
4H	23.7	29.42	5.72	1.94	1.22	24.11

Notes: * = calculated based on mbsf-mcd relationship for splice shown in Figure **F6,** p. 22. † = within the splice, the following equations apply: cmcd = mcd/growth factor, mcd = mbsf + cumulative depth offset, mcd = cmcd × growth factor, mbsf = cmcd × growth factor – cumulative offset. Below the splice, the growth rate is not defined. Use cumulative offset to map mcd to mbsf. ‡ = floating splice. ND = not defined. This table is also available in **ASCII.**

Table T3. Splice tie points, Site 1232.

Hole, core, section, interval (cm)	Depth (mbsf)	Depth (mcd)	Depth (cmcd)		Hole, core, section, interval (cm)	Depth (mbsf)	Depth (mcd)	Depth (cmcd)
202-					202-			
1232C-1H-4, 30	3.66	3.66	3.00	Tie to	1232B-1H-1, 141	1.41	3.66	3.00
1232B-1H-6, 20	7.70	9.95	8.16	Tie to	1232C-2H-3, 5	7.77	9.95	8.16
1232C-2H-5,90	11.60	13.78	11.30	Tie to	1232B-2H-2, 25	10.84	13.78	11.30
1232B-2H-6, 10	16.68	19.62	16.08	Tie to	1232C-3H-2, 10	15.80	19.62	16.08
1232C-3H-4, 5	18.75	22.57	18.50	Tie to	1232B-3H-1, 75	19.35	22.57	18.50
1232B-3H-6, 110	27.21	30.43	24.94	Tie to	1232C-4H-1, 95	24.65	30.43	24.94
1232C-4H-5, 5	29.75	35.53	29.12	Tie to	1232B-4H-2, 80	30.40	35.53	29.12
1232B-4H-7, 35	37.45	42.58	34.90					

Note: This table is also available in **ASCII.**

Table T4. OSUS-MS measurements, Hole 1232A.

Core, section, interval (cm)	Depth (mbsf)	Depth (mcd)	Magnetic susceptibility (instrument units)	Run number	Depth from top of core (cm)
202-1232A-					
1H-1, 5.0	0.05	5.99	239	92	6.0
1H-1, 10.0	0.10	6.04	198	92	11.0
1H-1, 15.0	0.15	6.09	194	92	16.0
1H-1, 20.0	0.20	6.14	192	92	21.0
1H-1, 25.0	0.25	6.19	199	92	26.0
1H-1, 30.0	0.30	6.24	223	92	31.0
1H-1, 35.0	0.35	6.29	223	92	36.0
1H-1, 40.0	0.40	6.34	216	92	41.0
1H-1, 45.0	0.45	6.39	220	92	46.0
1H-1, 50.0	0.50	6.44	245	92	51.0
1H-1, 55.0	0.55	6.49	254	92	56.0
1H-1, 60.0	0.60	6.54	259	92	61.0
1H-1, 65.0	0.65	6.59	257	92	66.0
1H-1, 70.0	0.70	6.64	263	92	71.0
1H-1, 75.0	0.75	6.69	266	92	76.0
1H-1, 80.0	0.80	6.74	245	92	81.0
1H-1, 85.0	0.85	6.79	254	92	86.0
1H-1, 90.0	0.90	6.84	267	92	91.0
1H-1, 95.0	0.95	6.89	288	92	96.0
1H-1, 100.0	1.00	6.94	277	92	101.0
1H-1, 105.0	1.05	6.99	248	92	106.0
1H-1, 110.0	1.10	7.04	256	92	111.0
1H-1, 115.0	1.15	7.09	261	92	116.0
1H-1, 120.0	1.20	7.14	274	92	121.0
1H-1, 125.0	1.25	7.19	252	92	126.0
1H-1, 130.0	1.30	7.24	278	92	131.0
1H-1, 135.0	1.35	7.29	297	92	136.0
1H-1, 140.0	1.40	7.34	323	92	141.0
1H-1, 145.0	1.45	7.39	343	92	146.0
1H-2, 5.0	1.56	7.50	256	93	156.0
1H-2, 10.0	1.61	7.55	255	93	161.0
1H-2, 15.0	1.66	7.60	283	93	166.0
1H-2, 20.0	1.71	7.65	367	93	171.0
1H-2, 25.0	1.76	7.70	376	93	176.0
1H-2, 30.0	1.81	7.75	385	93	181.0
1H-2, 35.0	1.86	7.80	408	93	186.0
1H-2, 40.0	1.91	7.85	365	93	191.0
1H-2, 45.0	1.96	7.90	363	93	196.0
1H-2, 50.0	2.01	7.95	365	93	201.0
1H-2, 55.0	2.06	8.00	338	93	206.0
1H-2, 60.0	2.11	8.05	323	93	211.0
1H-2, 65.0	2.16	8.10	339	93	216.0
1H-2, 70.0	2.21	8.15	340	93	221.0
1H-2, 75.0	2.26	8.20	384	93	226.0
1H-2, 80.0	2.31	8.25	393	93	231.0
1H-2, 85.0	2.36	8.30	403	93	236.0
1H-2, 90.0	2.41	8.35	404	93	241.0
1H-2, 95.0	2.46	8.40	438	93	246.0
1H-2, 100.0	2.51	8.45	467	93	251.0
1H-2, 105.0	2.56	8.50	533	93	256.0
1H-2, 110.0	2.61	8.55	608	93	261.0
1H-2, 115.0	2.66	8.60	544	93	266.0
1H-2, 120.0	2.71	8.65	530	93	271.0
1H-2, 125.0	2.76	8.70	536	93	276.0
1H-2, 130.0	2.81	8.75	508	93	281.0
1H-2, 135.0	2.86	8.80	489	93	286.0
1H-2, 140.0	2.91	8.85	535	93	291.0
1H-2, 145.0	2.96	8.90	460	93	296.0
1H-3, 5.0	3.06	9.00	440	94	305.0
1H-3, 10.0	3.11	9.05	474	94	310.0
1H-3, 15.0	3.16	9.10	517	94	315.0
1H-3, 20.0	3.21	9.15	599	94	320.0
1H-3, 25.0	3.26	9.20	640	94	325.0
1H-3, 30.0	3.31	9.25	639	94	330.0

Note: Only a portion of this table appears here. The complete table is available in **ASCII**.

Table T5. OSUS-MS measurements, Hole 1232B.

Core, section, interval (cm)	Depth (mbsf)	Depth (mcd)	Magnetic susceptibility (instrument units)	Run number	Depth from top of core (cm)
202-1232B-					
1H-1, 2.5	0.03	2.27	163	152	2.5
1H-1, 5.0	0.05	2.29	170	152	5.0
1H-1, 7.5	0.08	2.32	170	152	7.5
1H-1, 10.0	0.10	2.34	164	152	10.0
1H-1, 12.5	0.12	2.37	159	152	12.5
1H-1, 15.0	0.15	2.39	163	152	15.0
1H-1, 17.5	0.17	2.41	165	152	17.5
1H-1, 20.0	0.20	2.44	167	152	20.0
1H-1, 22.5	0.22	2.46	167	152	22.5
1H-1, 25.0	0.25	2.49	168	152	25.0
1H-1, 27.5	0.28	2.52	169	152	27.5
1H-1, 30.0	0.30	2.54	171	152	30.0
1H-1, 32.5	0.32	2.57	173	152	32.5
1H-1, 35.0	0.35	2.59	180	152	35.0
1H-1, 37.5	0.38	2.62	192	152	37.5
1H-1, 40.0	0.40	2.64	206	152	40.0
1H-1, 42.5	0.43	2.66	215	152	42.5
1H-1, 45.0	0.45	2.69	219	152	45.0
1H-1, 47.5	0.47	2.71	226	152	47.5
1H-1, 50.0	0.50	2.74	240	152	50.0
1H-1, 52.5	0.52	2.77	248	152	52.5
1H-1, 55.0	0.55	2.79	255	152	55.0
1H-1, 57.5	0.57	2.82	265	152	57.5
1H-1, 60.0	0.60	2.84	271	152	60.0
1H-1, 62.5	0.62	2.87	287	152	62.5
1H-1, 65.0	0.65	2.89	325	152	65.0
1H-1, 67.5	0.68	2.91	350	152	67.5
1H-1, 70.0	0.70	2.94	285	152	70.0
1H-1, 72.5	0.73	2.96	224	152	72.5
1H-1, 75.0	0.75	2.99	221	152	75.0
1H-1, 77.5	0.77	3.02	234	152	77.5
1H-1, 80.0	0.80	3.04	249	152	80.0
1H-1, 82.5	0.82	3.07	260	152	82.5
1H-1, 85.0	0.85	3.09	266	152	85.0
1H-1, 87.5	0.88	3.12	281	152	87.5
1H-1, 90.0	0.90	3.14	340	152	90.0
1H-1, 92.5	0.93	3.16	424	152	92.5
1H-1, 95.0	0.95	3.19	459	152	95.0
1H-1, 97.5	0.98	3.21	442	152	97.5
1H-1, 100.0	1.00	3.24	454	152	100.0
1H-1, 102.5	1.02	3.27	508	152	102.5
1H-1, 105.0	1.05	3.29	568	152	105.0
1H-1, 107.5	1.08	3.32	584	152	107.5
1H-1, 110.0	1.10	3.34	532	152	110.0
1H-1, 112.5	1.12	3.37	518	152	112.5
1H-1, 115.0	1.15	3.39	546	152	115.0
1H-1, 117.5	1.17	3.41	536	152	117.5
1H-1, 120.0	1.20	3.44	476	152	120.0
1H-1, 122.5	1.23	3.46	481	152	122.5
1H-1, 125.0	1.25	3.49	522	152	125.0
1H-1, 127.5	1.27	3.52	537	152	127.5
1H-1, 130.0	1.30	3.54	508	152	130.0
1H-1, 132.5	1.33	3.57	469	152	132.5
1H-1, 135.0	1.35	3.59	381	152	135.0
1H-1, 137.5	1.38	3.62	285	152	137.5
1H-1, 140.0	1.40	3.64	222	152	140.0
1H-1, 142.5	1.42	3.66	197	152	142.5
1H-1, 145.0	1.45	3.69	177	152	145.0
1H-1, 147.5	1.48	3.71	142	152	147.5
1H-2, 2.5	1.52	3.77	264	153	152.5
1H-2, 5.0	1.55	3.79	315	153	155.0
1H-2, 7.5	1.58	3.82	325	153	157.5
1H-2, 10.0	1.60	3.84	300	153	160.0
1H-2, 12.5	1.62	3.87	275	153	162.5

Note: Only a portion of this table appears here. The complete table is available in **ASCII**.

Table T6. Lithologic Unit I, Site 1232.

Unit	Top			Base			Description	Interpretation
		Depth			Depth			
	Hole, core	(mbsf)	(mcd)	Hole, core	(mbsf)	(mcd)		
I	202-			202-				
	1232A-1H	0.0	5.9	1232A-39X	362.0	381.7	Light gray to gray silty clay interbedded with dark gray coarser layers	Turbidite sequences
	1232B-1H	0.0	2.2	1232B-10H	90.5	98.9		
	1232C-1H	0.0	0.0	1232C-4H	33.3	39.0		

Table T7. Coarse-grained layers, Site 1232. (See table note. Continued on next three pages.)

Core, section	Bottom depth (cm)	(mbsf)	(mcd)	Thickness of sandy silt layer (cm)
202-1232A-				
1H-3	62.0	3.63	9.57	7.0
1H-3	78.5	3.80	9.73	1.0
1H-3	93.5	3.94	9.89	1.5
1H-3	115.0	4.16	10.10	5.5
1H-3	140.0	4.41	10.35	8.0
1H-4	22.0	4.74	10.68	6.0
1H-4	27.0	4.79	10.73	1.0
1H-4	54.0	5.06	11.00	12.0
1H-4	80.0	5.32	11.26	1.5
1H-4	126.0	5.78	11.72	0.2
1H-4	140.0	5.92	11.86	7.5
1H-5	31.0	6.33	12.27	16.5
1H-5	65.0	6.67	12.61	13.0
1H-5	95.0	6.97	12.91	1.0
1H-5	123.0	7.25	13.19	0.9
1H-5	135.0	7.37	13.31	0.5
1H-5	141.0	7.43	13.37	6.0
1H-6	4.0	7.56	13.50	1.0
1H-6	29.0	7.81	13.75	3.0
1H-6	58.0	8.10	14.04	6.0
1H-6	72.0	8.24	14.18	4.0
1H-6	86.0	8.38	14.32	0.5
1H-6	101.5	8.53	14.48	3.0
1H-6	123.0	8.75	14.69	6.5
3H-1	7.0	18.57	22.85	7.0
3H-1	24.0	18.74	23.02	3.0
3H-1	50.0	19.00	23.28	7.0
3H-1	58.0	19.08	23.36	0.5
3H-1	62.0	19.12	23.40	0.5
3H-1	65.0	19.15	23.43	0.5
3H-1	88.0	19.38	23.66	5.0
3H-1	102.5	19.52	23.81	4.0
3H-1	111.5	19.61	23.90	1.0
3H-1	116.5	19.67	23.94	1.5
3H-1	125.0	19.75	24.03	2.0
3H-1	135.0	19.85	24.13	2.0
3H-1	143.0	19.93	24.21	1.5
3H-2	28.0	20.27	24.55	6.0
3H-2	38.0	20.37	24.65	2.0
3H-2	46.5	20.45	24.74	0.5
3H-2	60.5	20.59	24.88	1.0
3H-2	67.5	20.67	24.94	0.5
3H-2	74.0	20.73	25.01	0.5
3H-2	80.0	20.79	25.07	0.5
3H-2	129.5	21.28	25.57	7.5
3H-2	146.0	21.45	25.73	0.5
3H-3	2.5	21.52	25.81	1.5
3H-3	17.0	21.67	25.95	3.0
3H-3	26.0	21.76	26.04	1.5
3H-3	65.0	22.15	26.43	10.0
3H-3	73.0	22.23	26.51	1.5
3H-3	80.0	22.30	26.58	2.0
3H-3	87.0	22.37	26.65	1.5
3H-3	100.5	22.50	26.78	3.5
3H-3	115.0	22.65	26.93	2.0
3H-3	137.0	22.87	27.15	4.0
3H-4	8.0	23.09	27.37	8.0
3H-4	35.0	23.36	27.64	2.5
3H-4	43.5	23.44	27.73	0.5
3H-4	52.5	23.53	27.82	1.0
3H-4	76.0	23.77	28.05	1.5
3H-4	108.5	24.09	28.38	0.5
3H-4	128.0	24.29	28.57	4.0
3H-4	145.0	24.46	28.74	4.5
3H-5	38.0	24.89	29.17	7.0
3H-5	59.0	25.10	29.38	3.5
3H-5	86.5	25.38	29.66	7.5
3H-5	110.0	25.61	29.89	4.0
4H-1	11.0	27.11	32.49	4.0
4H-1	33.0	27.33	32.71	4.0
4H-1	51.0	27.51	32.89	3.5
4H-1	58.5	27.58	32.97	2.5
4H-1	68.5	27.68	33.06	3.5
4H-1	126.0	28.26	33.64	5.0
4H-2	34.0	28.85	34.23	6.5
4H-2	81.5	29.33	34.71	5.0
4H-2	136.5	29.88	35.26	3.5
4H-3	26.0	30.28	35.66	6.0
4H-3	95.0	30.97	36.35	3.0
4H-3	147.0	31.49	36.87	2.0
4H-4	6.0	31.61	36.99	6.0
4H-4	62.0	32.17	37.55	1.5
4H-4	88.5	32.44	37.81	0.5
4H-4	112.5	32.67	38.06	2.0
4H-5	9.5	33.15	38.53	0.5
4H-5	70.0	33.76	39.14	1.0
4H-5	123.5	34.29	39.67	4.0
4H-5	146.0	34.52	39.90	4.0
4H-6	50.0	35.07	40.45	20.0
4H-6	62.0	35.19	40.57	2.0
4H-6	87.0	35.44	40.82	5.0
4H-6	91.0	35.48	40.86	1.0
4H-6	136.0	35.93	41.31	4.0
5H-1	120.0	37.70	43.13	6.0
5H-2	87.0	38.88	44.31	5.0
5H-6	96.0	45.05	50.48	7.0
5H-6	106.0	45.15	50.58	3.0
5H-6	120.0	45.29	50.72	4.0
5H-6	129.0	45.38	50.81	1.0
5H-6	144.0	45.53	50.96	2.0
5H-7	8.0	45.68	51.11	7.0
5H-7	50.0	46.10	51.53	19.0
5H-7	68.0	46.28	51.71	9.0
6H-1	70.0	46.70	60.35	1.0
6H-1	116.0	47.16	60.81	10.0
6H-1	133.0	47.33	60.98	3.0
6H-2	13.0	47.63	61.29	13.0
6H-2	40.0	47.90	61.56	3.0
6H-2	50.0	48.00	61.66	1.0
6H-2	88.0	48.38	62.04	6.0
6H-2	100.0	48.50	62.16	3.0
6H-2	120.0	48.70	62.36	4.0
6H-2	141.0	48.91	62.57	1.0
6H-3	20.0	49.20	62.88	10.0
6H-3	37.0	49.37	63.05	6.0
6H-3	53.0	49.53	63.21	4.0
6H-3	62.0	49.62	63.30	3.0
6H-3	133.0	50.33	64.01	3.0
6H-4	8.0	50.58	64.27	7.0
6H-4	38.0	50.88	64.57	7.0
6H-4	50.0	51.00	64.69	2.0
6H-4	78.0	51.28	64.97	10.0
6H-4	99.0	51.49	65.18	4.0
6H-4	127.0	51.77	65.46	18.0
6H-5	11.0	52.11	65.81	9.0
6H-5	34.0	52.34	66.04	6.0
6H-5	63.0	52.63	66.33	11.0
6H-5	94.0	52.94	66.64	6.0
6H-5	127.0	53.27	66.97	7.0
6H-5	144.0	53.44	67.14	4.0
6H-6	15.0	53.65	67.36	13.0
6H-6	40.0	53.90	67.61	12.0
6H-6	74.0	54.24	67.95	6.0
6H-6	96.0	54.46	68.17	5.0
6H-6	125.0	54.75	68.46	15.0
6H-6	144.0	54.94	68.65	4.0
6H-7	13.0	55.13	68.85	3.0
6H-7	36.0	55.36	69.08	6.0
6H-7	61.0	55.61	69.33	4.0
7H-1	19.0	55.69	71.30	10.0
7H-1	32.0	55.82	71.43	2.0
7H-1	38.0	55.88	71.49	2.0
7H-1	67.0	56.17	71.78	5.0
7H-1	78.0	56.28	71.89	4.0
7H-1	139.0	56.89	72.50	9.0
7H-2	6.0	57.06	72.68	6.0
7H-2	101.0	58.01	73.63	25.0
7H-2	121.0	58.21	73.83	5.0
7H-2	141.0	58.41	74.03	7.0
7H-3	29.0	58.79	74.41	6.0
7H-3	34.0	58.84	74.46	1.0
7H-3	50.0	59.00	74.62	10.0
7H-3	64.0	59.14	74.76	5.0
7H-3	70.0	59.20	74.82	2.0
7H-3	90.0	59.40	75.02	10.0
7H-3	109.0	59.59	75.21	3.0
7H-3	114.0	59.64	75.26	1.0
7H-3	121.0	59.71	75.33	2.0
7H-3	132.0	59.82	75.44	4.0
7H-3	138.0	59.88	75.50	3.0
7H-4	7.0	60.07	75.71	5.0
7H-4	35.0	60.35	75.99	2.0
7H-4	57.0	60.57	76.21	6.0
7H-4	111.0	61.11	76.75	4.0
7H-4	122.0	61.22	76.86	4.0
7H-4	138.0	61.38	77.02	4.0
7H-4	145.0	61.45	77.09	3.0
7H-5	43.0	61.93	77.58	6.0
7H-5	82.0	62.32	77.97	21.0
7H-5	122.0	62.72	78.37	13.0
7H-6	43.0	63.43	79.09	19.0
7H-6	58.0	63.58	79.24	9.0
8H-1	52.0	65.52	81.82	52.0
8H-1	61.0	65.61	81.91	1.5
8H-1	82.0	65.82	82.12	4.5
8H-1	102.0	66.02	82.32	2.0
8H-1	145.0	66.45	82.75	1.5
8H-2	27.5	66.78	83.08	1.5
8H-2	35.5	66.86	83.17	3.0
8H-2	52.0	67.02	83.33	4.5
8H-2	60.0	67.10	83.41	3.5
8H-2	83.5	67.33	83.64	5.0
9H-2	33.0	76.33	92.81	1.0
9H-2	94.0	76.94	93.42	0.5
9H-2	95.5	76.96	93.43	0.5
9H-2	88.0	76.88	93.36	0.5
9H-2	126.5	77.26	93.75	1.5
9H-3	74.0	78.24	94.73	0.5
9H-3	7.5	77.57	94.07	0.5
9H-3	93.5	78.43	94.93	1.5
9H-3	122.5	78.72	95.21	2.0
9H-4	36.5	79.36	95.86	1.5
9H-4	58.5	79.58	96.08	4.5
9H-4	66.0	79.66	96.16	1.5
9H-4	88.0	79.88	96.38	5.5
9H-4	94.0	79.94	96.44	1.5
9H-4	115.5	80.15	96.65	2.5
9H-4	134.0	80.34	96.84	2.5
9H-5	5.0	80.55	97.06	5.0
9H-5	26.0	80.76	97.27	3.5
9H-5	40.0	80.90	97.41	2.5
9H-5	66.5	81.17	97.68	3.0
9H-5	87.0	81.37	97.88	5.5

Table T7 (continued).

Core, section	Bottom depth (cm)	(mbsf)	(mcd)	Thickness of sandy silt layer (cm)
9H-5	114.5	81.64	98.15	13.5
9H-5	125.5	81.75	98.26	2.0
9H-5	145.5	81.96	98.46	2.5
9H-6	26.0	82.26	98.78	7.0
9H-6	31.5	82.32	98.83	2.0
9H-6	38.0	82.38	98.90	1.0
9H-6	67.0	82.67	99.19	6.0
9H-6	84.0	82.84	99.36	3.0
9H-6	92.0	82.92	99.44	0.5
9H-6	113.0	83.13	99.65	2.0
9H-6	118.0	83.18	99.70	0.5
9H-6	125.0	83.25	99.77	2.5
9H-6	145.0	83.45	99.97	4.0
10H-1	22.5	84.22	100.71	3.0
10H-1	41.5	84.42	100.89	7.0
10H-1	58.5	84.58	101.07	1.5
10H-1	89.5	84.89	101.38	12.5
10H-1	117.5	85.18	101.65	3.0
10H-1	150.5	85.50	101.99	6.5
10H-2	3.0	85.54	102.02	3.0
10H-2	9.0	85.60	102.08	1.0
10H-2	27.5	85.79	102.26	0.5
10H-2	39.5	85.90	102.39	2.0
10H-2	49.5	86.00	102.49	2.5
10H-2	72.5	86.24	102.71	3.5
10H-2	78.5	86.29	102.78	0.5
10H-2	109.5	86.61	103.08	1.5
10H-2	128.0	86.79	103.27	3.0
10H-2	150.5	87.01	103.50	0.5
11H-4	139.5	99.43	115.90	1.0
11H-4	142.5	99.46	115.93	1.0
11H-4	148.0	99.51	115.99	2.5
11H-5	15.5	99.68	116.17	0.5
11H-5	18.5	99.71	116.19	0.5
11H-5	23.0	99.76	116.24	1.5
11H-5	35.0	99.88	116.36	1.0
11H-5	41.5	99.94	116.43	0.5
11H-5	63.5	100.17	116.64	2.5
11H-5	65.0	100.18	116.66	0.5
11H-5	68.5	100.21	116.69	2.5
11H-5	75.5	100.29	116.76	0.5
11H-5	103.5	100.57	117.04	10.0
11H-5	132.0	100.85	117.33	4.5
11H-5	136.0	100.89	117.37	3.0
11H-6	18.5	101.22	117.71	2.0
11H-6	23.0	101.27	117.75	3.0
11H-6	46.0	101.50	117.98	1.5
11H-6	73.0	101.77	118.25	1.5
11H-6	77.0	101.81	118.29	3.0
11H-6	99.0	102.03	118.51	9.0
11H-6	112.5	102.17	118.64	0.5
11H-6	122.0	102.26	118.74	0.5
11H-6	129.0	102.33	118.81	1.0
11H-6	135.5	102.39	118.88	1.0
11H-6	151.0	102.55	119.03	5.5
11H-7	6.5	102.61	119.10	6.5
11H-7	16.5	102.71	119.19	1.0
11H-7	48.5	103.04	119.51	4.0
11H-CC	6.0	103.18	119.66	6.0
12H-1	11.0	103.11	119.87	9.0
12H-1	25.0	103.25	120.01	1.0
12H-1	40.0	103.40	120.16	6.0
12H-1	68.0	103.68	120.44	12.0
12H-1	87.0	103.87	120.63	3.0
12H-1	104.0	104.04	120.80	1.0
12H-1	131.0	104.31	121.07	15.0
12H-1	141.0	104.41	121.17	1.0
12H-2	10.0	104.61	121.37	3.0
12H-2	32.0	104.83	121.59	10.0
12H-2	51.0	105.02	121.78	1.0
12H-2	60.0	105.11	121.87	1.0
12H-2	110.0	105.61	122.37	10.0
12H-2	133.0	105.84	122.60	13.0
12H-3	3.0	106.06	122.82	2.0
12H-3	134.0	107.37	124.13	8.0
12H-4	9.0	107.64	124.40	8.0
12H-4	68.0	108.23	124.99	9.0
12H-4	76.0	108.31	125.07	1.0
15X-2	28.0	132.68	149.89	1.8
15X-2	79.5	133.20	150.40	1.5
16X-1	42.0	141.02	158.23	6.0
16X-1	63.0	141.23	158.44	3.0
16X-1	97.0	141.57	158.78	2.0
16X-1	136.0	141.96	159.17	12.0
16X-2	18.0	142.28	159.49	0.5
16X-2	29.0	142.39	159.60	0.5
16X-2	57.0	142.67	159.88	0.5
16X-2	109.0	143.19	160.40	3.0
18X-1	9.0	159.99	177.20	2.0
18X-1	39.0	160.29	177.50	8.0
18X-1	44.0	160.34	177.55	1.0
18X-1	66.0	160.56	177.77	0.5
18X-1	89.0	160.79	178.00	1.0
18X-1	116.0	161.06	178.27	1.0
18X-1	123.0	161.13	178.34	1.0
18X-1	143.0	161.33	178.54	1.0
18X-2	11.0	161.51	178.72	2.0
18X-2	28.0	161.68	178.89	1.0
18X-2	50.0	161.90	179.11	0.5
18X-2	147.0	162.87	180.08	1.0
18X-3	16.0	163.06	180.28	0.5
18X-3	49.0	163.39	180.61	1.0
18X-3	70.0	163.60	180.82	1.0
18X-3	94.0	163.84	181.06	0.5
18X-3	111.0	164.01	181.23	1.0
18X-3	123.0	164.13	181.35	0.5
18X-3	139.0	164.29	181.51	0.5
18X-4	22.0	164.62	181.84	1.0
18X-4	46.0	164.86	182.08	1.0
18X-4	61.0	165.01	182.23	0.5
18X-4	85.0	165.25	182.47	1.0
18X-4	92.0	165.32	182.54	1.0
18X-4	108.0	165.48	182.70	1.0
19X-1	14.0	169.64	186.85	3.0
19X-1	92.0	170.42	187.63	4.0
19X-1	143.0	170.93	188.14	1.5
19X-2	24.0	171.24	188.46	3.5
19X-2	42.0	171.42	188.64	2.0
19X-2	52.5	171.52	188.74	2.5
19X-2	67.0	171.67	188.89	2.0
19X-2	83.0	171.83	189.05	3.5
20X-1	13.5	179.34	196.54	5.0
20X-1	74.5	179.95	197.15	0.5
20X-1	132.0	180.52	197.73	0.5
20X-2	44.5	181.15	198.35	1.5
20X-2	71.0	181.41	198.62	2.5
20X-2	99.0	181.69	198.90	0.5
22X-3	79.5	201.90	220.24	1.0
22X-4	42.0	203.02	220.45	0.5
22X-4	62.5	203.23	220.66	0.5
22X-4	75.0	203.35	220.57	0.5
22X-4	88.0	203.48	220.70	0.5
22X-4	98.5	203.59	220.80	0.5
22X-5	5.0	203.65	220.88	0.5
22X-5	15.5	203.76	220.99	1.0
22X-5	24.5	203.85	221.07	0.5
22X-5	38.0	203.98	221.21	1.0
22X-5	52.5	204.12	221.35	0.5
22X-5	65.5	204.26	221.49	4.0
23X-1	47.5	208.18	225.38	1.0
23X-2	6.5	209.26	226.48	0.5
23X-2	13.0	209.33	226.54	1.0
23X-2	72.0	209.92	227.13	1.0
23X-3	13.0	210.83	228.04	1.0
23X-3	60.5	211.30	228.51	0.5
23X-3	105.5	211.76	228.96	0.5
23X-3	134.0	212.04	229.25	0.5
23X-4	38.0	212.59	229.80	5.0
23X-4	68.5	212.90	230.10	3.5
23X-4	109.5	213.30	230.51	1.0
23X-4	144.0	213.65	230.86	4.5
23X-5	11.5	213.82	231.04	0.5
23X-5	23.0	213.94	231.15	0.5
23X-5	63.0	214.34	231.55	5.0
23X-5	107.5	214.79	231.99	0.5
23X-5	129.5	215.01	232.21	0.5
23X-5	131.5	215.02	232.24	0.5
23X-5	138.5	215.10	232.30	0.5
23X-CC	6.5	215.24	232.45	0.5
24X-1	39.5	217.70	234.90	1.0
24X-1	46.5	217.76	234.98	1.0
24X-1	56.5	217.87	235.07	0.5
24X-1	76.5	218.07	235.27	0.5
24X-1	145.0	218.75	235.96	1.0
24X-2	51.5	219.32	236.54	0.5
24X-2	77.0	219.58	236.79	1.0
25X-1	3.0	226.93	244.14	1.5
25X-1	44.0	227.34	244.55	1.0
25X-1	74.5	227.65	244.85	0.5
25X-1	108.0	227.98	245.19	0.5
25X-2	70.0	229.05	246.28	1.0
25X-2	78.5	229.13	246.37	0.5
25X-2	125.0	229.60	246.83	0.5
25X-3	82.5	230.68	247.90	0.5
25X-3	100.0	230.85	248.08	1.0
25X-3	25.5	230.10	247.34	1.0
27X-2	1.0	247.61	265.26	1.0
27X-2	15.0	247.75	265.40	1.0
27X-2	43.0	248.03	265.68	2.0
27X-2	68.0	248.28	265.93	1.0
27X-2	111.0	248.71	266.36	1.0
27X-2	132.0	248.92	266.57	1.0
27X-3	7.0	249.17	266.82	1.0
27X-3	21.0	249.31	266.96	1.0
27X-3	66.0	249.76	267.41	0.5
27X-3	86.0	249.96	267.61	1.0
27X-3	95.0	250.05	267.70	1.0
27X-3	124.5	250.35	267.99	0.5
27X-3	149.0	250.59	268.24	1.0
27X-4	21.5	250.82	268.46	1.0
27X-4	46.0	251.06	268.71	1.0
27X-4	54.0	251.14	268.79	1.0
27X-4	79.0	251.39	269.04	1.0
27X-4	97.0	251.57	269.22	0.5
27X-4	120.0	251.80	269.45	1.5
27X-4	133.5	251.93	269.58	0.5
27X-5	102.0	253.12	270.76	1.0
27X-5	120.5	253.30	270.95	0.5
27X-5	136.5	253.46	271.11	0.5
27X-6	11.5	253.71	271.36	1.0
27X-6	23.0	253.83	271.47	1.0
27X-6	29.5	253.90	271.54	1.0
27X-6	91.0	254.51	272.15	1.5
27X-7	15.5	254.76	272.40	0.5

Table T7 (continued).

Core, section	Bottom depth (cm)	(mbsf)	(mcd)	Thickness of sandy silt layer (cm)
27X-7	46.5	255.07	272.71	1.5
27X-7	74.0	255.34	272.99	1.0
27X-7	82.0	255.42	273.07	1.0
27X-7	101.0	255.61	273.26	1.0
27X-7	104.0	255.64	273.29	1.0
28X-1	45.0	256.15	273.96	1.0
28X-1	98.0	256.68	274.49	0.5
28X-1	136.5	257.07	274.88	0.5
28X-2	16.5	257.36	275.17	0.5
28X-2	45.5	257.64	275.45	0.5
28X-2	69.0	257.88	275.69	0.5
28X-2	96.5	258.15	275.96	0.5
28X-3	106.0	259.73	277.54	1.0
28X-4	109.0	261.25	279.06	0.5
28X-4	123.0	261.39	279.20	0.5
28X-5	51.5	262.17	279.98	1.0
28X-5	62.5	262.27	280.08	0.5
28X-5	87.0	262.52	280.33	0.5
28X-5	146.0	263.11	280.92	1.0
28X-6	38.0	263.53	281.34	0.5
28X-6	54.0	263.69	281.50	0.5
28X-6	93.5	264.08	281.89	0.5
28X-7	15.0	264.31	282.12	1.0
28X-7	28.0	264.44	282.25	0.5
28X-7	46.0	264.62	282.43	0.5
28X-7	57.5	264.73	282.55	1.0
30X-7	48.0	283.97	302.27	1.0
30X-7	55.5	284.15	302.35	0.5
30X-7	81.0	284.30	302.60	0.5
31X-1	72.5	285.42	303.86	1.0
31X-1	88.5	285.58	304.02	2.0
31X-2	51.0	286.71	305.13	0.5
31X-2	54.0	286.74	305.16	0.5
31X-3	76.5	288.46	306.89	1.0
31X-3	126.5	288.96	307.39	4.0
31X-4	33.0	289.53	307.95	0.5
31X-4	55.0	289.75	308.17	1.5
31X-5	80.0	291.50	309.91	0.5
31X-5	81.0	291.51	309.92	0.5
31X-5	129.0	291.99	310.40	0.5
31X-5	141.0	292.11	310.52	0.5
31X-6	101.0	293.21	311.61	0.5
31X-6	105.5	293.26	311.65	0.5
31X-7	13.5	293.83	312.23	1.0
31X-7	26.5	293.96	312.36	0.5
31X-CC	9.0	294.31	312.69	2.0
32X-1	4.5	294.35	313.10	0.5
32X-1	27.0	294.57	313.32	0.5
32X-1	143.0	295.73	314.48	7.0
32X-2	8.0	295.85	314.61	0.5
32X-2	108.5	296.86	315.61	0.5
32X-3	55.0	297.82	316.59	0.5
32X-3	61.0	297.88	316.65	0.5
32X-3	99.0	298.26	317.03	0.5
32X-3	115.0	298.42	317.19	0.5
32X-3	146.0	298.73	317.50	0.5
32X-4	19.5	298.96	317.74	0.5
32X-4	50.0	299.27	318.05	0.5
32X-4	90.0	299.67	318.45	0.5
32X-5	24.0	300.51	319.30	0.5
32X-5	26.0	300.53	319.32	0.5
32X-5	90.0	301.17	319.96	0.5
32X-6	13.0	301.90	320.70	0.5
32X-6	56.0	302.33	321.13	0.5
32X-6	106.0	302.83	321.63	0.5
32X-6	120.0	302.97	321.77	0.5
32X-CC	15.0	303.89	322.71	6.0
33X-1	30.0	304.20	323.15	0.5
33X-1	59.0	304.49	323.44	1.0
33X-1	17.5	304.08	323.02	1.0
33X-1	95.0	304.85	323.80	0.5
33X-1	111.0	305.01	323.96	0.5
33X-1	125.5	305.15	324.11	0.5
33X-1	142.5	305.33	324.27	1.5
33X-2	81.0	306.22	325.17	6.0
33X-2	106.5	306.48	325.42	0.5
33X-2	119.5	306.61	325.55	0.5
33X-2	128.0	306.69	325.64	0.5
33X-3	6.0	306.98	325.93	0.5
33X-3	25.0	307.17	326.12	0.5
202-1232B-				
1H-1	70.0	0.70	2.94	1.0
1H-1	96.0	0.96	3.20	1.0
1H-1	108.0	1.08	3.32	1.0
1H-1	129.0	1.29	3.53	1.0
1H-2	8.0	1.58	3.82	7.0
1H-2	13.0	1.63	3.87	1.0
1H-2	57.0	2.07	4.31	4.0
1H-2	80.0	2.30	4.54	1.5
1H-2	89.0	2.39	4.63	1.0
1H-2	103.0	2.53	4.77	2.0
1H-2	122.0	2.72	4.96	4.0
1H-2	146.0	2.96	5.20	2.0
1H-3	5.0	3.05	5.30	5.0
1H-3	39.0	3.39	5.64	6.0
1H-3	71.0	3.71	5.96	3.0
1H-3	101.0	4.01	6.26	3.0
1H-3	137.0	4.37	6.62	1.0
1H-4	6.5	4.57	6.82	0.5
1H-4	103.0	5.53	7.78	1.0
1H-5	58.0	6.58	8.83	3.0
1H-5	85.0	6.85	9.10	2.5
1H-5	109.0	7.09	9.34	1.0
1H-5	137.0	7.37	9.62	7.0
1H-6	81.0	8.31	10.56	2.0
1H-6	109.0	8.59	10.84	1.0
1H-6	136.0	8.86	11.11	2.0
2H-1	2.0	9.12	12.02	1.0
2H-1	70.0	9.80	12.70	8.0
2H-1	112.0	10.22	13.12	10.0
2H-2	13.0	10.73	13.62	6.0
2H-2	33.0	10.93	13.82	1.0
2H-2	56.0	11.16	14.05	2.0
2H-2	113.0	11.73	14.62	1.0
2H-2	128.0	11.88	14.77	6.0
2H-3	25.0	12.35	15.23	2.0
2H-3	83.0	12.93	15.81	3.0
2H-4	20.0	13.80	16.67	1.0
2H-4	56.0	14.16	17.03	4.0
2H-4	83.0	14.43	17.30	3.0
2H-4	123.0	14.83	17.70	1.0
2H-5	2.0	15.12	17.99	2.0
2H-5	48.0	15.58	18.45	1.0
2H-5	64.0	15.74	18.61	2.0
2H-5	99.0	16.09	18.96	4.0
2H-5	117.0	16.27	19.14	1.0
2H-5	133.0	16.43	19.30	1.0
2H-6	2.0	16.62	19.49	1.0
2H-6	29.0	16.89	19.76	5.0
2H-6	76.0	17.36	20.23	2.0
2H-6	110.0	17.70	20.57	1.0
2H-7	4.0	18.14	21.01	4.0
2H-7	23.0	18.33	21.20	2.0
3H-6	68.0	26.78	30.01	3.0
3H-6	74.0	26.84	30.07	1.0
3H-6	84.0	26.94	30.17	3.0
3H-6	130.0	27.40	30.63	4.0
3H-6	150.0	27.60	30.83	4.0
3H-7	5.0	27.65	30.89	5.0
3H-7	17.0	27.77	31.01	2.0
3H-7	25.0	27.85	31.09	2.0
3H-7	42.0	28.02	31.26	3.0
3H-7	57.0	28.17	31.41	3.0
3H-7	65.0	28.25	31.49	4.0
4H-1	41.0	28.51	33.58	25.0
4H-1	48.0	28.58	33.65	1.0
4H-1	69.0	28.79	33.86	4.0
4H-1	91.0	29.01	34.08	6.0
4H-1	97.0	29.07	34.14	1.0
4H-1	101.0	29.11	34.18	1.0
4H-1	104.0	29.14	34.21	1.0
4H-1	111.0	29.21	34.28	1.0
4H-1	125.0	29.35	34.42	2.0
4H-1	139.0	29.49	34.56	4.0
4H-1	147.0	29.57	34.64	1.0
4H-2	9.0	29.69	34.76	3.0
4H-2	17.0	29.77	34.84	2.0
4H-2	23.0	29.83	34.90	1.0
4H-2	55.0	30.15	35.22	6.0
4H-2	63.0	30.23	35.30	2.0
4H-2	70.0	30.30	35.37	1.0
4H-2	76.0	30.36	35.43	1.0
4H-2	83.0	30.43	35.50	2.0
4H-2	94.0	30.54	35.61	1.0
4H-2	101.0	30.61	35.68	2.0
4H-2	141.0	31.01	36.08	6.0
4H-3	3.0	31.13	36.21	1.0
4H-3	7.0	31.17	36.25	2.0
4H-3	11.0	31.21	36.29	1.0
4H-3	21.0	31.31	36.39	2.0
4H-3	27.0	31.37	36.45	2.0
4H-3	62.0	31.72	36.80	13.0
4H-3	69.0	31.79	36.87	1.0
4H-3	74.0	31.84	36.92	1.0
4H-3	80.0	31.90	36.98	2.0
4H-3	90.0	32.00	37.08	3.0
4H-3	101.0	32.11	37.19	2.0
4H-3	118.0	32.28	37.36	5.0
4H-3	133.0	32.43	37.51	3.0
4H-4	13.0	32.73	37.81	2.0
4H-4	72.0	33.32	38.40	3.0
4H-4	87.0	33.47	38.55	1.0
4H-4	110.0	33.70	38.78	3.0
4H-4	123.0	33.83	38.91	2.0
4H-4	141.0	34.01	39.09	4.0
4H-4	150.0	34.10	39.18	2.0
4H-5	7.0	34.17	39.26	2.0
5H-3	18.0	40.78	45.87	9.0
5H-3	25.0	40.85	45.94	1.0
5H-3	59.5	41.19	46.28	0.5
5H-3	61.5	41.22	46.31	0.5
5H-3	64.0	41.24	46.33	1.0
5H-3	75.0	41.35	46.44	9.0
5H-3	97.0	41.57	46.66	6.5
5H-3	106.0	41.66	46.75	1.0
5H-3	120.5	41.81	46.90	0.5
5H-3	128.0	41.88	46.97	6.5
5H-4	10.5	42.21	47.31	3.5
5H-4	24.5	42.35	47.46	4.0
5H-4	33.0	42.43	47.54	1.5
5H-4	41.5	42.51	47.62	0.5
5H-4	50.0	42.60	47.71	6.5
5H-4	60.0	42.70	47.81	2.5

Table T7 (continued).

Core, section	Bottom depth (cm)	(mbsf)	(mcd)	Thickness of sandy silt layer (cm)
5H-4	65.0	42.75	47.86	0.5
5H-4	83.0	42.93	48.04	1.0
5H-4	107.5	43.17	48.28	1.5
5H-4	137.5	43.47	48.58	0.5
5H-5	23.0	43.83	48.95	1.5
5H-5	57.0	44.17	49.29	1.0
5H-5	77.5	44.38	49.49	0.5
5H-5	82.0	44.42	49.54	3.5
5H-5	134.5	44.94	50.06	0.5
5H-5	141.5	45.01	50.13	7.0
5H-5	151.0	45.11	50.23	1.5
5H-6	1.0	45.11	50.24	0.5
5H-6	23.5	45.33	50.47	3.5
5H-6	44.0	45.54	50.67	5.0
5H-6	61.0	45.71	50.84	2.0
5H-6	70.0	45.80	50.93	2.5
5H-6	88.5	45.99	51.12	1.5
5H-6	89.5	45.99	51.12	0.5
5H-6	95.5	46.06	51.19	5.0
5H-6	104.5	46.15	51.28	1.0
5H-6	118.0	46.28	51.41	1.5
5H-7	5.5	46.65	51.79	5.5
5H-7	32.5	46.92	52.06	1.0
5H-7	52.0	47.12	52.26	0.5
5H-7	54.0	47.14	52.28	0.5
5H-CC	12.0	47.31	52.46	5.5
6H-1	15.0	47.25	52.37	0.5
6H-1	28.0	47.38	52.50	1.0
6H-1	66.5	47.76	52.88	0.5
6H-1	133.0	48.43	53.55	1.5
6H-2	41.0	49.01	54.14	6.0
6H-2	51.0	49.11	54.24	0.5
6H-2	96.5	49.56	54.69	6.5
6H-2	151.0	50.11	55.24	14.0
6H-3	1.5	50.13	55.26	1.5
6H-3	10.0	50.22	55.34	1.0
6H-3	24.5	50.37	55.49	2.0
6H-3	30.5	50.42	55.54	0.5
6H-7	34.0	56.50	61.62	15.0
6H-7	49.5	56.65	61.78	0.5
6H-CC	14.5	56.99	62.10	1.5
6H-CC	18.0	57.02	62.14	2.5
6H-CC	23.0	57.07	62.19	4.0
6H-CC	33.5	57.17	62.29	0.5
6H-CC	35.5	57.19	62.31	1.0
7H-1	6.0	56.66	61.92	1.0
7H-1	17.0	56.77	62.03	7.0
7H-1	29.0	56.89	62.15	3.0
7H-1	49.0	57.09	62.35	3.0
7H-1	56.0	57.16	62.42	1.0
7H-1	70.0	57.30	62.56	1.0
7H-1	104.0	57.64	62.90	13.0
7H-1	116.0	57.76	63.02	4.0
7H-1	131.0	57.91	63.17	3.0
7H-1	139.0	57.99	63.25	1.0
7H-2	14.0	58.24	63.52	14.0
7H-2	29.0	58.39	63.67	19.0
7H-2	32.0	58.42	63.70	1.0
7H-2	37.0	58.47	63.75	1.0
7H-2	47.0	58.57	63.85	2.0
7H-2	69.0	58.79	64.07	11.0
7H-2	97.0	59.07	64.35	7.0
7H-2	106.0	59.16	64.44	1.0
7H-2	126.0	59.36	64.64	1.0
7H-2	137.0	59.47	64.75	8.0
7H-3	6.0	59.66	64.95	3.0
7H-3	34.0	59.94	65.23	15.0
7H-3	45.0	60.05	65.34	4.0
7H-3	64.0	60.24	65.53	4.0
7H-3	86.0	60.46	65.75	4.0
7H-3	113.0	60.73	66.02	9.0
7H-3	141.0	61.01	66.30	10.0
7H-4	4.0	61.14	66.44	1.0
7H-4	27.0	61.37	66.67	8.0
7H-4	45.0	61.55	66.85	4.0
7H-4	68.0	61.78	67.08	11.0
7H-4	100.0	62.10	67.40	7.0
7H-4	117.0	62.27	67.57	3.0
7H-4	137.0	62.47	67.77	6.0
7H-5	10.0	62.70	68.01	3.0
7H-5	40.0	63.00	68.31	14.0
7H-5	60.0	63.20	68.51	2.0
7H-5	81.0	63.41	68.72	3.0
7H-5	105.0	63.65	68.96	4.0
7H-5	132.0	63.92	69.23	8.0
7H-6	2.0	64.12	69.43	2.0
7H-6	19.0	64.29	69.60	1.0
7H-6	61.0	64.71	70.02	3.0
7H-6	82.0	64.92	70.23	3.0
7H-6	121.0	65.31	70.62	10.0
7H-7	68.0	66.28	71.61	13.0
8H-1	72.0	66.82	72.23	1.0
9H-4	31.0	75.91	84.02	3.0
9H-4	45.0	76.05	84.16	1.0
9H-4	65.0	76.25	84.36	3.0
9H-4	82.0	76.42	84.53	1.0
9H-4	106.0	76.66	84.77	1.0
9H-4	116.0	76.76	84.87	2.0
9H-4	130.0	76.90	85.01	2.0
9H-5	9.0	77.19	85.33	1.0
9H-5	65.0	77.75	85.89	3.0
9H-6	14.0	78.74	86.89	1.0
9H-6	26.0	78.86	87.01	3.0
9H-6	38.0	78.98	87.13	4.0
9H-6	48.0	79.08	87.23	2.0
9H-6	79.0	79.39	87.54	2.0
9H-6	89.0	79.49	87.64	3.0
9H-6	95.0	79.55	87.70	1.0
9H-6	145.0	80.05	88.20	2.0
9H-7	21.0	80.31	88.47	4.0
9H-7	34.0	80.44	88.60	2.0
9H-7	45.0	80.55	88.71	2.0
9H-7	67.0	80.77	88.93	2.0
9H-7	82.0	80.92	89.08	1.0
10H-1	57.0	81.17	89.58	3.0
10H-1	96.0	81.56	89.97	3.0
10H-2	6.0	82.16	90.59	2.0
10H-2	15.0	82.25	90.68	3.0
10H-2	36.0	82.46	90.89	3.0
10H-2	56.0	82.66	91.09	2.0
10H-2	83.0	82.93	91.36	3.0
10H-2	93.0	83.03	91.46	2.0
10H-3	42.0	84.02	92.46	11.0
10H-3	74.0	84.34	92.78	1.0
10H-3	100.0	84.60	93.04	1.0
10H-4	38.0	85.48	93.95	2.0
10H-5	7.0	86.67	95.15	1.0
10H-5	38.0	86.98	95.46	3.0
10H-5	112.0	87.72	96.20	2.0
10H-5	134.0	87.94	96.42	6.0
10H-5	141.0	88.01	96.49	2.0
10H-6	12.0	88.22	96.72	6.0
10H-6	19.0	88.29	96.79	2.0
10H-6	42.0	88.52	97.02	3.0
10H-6	64.0	88.74	97.24	3.0
10H-6	89.0	88.99	97.49	8.0
10H-6	113.0	89.23	97.73	4.0
10H-6	127.0	89.37	97.87	2.0
10H-7	6.0	89.66	98.16	6.0
10H-7	24.0	89.84	98.34	5.0
10H-7	55.0	90.15	98.65	11.0
10H-7	66.0	90.26	98.76	2.0
202-1232C-				
1H-2	26.0	1.76	1.77	3.0
1H-4	44.0	3.79	3.83	1.0
1H-4	72.0	4.07	4.11	1.0
3H-3	100.0	18.20	21.99	8.0
3H-3	118.0	18.38	22.17	2.0
3H-3	130.0	18.50	22.29	1.0
3H-3	137.0	18.57	22.36	0.5
3H-4	45.0	19.15	22.94	9.0
3H-4	80.0	19.50	23.29	5.0
3H-4	99.0	19.69	23.48	1.0
3H-4	107.0	19.77	23.56	1.0
3H-4	123.0	19.93	23.72	3.0
3H-5	3.0	20.23	24.03	3.0
3H-5	27.0	20.47	24.27	5.0
3H-5	35.0	20.55	24.35	1.0
3H-5	45.0	20.65	24.45	1.0
3H-5	56.0	20.76	24.56	1.0
3H-5	82.0	21.02	24.82	6.0
3H-5	124.0	21.44	25.24	7.0
3H-5	149.0	21.69	25.49	4.0
3H-6	9.0	21.79	25.60	9.0
3H-6	43.0	22.13	25.94	7.0
4H-1	19.0	23.89	29.61	16.0
4H-1	39.0	24.09	29.81	4.0
4H-1	46.5	24.17	29.89	1.5
4H-1	55.0	24.25	29.97	1.0
4H-1	60.0	24.30	30.02	0.5
4H-1	81.0	24.51	30.23	3.0
4H-1	94.0	24.64	30.36	4.0
4H-1	116.0	24.86	30.58	6.0
4H-1	128.0	24.98	30.70	1.0
4H-1	140.0	25.10	30.82	7.0
4H-2	2.0	25.22	30.94	2.0
4H-2	8.5	25.28	31.00	0.5
4H-2	26.0	25.46	31.18	2.0
4H-2	38.0	25.58	31.30	2.0
4H-2	46.0	25.66	31.38	1.0
4H-2	57.0	25.77	31.49	1.0
4H-2	100.0	26.20	31.92	6.0
4H-2	108.0	26.28	32.00	2.0
4H-2	113.0	26.33	32.05	1.0
4H-2	124.0	26.44	32.16	2.0
4H-2	147.0	26.67	32.39	8.0
4H-3	20.0	26.90	32.63	8.0
4H-3	30.0	27.00	32.73	0.5
4H-3	36.0	27.06	32.79	4.0
4H-3	40.0	27.10	32.83	0.5
4H-3	52.0	27.22	32.95	1.0
4H-3	57.0	27.27	33.00	3.0
4H-3	63.0	27.33	33.06	1.5
4H-3	81.0	27.51	33.24	6.0
4H-3	83.0	27.53	33.26	0.5
4H-3	92.0	27.62	33.35	4.0
4H-3	101.0	27.71	33.44	0.5
4H-3	124.0	27.94	33.67	7.0
4H-3	148.0	28.18	33.91	3.0
4H-4	18.0	28.38	34.12	4.0
4H-4	25.0	28.45	34.19	0.5
4H-4	32.0	28.52	34.26	0.5

Note: This table is also available in **ASCII.**

Table T8. Distribution of calcareous nannofossils, Hole 1232A.

Core, section, interval (cm)	Depth (mbsf)	Depth (mcd)	Preservation	Abundance	*Calcidiscus leptoporus*	*Coccolithus pelagicus*	*Emiliania huxleyi*	*Gephyrocapsa caribbeanica*	*Gephyrocapsa muellerae*	*Gephyrocapsa oceanica*	*Gephyrocapsa* spp. (medium)	*Gephyrocapsa* spp. (small)	*Helicosphaera carteri*	*Pseudoemiliania lacunosa*	*Reticulofenestra asanoi*	*Reticulofenestra producta*
202-1232A-																
1H-1	0.00	5.94	M	F	F	F	C					D				
1H-1	1.51	7.45	M	F	F		R		R		F	C	R			
1H-4, 21	4.73	10.67	M	R	F	F	F					F				
1H-5, 21	6.23	12.17	M	R	R		R					C				
1H-CC	8.95	14.89	M	R		R	F		cf.	F	F	C	R			
3H-CC	28.20	32.48	G	C	F	F	F		C		C	A	F			
4H-2, 20	28.71	34.09	G	C	R	F	R		F			A				
4H-5, 50	33.56	38.94	F	M	F		R		F			F	R			
4H-CC	36.74	42.12	M	F	F	F					F	D	R			
5H-CC	46.27	51.70		B												
6H-CC	55.68	69.33	M	F	R	R	R					F				
7H-CC	63.96	79.57	M	R		R	R					R				
8H-CC	74.80	91.10		B												
9H-CC	83.89	100.37	M	F	R	R	R					F				
10H-CC	92.43	108.91	M	A	F		R					A				
11H-CC	103.12	119.60	M	F	R							F				
12H-CC	112.83	129.59		B												
13X-CC	119.94	137.15	M	C	F	R	R		F			C	R			
14X-1, 29	121.59	138.80	M	C	R	R						R				
14X-CC	121.90	139.11	M	R	R						R	R				
15X-CC	133.27	150.48	P	R		R		R				R				
16X-CC	143.36	160.57		B												
17X-CC	150.30	167.51		B												
18X-CC	165.65	182.86	P	R	R	R										R
19X-CC	171.94	189.15	P	R	R	R										R
20X-CC	184.30	201.51	P	R		R										R
21X-CC	192.59	209.80		B												
22X-CC	204.42	221.63	M	F		R					F					
23X-CC	215.17	232.38	P	R		R					R	R				
24X-CC	220.10	237.31	P	R		R					R					
25X-CC	236.35	253.56	M	C		R					F		R			
26X-CC	245.92	263.35	M	C	R	R					C			R		
27X-CC	255.65	273.31	M	R	R	R		R			R	R				
28X-CC	265.23	283.04	P	R		R		R				R				
29X-CC	274.81	292.93	M	R		R						R				
30X-CC	284.55	302.85	M	R	R	R						R	R	R		
31X-CC	294.17	312.60		B												
32X-CC	303.81	322.56	M	R	R	R					R	R	R	R		
33X-CC	310.90	329.85	M	R	R	R					R	R				
34X-CC	323.03	341.98		B												
35X-CC	332.61	351.78		B												
36X-CC	342.17	361.52	M	R		R						R				
37X-CC	351.78	371.25	P	R		R						R				
38X-CC	361.48	381.10	P	R	R											R
39X-CC	361.70	381.35	P	R	R						R	R				

Notes: Preservation: G = good, M = moderate, P = poor. Abundance: A = abundant, C = common, F = few, R = rare, B = barren. cf. = taxon similar to described species but taxonomic affinity uncertain.

Table T9. Distribution of foraminifers, Hole 1232A.

Core, section, interval (cm)	Depth (mbsf)	Depth (mcd)	Preparation	Preservation	Abundance	Benthic/planktonic foraminifers (%)	Remarks	*Globigerina bulloides*	*Globigerinoides ruber*	*Globigerinoides ruber* pink	*Globorotalia crassaformis*	*Globigerinita glutinata*	*Globorotalia inflata*	*Globorotalia scitula*	*Globorotalia tosaensis*	*Globorotalia truncatulinoides*	*Neogloboquadrina pachyderma*	*Orbulina suturalis*	*Streptochilus* sp.	Biozone/ comments
202-1232A-																				
Mudline	0.00	5.94	S	M	F	1/99		F					A			R				PT1a
1H-1, base	1.51	7.45	S	P	F	1/99		F					A	R		C				PT1a
1H-CC	8.95	14.89	S	P	T															PT1a
2H-CC							Empty tube													PT1a
3H-CC	28.20	32.48	S	G	A	1/99		A	R				A			C		R		PT1a
4H-CC	36.74	42.12	S	M	F	1/99		C					C	R		R	F			PT1a
5H-CC	46.27	51.70	S	M	R	5/95		C					C			R				PT1a
6H-CC	55.68	69.33	S	M	C	10/90		F					A			F				PT1a
7H-CC	63.96	79.57	S	P	T		Turbidite													PT1a
8H-5, 136–138	72.41	88.71	S	M	C	10/90	Above turbidite	F				R	C			R				PT1a
8H-5, 145–147	72.50	88.80	S	M	F	40/60	Turbidite	F					F	R		R				PT1a
8H-5, 148–150	72.53	88.83	S	M	C	30/70	Below turbidite	C					C			F				PT1a
8H-CC	74.80	91.10	S	M	R	1/99	Radiolarians: A						R	R						PT1a
9H-CC	83.89	100.37	S	P	R	1/99							R			R				PT1a
10H-CC	92.43	108.91	S	G	C	10/90		C					A	R		F	R			PT1a
11H-CC	103.12	119.60	S	P	F	10/90		C					C			C				PT1a
12H-CC	112.83	129.59	S	M	F	5/95		C					F	R						PT1a
13X-CC	119.94	137.15	S	G	A	5/95		A					C			F				PT1a
14X-CC	121.90	139.11	S	M	F	35/65	Radiolarians: A	C					C			R				PT1a
15X-CC	133.27	150.48	S	P	T		Radiolarians: R													PT1a
16X-CC	143.36	160.57	S	P	T		Radiolarians: R													PT1a
17X-CC	150.30	167.51	S	P	T		Radiolarians: R													PT1a
18X-CC	165.65	182.86	S	P	R	1/99	Radiolarians: R	R					R			R				PT1a
19X-CC	171.94	189.15	S	P	T		Radiolarians: R													PT1a
20X-CC	184.30	201.51	S	P	T		Radiolarians: R													PT1a
21X-CC	192.59	209.80	S	M	F	60/40	Radiolarians: R	F				R	C	R						PT1a
22X-CC	204.42	221.63	S	C	M	10/90	Radiolarians: R	F			R	R	A	R	R	R	R	F		
23X-CC	215.17	232.38	S	P	T		Radiolarians: R													
24X-CC	220.10	237.31	S	P	T		Radiolarians: R													
25X-CC	236.35	253.56	S	M	F	10/90	Radiolarians: R	F				F	C							
26X-CC	245.92	263.35	S	M	C	3/97	Radiolarians: R				R		A	C	F	R				PT1b
27X-CC	255.65	273.31	S	P	T		Radiolarians: R													PT1b
28X-CC	265.23	283.04	S	P	R	1/99	Radiolarians: R				R	F	F		R					PT1b
29X-CC	274.81	292.93	S	P	T		Radiolarians: R													PT1b
30X-CC	284.55	302.85	S	P	T		Radiolarians: R													PT1b
31X-CC	294.17	312.60	S		B		Radiolarians: A													PT1b
32X-CC	303.81	322.56	S	M	F	50/50	Radiolarians: R				R	F	R		R	R			R	PT1b
33X-CC	310.90	329.85	S	G	C	15/85	Radiolarians: R				R		A	R	C	C				PT1b
34X-CC	323.03	341.98	S	P	R	1/99	Radiolarians: R													PT1b
35X-CC	332.61	351.78	S	P	T															PT1b
36X-CC	342.17	361.52	S	G	C	5/95	Radiolarians: R				A	C	R	R	R	C				PT1b
37X-CC	351.78	371.25	S		B															PT1b
38X-CC	361.48	381.10	S		B															PT1b
39X-CC	361.70	381.35	S	P	T		Radiolarians: R				R			R						PT1b

Notes: Preparation: S = sieve. Preservation: G = good, M = moderate, P = poor. Abundance: A = abundant, C = common, F = few, R = rare, T = trace, B = barren.

Table T10. Distribution of diatoms, Hole 1232A. (**See table notes.** Continued on next page.)

Core, section, interval (cm)	Depth (mbsf)	Depth (mcd)	Method	Preservation	Abundance	*A. africana/A. tabularis*	*Azpeitia nodulifera*	*Chaetoceros* resting spores	*Hemidiscus cuneiformis*	*Fragilariopsis doliolus*	*Thalassionema nitzschioides*	*Thalassiosira eccentrica* grp.	*Thalassiosira oestrupii*	Freshwater forms	Marine benthic forms	Marine neritic forms	Diatom fragments	Remarks
202-1232A-																		
Mudline	0.00	0.00	S	M	F			C				F		F	T		C	
1H-1	1.50	7.44	S	M	C			A				C	C		T		C	
1H-4, 80	5.30	11.24	S	M	C			C		T							*	
1H-CC	8.98	14.92	S	M	F			A				F	F	C	T		C	
3H-CC	28.29	32.57	S	G	C			A			T	C	C		T		C	
4H-2, 10	28.60	33.98	S	M	F		T	A				F			T		C	Top of turbidite
4H-2, 20	28.70	34.08	S	M	C			A				C	F	F	T	T	C	10 cm from turbidite top
4H-2, 30	28.80	34.18	S	M	F			A				F			T		C	20 cm from turbidite top
4H-5, 50	29.00	34.38	S	M	C			A				C	C		T	T	T	Hemipelagic greenish mud
4H-CC	36.85	42.23	S	M	F			F					F	C	T		C	
5H-6, 110	45.10	50.53	S	P	R			F						C			T	Turbidite—finer material (muddy)
5H-6, 115	45.15	50.58	S	P	R			F						C			T	Turbidite—finer material (coarse silt)
5H-6, 118	45.18	50.61	S	P	T												T	Base of turbidite—coarser material (fine sand)
5H-6, 120	45.20	50.63	S	M	C			A			T		C	F	T		C	Top of hemipelagic sequence below turbidite
5H-CC	46.34	51.77	S	G	C			F					F	C	F	T	*	
6H-CC	55.91	69.56	S	M	C			C						F	F	F	*	
7H-3, 121	59.71	75.32	S	P	C		T	A			T	C	C			T	T	Turbidite
7H-5, 44	63.44	79.05	S	M	F	T		A			R	T	T		T	T	*	
7H-5, 60	63.60	79.21	S	P	R		T							T		T	T	
7H-5, 65	63.65	79.26	S	P	F		R	F			T			T		T	C	(*Delphineis*)
7H-5, 80	63.80	79.41	S	P	F			T				T				T	T	(*Delphineis/Actinoptychus*)
7H-CC	63.97	79.58	S	M	F			F							R	T	*	
8H-6, 55	73.05	89.35	S	M	F		T	F				R		R	R	R	*	Hemipelagic greenish mud
8H-6, 80	73.30	89.60	S	M	C		R	C	T			F		T	T	T	*	Hemipelagic greenish mud
8H-CC	74.94	91.24	S	M	C			C			T	T	T	T	T	T	*	
9H-3, 135	78.85	95.33	S	M	F			F			R	T	T			T	C	
9H-CC	83.94	100.42	S	M	F			F						T	T		C	
10H-CC	92.73	109.21	S	G	C			A			T	C	C	T		T	C	
11H-2, 60	95.60	112.08	S	P	T			T						T				
11H-5, 74	100.24	116.72	S	P	T												T	Yellowish green carbonate concretion
11H-CC	103.25	119.73	S	P	T												T	
12H-2, 70	105.20	121.96	S	P	T												T	
12H-4, 120	108.70	125.46	S	P	T												T	
12H-6, 25	110.75	127.51	S	P	T			T									T	Olive mud
12H-CC	113.02	129.78	S	P	T			T				T					T	
13X-1, 140	113.90	131.11	S	P	F			F			T	T	T		T	T	T	
13X-2, 80	114.80	132.01	S		B													
13X-CC	120.02	137.23	S	P	T												T	
14X-CC	121.90	139.11	S	P	R			T				T			T		T	
15X-CC	133.40	150.61	S	P	R			F				T		T	T		T	
16X-CC	143.57	160.78	S	P	F			C			T			T	T		T	
17X-CC	150.38	167.59	S	P	T									T			T	
18X-1, 85	160.75	177.96	S		B													
18X-CC	165.77	182.98	S	P	T			R			R	T		T	T		*	
19X-1, 93	170.43	187.64	S	M	F	T		C			T	T	T		T	T	C	
19X-CC	172.04	189.25	S	P	R			F				R	C	T	T	R	*	
20X-CC	184.55	201.76	S	P	T								C	T	T		*	
21X-CC	192.67	209.88	S	P	R			R				T		R		T	*	
22X-CC	204.63	221.84	S	P	R			R				T	T	R	R	T	*	
23X-5, 62	213.70	230.91	S	M	R			R			T			F	T	T	*	Base of turbidite—coarser material (fine sand)
23X-CC	215.42	232.63	S	M	R			T						F		T	*	
24X-CC	220.17	237.38	S	P	R			T						R	T	T	*	
25X-CC	236.67	253.88	S	P	T			T						T			*	
26X-CC	246.28	263.71	S	P	T	T		T							T		*	
27X-CC	255.80	273.46	S	P	R			A				F		C			T	
28X-CC	265.56	283.37	S	P	F			C			T	T		C	T		T	
29X-CC	275.13	293.25	S	P	T												T	
30X-CC	284.78	303.08	S	P	R										T		T	
31X-CC	294.57	313.00	S	P	F			C			T	T				C	A	Opal rich, many fragments, and strongly silicified forms; different assemblage from previous samples
32X-CC	304.05	322.80	S	P	F			F				T	T	T			C	

Table T10 (continued).

Core, section, interval (cm)	Depth (mbsf)	Depth (mcd)	Method	Preservation	Abundance	*A. africana/A. tabularis*	*Azpeitia nodulifera*	*Chaetoceros* resting spores	*Hemidiscus cuneiformis*	*Fragilariopsis doliolus*	*Thalassionema nitzschioides*	*Thalassiosira eccentrica* grp.	*Thalassiosira oestrupii*	Freshwater forms	Marine benthic forms	Marine neritic forms	Diatom fragments	Remarks
33X-CC	311.18	330.13	S	P	F		T	C				F	T			T	A	
34X-3, 120	317.70	336.65	S	P	T		T	T					T				*	
34X-5, 54	320.04	338.99	S	P	F		R	F			T	R	T	T	T	R	*	
34X-7, 5	323.00	341.95	S	P	T			T									*	
34X-7, 45	323.25	342.20	S	P	T			T			T					T	*	
34X-CC	323.30	342.25	S	P	T												T	
35X-CC	332.83	352.00	S	P	T											T	T	
36X-CC	342.37	361.72	S	P	T												T	
37X-CC	352.10	371.57	S	P	T			T				T		T			*	
38X-CC	361.68	381.30	S	P	T			T						T			*	
39X-CC	361.96	381.61	S	M	T									T			*	

Notes: Preparation: S = smear slide. Preservation: G = good, M = moderate, P = poor. Abundance: C = common, R = rare, F = few, T = trace, B = barren. * = not considered.

Table T11. Headspace gas concentrations, Hole 1232A.

Core, section, interval (cm)	Depth (mbsf)	Depth (mcd)	C_1 (ppmv)
202-1232A-			
1H-4, 0–5	4.52	10.46	2
3H-4, 0–5	23.01	27.29	3,278
4H-4, 0–5	31.55	36.93	5,010
5H-4, 0–5	41.05	46.48	6,123
6H-4, 0–5	50.54	64.19	9,080
7H-4, 0–5	60.03	75.64	11,031
8H-4, 0–5	69.53	85.83	11,329
9H-4, 0–5	79.02	95.50	21,452
10H-4, 0–5	88.54	105.02	3,744
11H-4, 0–5	98.03	114.51	8,510
12H-4, 0–5	107.55	124.31	11,426
13X-4, 0–5	117.01	134.22	26,639
15X-2, 0–5	132.40	149.61	11,353
16X-2, 0–5	142.10	159.31	11,432
18X-4, 0–5	164.41	181.62	34,343
19X-2, 0–5	171.01	188.22	24,965
20X-3, 0–5	182.20	199.41	19,217
21X-3, 0–5	191.79	209.00	33,323
22X-4, 0–5	202.61	219.82	16,791
23X-4, 0–5	212.21	229.42	26,053
24X-2, 0–5	218.81	236.02	21,356
25X-4, 0–5	231.38	248.59	10,072
26X-4, 0–5	240.97	258.40	29,887
27X-4, 0–5	250.59	268.25	8,883
28X-4, 0–5	260.16	277.97	12,358
29X-4, 0–5	269.79	287.91	13,387
30X-4, 0–5	279.49	297.79	23,291
31X-4, 0–5	289.19	307.62	32,375
32X-4, 0–5	298.80	317.55	17,060
33X-4, 0–5	308.43	327.38	29,822
35X-4, 0–5	327.64	346.81	16,741
36X-4, 0–5	337.23	356.58	24,902
37X-4, 0–5	346.83	366.30	14,322
38X-4, 0–5	356.52	376.14	19,401

Table T12. Interstitial water geochemical data, Holes 1232A and 1232B.

Core, section, interval (cm)	Depth (mbsf)	Depth (mcd)	pH	Alkalinity (mM)	Salinity	Cl^- (mM)	Na^+ (mM)	SO_4^{2-} (mM)	HPO_4^{2-} (μM)	NH_4^+ (mM)	H_4SiO_4 (μM)	Mn^{2+} (μM)	Fe^{2+} (μM)	Ca^{2+} (mM)	Mg^{2+} (mM)	B (μM)	Sr^{2+} (μM)	Ba^{2+} (μM)	Li^+ (μM)	K^+ (mM)
202-1232A-																				
1H-3, 145–150	4.46	10.40	7.82	23.4	34.0	563	478	8.4	71	1.28	419	19	BDL	7.0	50.1	488	76	7.2	19	10.8
3H-3, 145–150	22.95	27.23	7.82	35.9	34.0	572	483	1.0	137	1.93	472	21	17	5.9	52.2	540	77	14.6	19	11.3
4H-3, 145–150	31.47	36.85	7.83	36.1	34.0	567	478	0.6	115	2.08	516	15	22	5.6	51.9	528	76	16.8	19	11.2
5H-3, 145–150	40.98	46.41	7.86	33.8	35.0	562	472	1.2	79	2.19	431	9	24	6.0	51.5	480	73	10.7	16	11.0
6H-3, 145–150	50.48	64.13	7.81	35.0	34.0	574	481	1.1	52	2.18	419	8	36	6.6	53.1	478	72	9.4	16	10.5
7H-3, 140–150	59.91	75.52	7.87	36.4	34.0	566	469	0.6	108	2.46	454	12	51	6.6	55.0	521	72	13.6	19	11.2
8H-3, 140–150	69.42	85.72	7.95	33.5	33.0	568	471	0.7	158	2.35	485	22	69	5.3	54.9	563	75	27.0	23	11.1
9H-3, 140–150	78.91	95.39	7.95	31.9	34.0	563	473	1.0	84	2.04	513	5	40	3.5	53.1	540	72	27.6	22	10.9
10H-3, 140–150	88.43	104.91	8.01	30.9	33.0	569	477	0.7	103	1.88	468	6	22	3.5	53.7	484	67	12.6	16	9.8
11H-3, 140–150	97.91	114.39	7.99	29.9	34.0	573	482	0.8	101	1.93	446	5	35	4.3	52.2	471	68	9.9	15	10.0
12H-3, 140–150	107.43	124.19	7.90	30.9	34.0	569	479	0.7	95	2.05	419	8	44	4.9	51.5	445	67	10.0	16	9.3
13X-3, 140–150	116.90	134.11	7.94	30.9	34.0	567	484	1.4	107	2.38	546	5	6	4.9	48.5	471	68	13.2	19	10.2
16X-1, 140–150	142.00	159.21	7.94	30.8	34.0	565	476	1.7	134	2.52	409	8	10	6.2	50.7	430	73	15.3	19	9.2
19X-1, 140–150	170.90	188.11	7.94	29.3	34.0	566	481	1.1	87	2.16	511	6	13	4.3	49.3	415	68	15.2	19	9.2
22X-3, 140–150	202.51	219.72	8.09	22.4	34.0	561	468	1.8	119	2.02	598	10	22	4.5	49.7	417	71	29.6	20	10.5
25X-3, 140–150	231.27	248.48	8.00	19.1	33.0	564	476	4.7	87	1.85	417	8	20	4.3	49.4	400	74	20.1	17	9.3
28X-3, 140–150	260.07	277.88	7.99	26.3	33.0	565	475	2.4	115	2.17	591	4	15	4.4	51.2	366	67	25.7	19	9.4
31X-3, 140–150	289.09	307.52	7.95	29.0	34.0	572	482	1.3	115	2.24	534	9	12	4.5	51.9	365	65	24.3	19	8.8
34X-3, 140–150	317.90	336.85	8.09	29.7	34.0	567	480	0.6	94	2.60	587	4	BDL	3.8	50.4	337	63	15.5	19	9.5
37X-3, 140–150	346.72	366.19	8.01	27.9	34.0	564	485	1.0	106	2.52	555	8	BDL	4.3	45.8	325	66	30.1	20	8.3
202-1232B-																				
1H-3, 145–150	4.46	6.70	7.89	14.0	34.0	559	478	18.7	67	0.89	431	37	7	9.1	51.1	472	81	9.3	21	12.0
2H-3, 145–150	13.53	16.43	7.83	25.2	34.0	562	483	6.9	77	1.48	509	12	BDL	6.4	47.1	495	74	8.4	19	10.6
3H-3, 145–150	23.07	26.25	8.09	34.2	35.0	569	480	0.5	71	1.91	398	10	10	6.0	50.6	433	75	15.1	18	11.3
4H-3, 140–150	32.51	37.58	7.94	35.0	35.0	573	482	0.8	119	1.91	415	11	11	5.8	52.8	463	77	14.1	18	10.8
5H-3, 140–150	42.02	47.09	7.96	36.3	35.0	576	482	0.6	100	2.00	479	9	8	5.8	54.2	463	77	17.4	19	11.4
6H-3, 140–150	51.52	56.64	7.84	34.4	35.0	568	479	0.7	76	1.98	390	7	27	5.9	51.7	467	74	9.8	16	9.7
7H-3, 140–150	61.03	66.29	7.85	35.9	34.0	570	474	0.6	58	2.19	355	7	21	6.7	54.8	448	71	9.6	16	10.0
8H-3, 140–150	70.54	75.95	7.85	36.8	34.0	569	478	0.7	130	2.38	493	11	27	6.1	53.3	485	72	12.7	19	10.1
9H-3, 145–150	75.57	83.64	7.90	36.2	35.0	567	474	0.8	87	2.29	442	14	9	5.6	53.9	468	74	21.0	22	11.6
10H-3, 140–150	85.03	93.44	7.95	33.0	34.0	568	485	0.5	92	2.06	513	5	12	3.4	50.3	491	71	33.9	22	10.1

Note: BDL = below detection limit (Fe^{2+} = 6 μM).

Table T13. Inorganic carbon, calcium carbonate, total carbon, total organic carbon, and total nitrogen analyses, and TOC/TN ratio, Holes 1232A and 1232B. (See table note. Continued on next page.)

Core, section, interval (cm)	Depth (mbsf)	Depth (mcd)	IC (wt%)	$CaCO_3$ (wt%)	TC (wt%)	TOC (wt%)	TN (wt%)	TOC/TN (atomic)
202-1232A-								
1H-1, 74–75	0.74	6.68	0.08	0.7	0.43	0.35	0.02	16.08
1H-2, 74–75	2.25	8.19	0.03	0.3				
1H-3, 74–75	3.75	9.69	0.13	1.1	0.38	0.25	0.03	8.30
1H-4, 74–75	5.26	11.20	0.10	0.9				
1H-5, 74–75	6.76	12.70	0.07	0.6				
1H-6, 74–75	8.26	14.20	0.08	0.7				
3H-1, 72–73	19.22	23.50	0.11	0.9	0.24	0.13	0.01	7.24
3H-2, 72–73	20.71	24.99	0.08	0.7				
3H-3, 72–73	22.22	26.50	0.05	0.5	0.11	0.06	0.00	12.67
3H-4, 72–73	23.73	28.01	0.14	1.2				
3H-5, 72–73	25.23	29.51	0.12	1.0				
3H-6, 72–73	26.73	31.01	0.18	1.5				
3H-7, 19–20	27.71	31.99	0.10	0.9				
4H-1, 72–73	27.72	33.10	0.13	1.1	0.29	0.16	0.02	8.47
4H-2, 72–73	29.23	34.61	0.15	1.3				
4H-3, 72–73	30.74	36.12	0.17	1.5	0.31	0.14	0.01	8.39
4H-4, 72–73	32.27	37.65	0.17	1.4				
4H-5, 72–73	33.78	39.16	0.32	2.7				
4H-6, 72–73	35.29	40.67	0.32	2.7				
4H-7, 19–20	36.27	41.65	0.07	0.6				
5H-1, 74–75	37.24	42.67	0.23	1.9	0.31	0.08	0.01	6.21
5H-2, 74–75	38.75	44.18	0.10	0.8				
5H-3, 74–75	40.27	45.70	0.12	1.0				
5H-4, 74–75	41.79	47.22	0.07	0.6	0.21	0.14	0.01	9.98
5H-5, 74–75	43.31	48.74	0.09	0.8				
5H-6, 74–75	44.83	50.26	0.07	0.6				
5H-7, 20–21	45.80	51.23	0.10	0.8				
6H-1, 74–75	46.74	60.39	0.06	0.5	0.18	0.12	0.01	7.70
6H-2, 74–75	48.25	61.90	0.16	1.3				
6H-3, 74–75	49.77	63.42	0.40	3.4				
6H-4, 74–75	51.28	64.93	0.06	0.5	0.09	0.03		
6H-5, 74–75	52.79	66.44	0.10	0.9				
6H-6, 74–75	54.30	67.95	0.06	0.5				
6H-7, 20–21	55.27	68.92	0.10	0.8				
7H-1, 74–75	56.24	71.85	0.08	0.6	0.36	0.28	0.02	11.65
7H-2, 74–75	57.75	73.36	0.11	1.0				
7H-3, 74–75	59.25	74.86	0.16	1.3	0.41	0.25	0.02	9.45
7H-4, 74–75	60.77	76.38	0.06	0.5				
7H-5, 74–75	62.28	77.89	0.10	0.8				
7H-6, 20–22	63.25	78.86	0.12	1.0				
8H-1, 74–75	65.74	82.04	0.12	1.0	0.45	0.33	0.03	10.93
8H-3, 74–75	68.76	85.06	0.23	1.9				
8H-5, 74–75	71.79	88.09	0.23	1.9				
8H-6, 74–75	73.31	89.61	0.06	0.5	0.13	0.07		
9H-1, 74–75	75.24	91.72	3.23	26.9	3.44	0.21	0.03	5.66
9H-3, 74–75	78.25	94.73	0.10	0.8	0.30	0.20	0.02	8.01
9H-3, 86–88	78.37	94.85	0.12	1.0				
9H-5, 74–75	81.27	97.75	0.13	1.0				
10H-1, 74–75	84.74	101.22	0.08	0.7				
10H-3, 74–75	87.77	104.25	0.04	0.3	0.10	0.06		
10H-5, 74–75	90.80	107.28	1.69	14.1	2.05	0.36	0.04	7.20
11H-1, 74–75	94.24	110.72	0.09	0.8				
11H-3, 74–75	97.25	113.73	0.32	2.7	0.42	0.10	0.01	7.55
11H-5, 74–75	100.27	116.75	0.11	1.0				
11H-6, 74–75	101.78	118.26	0.05	0.5	0.09			
12H-1, 74–75	103.74	120.50	0.08	0.7	0.13	0.05	0.01	4.96
12H-3, 74–75	106.77	123.53	0.07	0.6				
12H-5, 74–76	109.81	126.57	0.07	0.6				
12H-7, 20–22	112.31	129.07	0.07	0.6				
13X-1, 74–75	113.24	130.45	0.66	5.5	0.84	0.18	0.03	5.93
13X-3, 74–75	116.24	133.45	0.42	3.5				
13X-5, 74–75	119.27	136.48	0.05	0.4				
15X-1, 74–75	131.64	148.85	0.06	0.5	0.27	0.21	0.02	7.50
16X-1, 74–75	141.34	158.55	0.09	0.7	0.32	0.23	0.02	8.40

Table T13 (continued).

Core, section, interval (cm)	Depth (mbsf)	Depth (mcd)	IC (wt%)	$CaCO_3$ (wt%)	TC (wt%)	TOC (wt%)	TN (wt%)	TOC/TN (atomic)
18X-1, 74–75	160.64	177.85	0.06	0.5				
18X-3, 74–75	163.65	180.86	0.46	3.8	0.64	0.18	0.02	6.28
19X-1, 74–75	170.24	187.45	0.15	1.2	0.23	0.08	0.01	7.84
20X-1, 74–75	179.94	197.15	0.05	0.4	0.14	0.09	0.01	6.29
20X-3, 74–75	182.94	200.15	0.04	0.4				
21X-1, 74–75	189.54	206.75	0.09	0.8	0.16	0.07	0.01	6.08
21X-3, 40–41	192.19	209.40	0.15	1.3				
22X-1, 74–75	198.84	216.05	0.48	4.0	0.68	0.20	0.02	7.39
22X-3, 74–75	201.85	219.06	0.08	0.7				
22X-5, 74–75	204.36	221.57	0.16	1.3				
23X-1, 74–75	208.44	225.65	0.07	0.6	0.22	0.15	0.02	7.54
23X-3, 74–75	211.44	228.65	0.05	0.4				
23X-5, 74–75	214.45	231.66	0.08	0.6				
24X-2, 74–76	219.55	236.76	0.08	0.7	0.18	0.10	0.09	1.02
25X-1, 74–75	227.64	244.85	0.24	2.0	0.33	0.09	0.01	6.04
25X-3, 74–75	230.61	247.82	0.09	0.7				
25X-5, 74–75	233.61	250.82	0.09	0.8				
26X-1, 74–75	237.24	254.67	0.06	0.5	0.13	0.07	0.01	4.85
26X-3, 74–75	240.21	257.64	0.08	0.7				
26X-5, 74–75	243.21	260.64	0.14	1.2				
27X-1, 74–75	246.84	264.50	0.12	1.0	0.19	0.07		
27X-3, 74–75	249.83	267.49	0.09	0.7				
27X-5, 74–75	252.82	270.48	0.09	0.8				
27X-7, 74–76	255.33	272.99	0.04	0.4				
28X-1, 74–75	256.44	274.25	0.10	0.8	0.37	0.27	0.02	13.41
28X-3, 74–75	259.41	277.22	0.76	6.3				
28X-5, 74–75	262.39	280.20	0.15	1.2				
28X-7, 74–75	264.90	282.71	0.11	0.9				
29X-1, 74–75	266.04	284.16	0.15	1.3				
29X-3, 74–75	269.03	287.15	0.14	1.2	0.45	0.31	0.03	9.80
29X-5, 74–75	272.02	290.14	0.08	0.7				
29X-7, 74–75	274.52	292.64	0.10	0.9				
30X-1, 74–75	275.74	294.04	0.06	0.5				
30X-3, 74–75	278.74	297.04	0.90	7.5	1.66	0.76	0.08	8.66
30X-5, 74–75	281.73	300.03	0.08	0.7				
30X-7, 74–75	284.23	302.53	0.09	0.8				
31X-3, 74–75	288.43	306.86	0.06	0.5	0.14	0.08	0.01	8.07
31X-5, 74–75	291.42	309.85	0.11	0.9				
32X-3, 74–75	298.03	316.78	0.11	1.0	0.27	0.16	0.02	7.96
32X-5, 74–75	301.05	319.80	0.13	1.1				
33X-3, 75–76	307.67	326.62	0.06	0.5	0.24	0.18	0.02	8.51
34X-1, 70–72	314.20	333.15	0.19	1.6				
34X-3, 74–75	317.24	336.19	0.09	0.8	0.16	0.07	0.01	5.82
34X-5, 74–75	320.25	339.20	0.10	0.9				
34X-7, 20–21	322.73	341.68	0.10	0.8				
35X-3, 74–75	326.87	346.04	0.16	1.3	0.44	0.28	0.03	8.16
35X-5, 74–75	329.89	349.06	0.08	0.6				
36X-3, 74–75	336.46	355.81	0.16	1.4	0.30	0.14	0.01	7.91
37X-3, 74–75	346.06	365.53	0.11	1.0	0.31	0.20	0.01	11.68
37X-5, 74–75	349.09	368.56	0.07	0.6				
38X-3, 74–75	355.75	375.37	0.23	1.9	0.52	0.29	0.05	4.47
38X-5, 74–75	358.76	378.38	0.09	0.8				
202-1232B-								
1H-4, 74–75	5.25	7.49	0.09	0.7				
1H-5, 74–75	6.75	8.99	0.11	1.0	0.15	0.04	0.01	3.92
2H-2, 74–75	11.33	14.23	0.06	0.5				
2H-4, 74–75	14.31	17.21	0.07	0.5	0.14	0.07		

Note: IC = inorganic carbon, TC = total carbon, TOC = total organic carbon, TN = total nitrogen.